3D concrete printing

The influence of printing process parameters on the mechanical properties, numerical modelling, and the exploration of sustainable printable solutions for humanitarian problems

K. Jansen

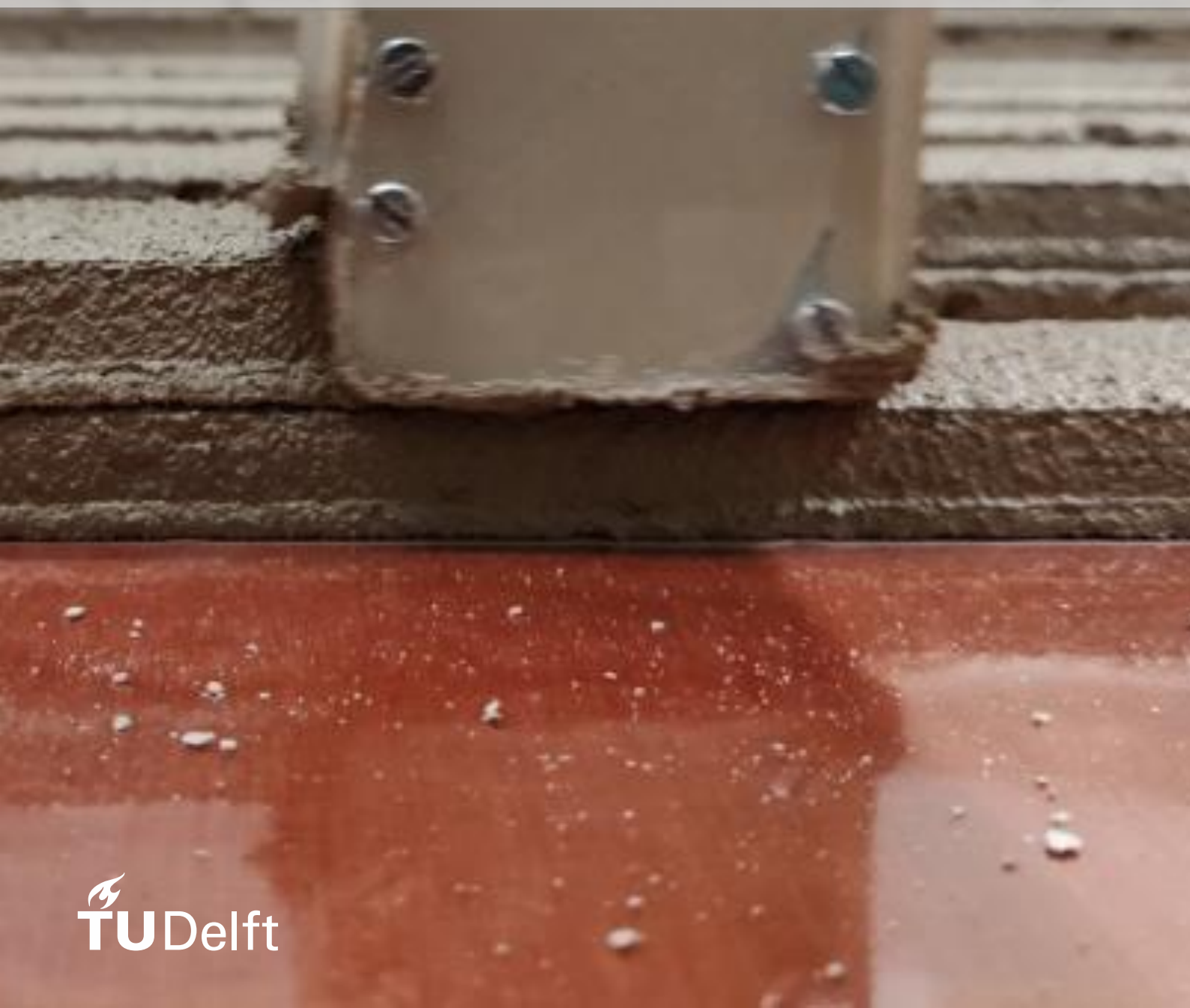

TU Delft

3D Concrete Printing

The influence of printing process parameters on the mechanical properties, numerical modelling, and the exploration of sustainable printable solutions for humanitarian problems

by

K. Jansen

to obtain the degree of Master of Science
on the faculty of Civil Engineering and Geosciences
at the Delft University of Technology.

To be defended publicly on Wednesday February 19, 2020 at 13:00.

Student number:	4587936	
Project duration:	May 2019 – February 2020	
Thesis committee:	Dr. O. Çopuroğlu,	TU Delft, chairman
	Dr. M. Luković,	TU Delft
	Dr. B. Šavija,	TU Delft
	ir. Y. Chen,	TU Delft

TU Delft Delft University of Technology

Acknowledgements

With my interest for concrete structures and the ambition to become a Structural Engineer, I started my master Structural Engineering in 2018, focusing on the track of concrete structures. After one year, the moment of starting my graduation project came faster than I expected, and Oğuzhan Çopuroğlu gave me the opportunity to do material research, on 3D printing of concrete. The fact that I could combine experimental research with numerical modelling, including the elaboration of a printable emergency shelter, made my research very interesting and diverse. Now, 10 months later, my master thesis is finished.

First of all, I would like to thank Oğuzhan. Not only for the opportunity you gave me to graduate on such an innovative topic, but also for the letting me free to include the modelling part of my research. The numerical modelling was something I thought would make the research more complete, as it is still a relevant research topic. Your idea to include a simple shelter design, definitely made the story more attractive and relevant for the future use of 3D concrete printing.

I could not have finished my thesis without the help and inspiration of my daily supervisor Yu Chen. Your ideas, enthusiasm, and your help, led to a better result of my research. All the interesting discussions we had, made me change my mind constantly, and gave me new research ideas. Thanks a lot for all your time and support, and good luck with the continuation of your PhD research!

I would also like to acknowledge my other committee members, Mladena Luković and Branko Šavija, for their positive, but critical feedback during the final stages of my research.

Carrying out all the experiments would have never been possible without the help of one person in particular, Maiko van Leeuwen. Thanks a lot for all your help! Thinking along with me to find solutions for all kind of problems during experiments, your help during the printing sessions, and the conversations we had about everything except my research, definitely made my time in the lab more fun.

I am also grateful for the interest that Anne Linde van Overmeir and Stefan Chaves Figueiredo showed during my research. The discussions we had about my experiments, definitely gave me new insights and helped me with the analysis. Your help during my printing sessions is also something that I very much appreciate!

During the printing sessions we needed the help of many more people. Printing would not have been possible without the help of Maarten Buitelaar, Hugo Kuenz, Ze Chang, and Yading Xu. Thank you for your time. For the CT scanning experiments, the help of Arjan Thijssen is much appreciated.

Finally, I would like to say Thank You to my family and friends for all the support and words of encouragement during my study.

Koen Jansen
Delft, January 2020

Summary

Concrete is one of the most widely applied construction materials worldwide. Although traditional construction processes are optimized in terms of efficiency, costs and material use, the main disadvantages are still related to the use of formwork, labour and limited freedom of shapes in architectural design. The future of concrete structures looks promising with the development of 3D concrete printing techniques. Over the last ten years, an incredible amount of research was performed on this new additive manufacturing technique. Research to 3D concrete printing systems and printable concrete mix designs led to the development of 3D printed bridges, houses and other pioneer structures. On the other hand, the influence of printing process parameters on the mechanical properties of printed elements, as well as methods to make printed concrete more ductile, like the implementation of (fiber)reinforcement, are still relevant topics in research.

The layer-wise construction process inevitably introduces interfaces between adjacent filaments. Literature showed that the bond strength between printed filaments is a crucial property, and highly influences the final mechanical properties. Therefore the experimental research of this master thesis focussed on the influence of printing process parameters, using a new printable concrete mixture developed at the TU Delft. Samples were tested in tension, compression and tensile splitting. The time interval between printing two filaments was the first parameter to investigate. Results showed that the tensile bond strength of samples printed with 10 minutes time interval decreased with more than 20% compared to a 20 second time interval. After 3 hours the bond strength decreased more dramatically, to a strength loss of 77%. The second variable in this research was therefore the effect of different curing regimes on the first filament printed for the three hour time interval samples, varying from a physical cover to the application of a water spray onto the filaments. Results were compared to the air cured samples printed with 3 hour time interval. Curing the filaments with a wet burlap or a layer of water spray, resulted in an increase of strength up to 101%. However, the application in practice is just as important, and therefore the water spray was considered to be the best option. Finally, the nozzle standoff distance with respect to the printed filament was a variable in this research, as a nozzle with backflow was used, which was not investigated yet. No significant differences were observed between nozzle standoff distances of <1mm and 10mm, because no pressure was exerted on the printed filaments. The anisotropic compressive strength and the tensile splitting strength were also tested, but were hardly influenced by the different printing process parameters, which supported the hypothesis that the bond strength is the most critical property.

The finished structures, like the 3D printed bridges and houses, show the potential of 3D concrete printing, but lack of design and calculation methods are still a limitation for the implementation of this technique in the national codes and guidelines. This is not only due to the influence of many process parameters on the bond strength, but also due to the anisotropic compressive strength properties of printed elements. Therefore, the second part of this research was a numerical research to investigate the possibilities to match the properties of a numerical finite element model with the experimental results, to be able to verify the strength or printed structures. The tensile bond strength test and the compressive strength test were simulated and both the interface and filament properties were assigned such that the numerical results matched the experimental results in tension. In compression it was possible to match two of the three loading directions.

In the final part of this master thesis, a hypothetical case study in Mali was studied. An emergency shelter scenario was chosen because the current shelter solutions, like plastic tents and improvised shelters with clay or mud walls, are mainly built for short term use. These shelters can be built in hours to days, but the indoor climate, safety as well as the health conditions inside the shelters can be improved. 3D printed shelters benefit both from the short construction time, better indoor climate, and provide a better feeling of safety, which possibly contributes the well-being of humans. The design of the emergency shelter was based on both the construction procedure, the green strength development of

printed filaments, and the final strength of the material. In the end, numerical calculations showed that the shelter fulfils the requirements and complies to the code, under the assumption that the shelter will be built in Mali, Africa. This assumption is related to specific wind pressure calculations. Other locations should also be possible if the maximum wind velocities do not exceed the maximum wind velocity in Mali. In the end, the 3D concrete printing technique shows potential for new solutions for humanitarian problems, and possibly let people realize that the investment in 3D concrete printed emergency shelters is feasible.

Abbreviations

3DCP **3** **D**imensional **C**oncrete **P**rinting

CNC **C**omputer **N**umerical **C**ontrolled

CSH **C**alcium **S**ilicate **H**ydrate

CT **C**omputed **T**omography

DIC **D**igital **I**mage **C**orrelation

FEA **F**inite **E**lement **A**nalysis

FE **F**inite **E**lement

HPCC **H**igh **P**erformance **C**alcined **C**lay

HPC **H**igh **P**erformance **C**oncrete

iDMC internal **D**isplacement **M**onitoring **C**entre

LCC **L**ow grade **C**alcined **C**lay

LF **L**imestone **F**iller

LVDT **L**inear **V**ariable **D**ifferential **T**ransformer

MK **M**eta **K**aolin

OPC **O**rdinary **P**ortland **C**ement

SCC **S**elf **C**ompacting **C**oncrete

SLS **S**erviceability **L**imit **S**tate

SP **S**uper **P**lasticizer

ULS **U**ltimate **L**imit **S**tate

VMA **V**iscosity **M**odifying **A**dmixture

Contents

1

Introduction

Concrete is one of the most widely applied construction materials worldwide (Bos et al., 2016). The design of traditionally cast concrete structures is associated with limited freedom of shapes. The construction process requires intensive labour, and use of formwork (Asprone et al., 2018b). The future of concrete structures however can be very different: 3D concrete printing (3DCP) shows opportunities that can change the design and construction of concrete structures considerably.

Over the last ten years, the development of 3DCP has made big progression, and more and more research is being performed on the process of 3D printed concrete. 3DCP is also referred to as additive manufacturing. In this technology, a computer model is used to create objects by joining materials (Asprone et al., 2018a). For 3D concrete printing this means that the construction process is automated by a 3D printing machine. Filaments of concrete are printed on top of each other without the need of labour and formwork (Bos et al., 2016; Panda et al., 2017; Wolfs et al., 2019).

This construction method has already been used in a variety of applications in building and civil engineering. In 2014, the Chinese company Winsun succeeded to partially print a concrete house. 3D printed hollow walls with diagonal connections were assembled at a building site, together with the windows, doors, and roof (Hager et al., 2016). In 2015 the same company printed a 5 storey building, using the same technique. In the Netherlands, a 3D printed pedestrian and bicycle bridge has been successfully tested, after which it was installed in Gemert (Salet et al., 2018).
Nowadays research is being performed on different kinds of reinforcement. If traditional reinforcement is used between the printed filaments, the effect of the reinforcement on the strength properties of the printed object is dependent on the bond strength between the printed filaments. Furthermore, installing the reinforcement requires labour or very complex installation strategies (Asprone et al., 2018b).
Asprone et al. (2018a) created a structural 3D printed beam with external reinforcement. Afterwards, a Finite Element Analysis was carried out to interpret the results. Panda et al. (2017) performed research on glass fiber reinforcement and also mentioned the addition of steel fibers as a possibility to improve the mechanical properties of the material. Another recent research topic is the addition of cable reinforcement in the printed concrete filament (Asprone et al., 2018b).

All these applications and research topics show that it is possible to make structural objects consisting of 3D printed concrete. At the same time, scientific articles also point out that there are no regulations or guidelines available for the design of a 3D printed structure. All designs mentioned above were based on experimental testing, and in some cases the results were verified by numerical analyses. Although it is very useful to have knowledge about the structural behaviour of a specific 3D printed object, there is no general design code available that provides a set of recommendations and calculation rules to design a 3D printed structure. This research therefore focused on two specific parts of the design process. The first part was experimental research to obtain mechanical properties of a sustainable concrete mixture developed by researchers from the Microlab, TU Delft. This part provided information on both the mechanical properties of the material and the influence of process parameters on the mechanical performance. The second part focused on numerical research where possibilities were investigated to

match the properties of a finite element model with the experimental results. For the continuation of this master thesis, this part is referred to as the development of a numerical material model. Finally, the developed material model was used used for the structural verification of a 3D printed emergency shelter.

1.1. The problem

To be able to design a structure, it is necessary to know the mechanical properties of the applied material. For conventionally cast concrete, test methods to obtain mechanical properties are well known and standardized. For calculations of a traditionally cast structural element, it is sufficient to assume that the material has heterogeneous mechanical properties.

The general problem related to 3DCP is that the printed elements cannot be qualified as an isotropic material, due to its layered structure (Le et al., 2012b). Furthermore, the printing process is not (yet) standardized, so different settings of the printing machine, as well as the environmental conditions, have a great influence on the final structural performance of the material. Below, a selection of parameters is presented to show the variety of process parameters that might influence the mechanical properties of 3D printed concrete elements:

Time intervals	A balance should be found between the buildability of the concrete, i.e. the capacity to remain stable and stacked during the printing process, and the bond strength properties between two printed filaments of concrete (Asprone et al., 2018a).
Nozzle standoff distance	The nozzle standoff distance can be explained as the height between the bottom of the nozzle and the printing surface. According to Panda et al. (2017) the nozzle standoff distance has an effect on the strength properties, i.e. a low nozzle standoff distance causes the printed filaments to be squeezed together, and a large nozzle standoff distance causes scatter in the results due to inaccurate positioning of individual filaments.
Printing speed	The printing speed should be optimized according to the flow rate of the concrete in order to avoid that micro voids develop in the microstructure of the concrete (Panda et al., 2017).
Object geometry	The geometry of the printed shape can have a negative influence on the strength properties. Costanzi et al. (2018) mentioned that a too small corner radius of rectangular filaments can lead to deviating material properties.
Geometry of the nozzle	Buswell et al. (2018) reported that changing the direction of a print path can lead to a higher porosity of the concrete. The size and geometry of the nozzle are two parameters for this aspect.
Printing environment	Wolfs et al. (2019) reported that the temperature, relative humidity, and the wind speed all have an influence on the interlayer adhesion.

The fresh state properties of mixtures also have an influence on the buildability, extrudability and pumpability, which indirectly influence the mechanical properties of the hardened material (Chen et al., 2019a; Le et al., 2012a). However, in this research, the mix design was a fixed parameter.

Finally, the problem related to 3D concrete printing is described as:

The lack of knowledge about the influence of the process parameters on the mechanical properties of 3D printed concrete, and the absence of a reliable material model for structural calculations.

1.2. Objectives

This research focused on the mechanical properties of 3D printed elements and the design process of a 3D printed building. Wolfs et al. (2019) and Le et al. (2012b) showed that the mechanical properties differ in the three loading directions as shown in Figure 1.1, and that the process parameters as described in section 1.1 have an influence on the final strength properties of the material. Therefore the main objective of this research was described as follows:

To find the influence of the process parameters on the mechanical performance of the material by means of lab-testing, to develop a reliable finite element material model and to use accumulated knowledge for the design of a hypothetical 3D printed concrete structure.

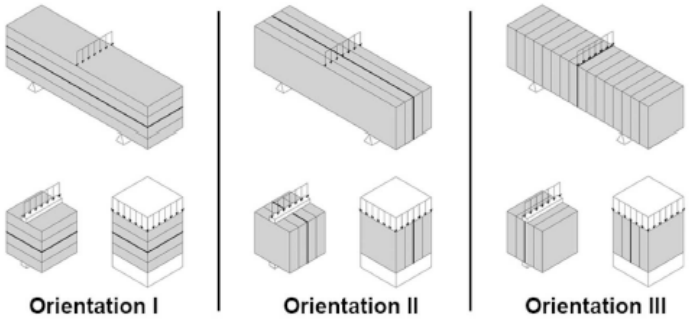

Figure 1.1: Impression of the layered structure of 3D printed concrete (Wolfs et al., 2019).

Research questions

To support the objective of this thesis, research questions were formulated to cover the three parts of the objective:

- How do the printing process parameters, like different time intervals, nozzle standoff distance and different curing conditions, influence the mechanical properties of 3D printed objects?
- Can the material behaviour in different directions be captured numerically, using a finite element program?
- How can the obtained knowledge about both the process parameters and the material model be used to design a 3D printed emergency shelter?

1.3. Scope

The topic on 3DCP has many variables that can influence the outcome of this research. As mentioned before, this research only focused on the mechanical properties of a developed material, by varying the process parameters. The cementitious material that was used during the experiments was a limestone and calcined clay-based sustainable concrete mixture. This material was developed by Chen et al. (2019b) at the Delft University of Technology. This mix design was successfully tested as a printable material.

To obtain the mechanical properties of the material, tests were carried out on samples. The tests were performed in both Stevin II lab and the Microlab at the TU Delft. Mechanical tests that were performed are compressive strength tests, bond strength tests, and tensile splitting strength tests. CT scanning of samples should provide extra information on the voids presents in the filaments and the interface. The information that was needed to perform these tests, and how to interpret and analyze the results, are explained later in this report.

The second part of this research was the step by step development of a reliable material model. The experimental tests were simulated in DIANA, to compare and match the experimental results with the

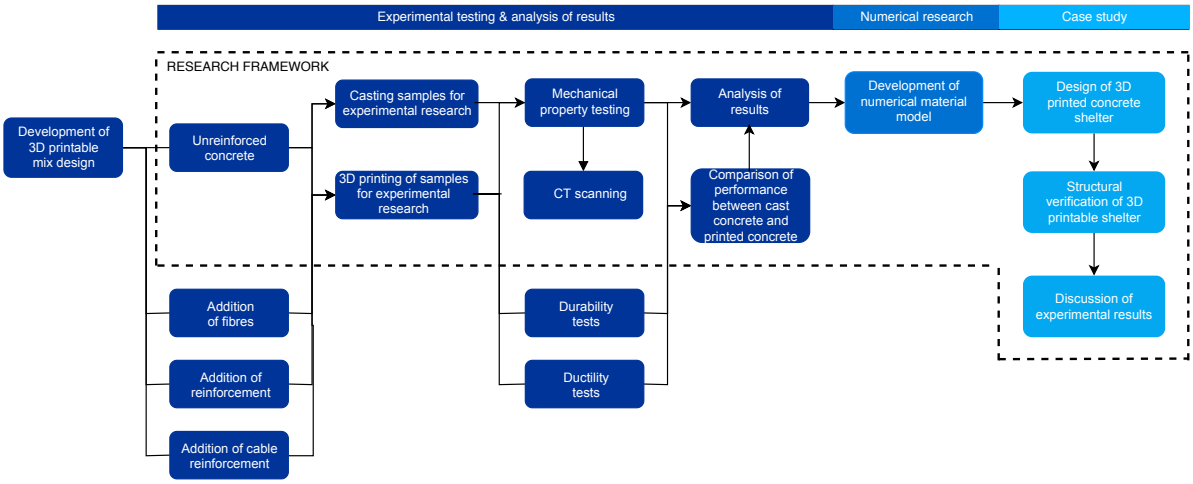

Figure 1.2: Outline of this thesis, including the research framework / scope.

numerical results. The goal was to use this model for structural verification of an emergency shelter.

Finally, the obtained knowledge about both the influence of process parameters on the mechanical properties of printed elements, and the developed material model, formed the basis for the elaboration of a case study. For 3DCP, not only the final strength is of importance, but an object must be buildable as well. This generally means that extruded filaments must have sufficient stiffness to bear the weight of the subsequent filaments, without deforming too much. For this reason, the buildability of an object is just as important than its final mechanical performance. This aspect requires a new way of thinking, and traditional design procedures do not comply. Also the lack of suitable calculation methods is still a limitation of the further development of 3DCP. During the case study, both the 3D printing aspects and structural verification were key aspects in the design process of an emergency shelter.

1.4. Risks

This research was highly dependant on the success of the performed experiments. Below the main risks are mentioned, and it is also described how problems were solved during this research:

1. **Mix design**
   Although the mix design was validated as a printable material, Chen et al. (2019a) mentioned that the buildability of the material was still a topic that needs additional research. During the printing process it could happen that the buildability of the material was not as expected. Problems with the mix design were however not observed, and no adaptations to the mix design were needed to make the material buildable.

2. **Experimental results**
   There was also a possibility that the results of the experiments gave inexplicable results or that experiments failed. The latter occurred during several direct tensile bond strength tests, mainly for the samples tested with a 3 hour time interval. The samples were printed again, larger samples were prepared, and the tests were performed again without problems.

2

Literature review

The starting point of this research project was to find relevant information needed to make a research plan. A proper research plan takes into account already finished research topics, combined with new research ideas to contribute to the general knowledge about 3DCP. Therefore this chapter shows a literature review where the most relevant information about 3DCP is presented. From background information, and critical mix design properties, to the variety of process parameters that have an influence on the final mechanical performance of 3D printed elements.

2.1. Background of 3DCP

The most commonly used type of 3D concrete printing is an extrusion based additive manufacturing technique. Filaments of concrete are positioned on top of each other, by means of a 3D concrete printer, to gradually form elements. The goals of this relatively new innovation are clear: create a new concrete manufacturing technique that, compared to traditionally cast concrete, saves costs, provides new architectural possibilities, and is environmentally friendly (Asprone et al., 2018b; Chen et al., 2019b; Labonnote et al., 2016; Wolfs et al., 2019). For 3DCP, no formwork is required, which means that intensive labour is less needed. Also the building speed in general increases, and therefore has economical benefits (Nerella et al., 2019). Panda et al. (2018) addressed the use of local materials to obtain an environmentally friendly mix-design, and to reduce the the carbon footprint of structures. For architectural design new opportunities arise. The use of free shapes in concrete design will be easier with 3DCP.

2.1.1. Examples from pioneers

The best way to explain the variety of projects suitable for 3DCP, is to show state-of-the-art projects. In Figure 2.1 the most striking examples are highlighted, with a short description added in the paragraph below.

(a) This example is a two storey house built in China in 2016. Two remarkable facts are that the reinforcement and plumbing for the walls were installed before the concrete was printed. Also the concrete used was traditional C30 [1] concrete, without any mix-design changes for printing. (Scott, 2016).

(b) The first 3D printed concrete bike bridge was opened in October 2017 in Gemert, the Netherlands. The bridge consists of six elements, connected by cables that are pre-stressed.

(c) A six-storey building designed by the WinSun Company in China. The over-all idea for this project was just as innovative as the 3D printing technique itself, namely a self-sufficient city located in the desert.

[1] Concrete with a characteristic compressive strength of 30 MPa, tested on cylindrical samples.

(a) (b)

(c) (d)

Figure 2.1: Impression of recently finished 3D printed projects.

(d) This is a project still to be realized in the Netherlands, early 2020. It is the world's first commercial housing project, where people can purchase a house via a real estate company. The residential houses have a futuristic shape and are therefore the perfect example to show the architectural possibilities of 3DCP.

The variety of examples shows already a lot of future possibilities. Researchers find more and more innovative ideas to make the disadvantages of 3DCP irrelevant. The amount of ongoing research to find new methods to implement reinforcement, use external reinforcement, to use external prestressing, and even to develop new structural elements without reinforcement, shows the willingness of the engineering industry to make this new durable construction method to a success.

2.1.2. General terminology explained

3D concrete printing involves new terms that might be unknown, or have a different interpretation in common engineering industries. This paragraph briefly describes the most important terms associated with 3DCP. Printability can be seen as an over-all quantification of a concrete mixture that is suitable for 3D printing, mainly depending on the pumpability, extrudability, open time, and buildability of the mixture.

Pumpability

This term is used to describe the capacity of concrete to pass through pipes and nozzles at the printing head, and is therefore mainly dependant on the mix-design (Le et al., 2012a).

Extrudability and open time

Extrudability can be best explained as a measure for how well a concrete mixture is suitable for 3D printing. Labonnote et al. (2016) defines extrudability as the ease and reliability of depositing material through a deposition device. This term is therefore mainly related to the mix-design. Chen et al. (2017) mentioned that the extrudability is also dependant on the open time of a concrete mixture, where the open time of the mixture can be best described as the age of the mix, after adding the water to start

the hydration.

Buildability
A critical parameter for 3D concrete printing is the buildability of the material. Chen et al. (2017) described the buildability of the material as shape stability, where Labonnote et al. (2016) defined buildability as the resistance of the wet material to deform under loads. According to Perrot et al. (2015) and Le et al. (2012a), the buildability can be qualified by the number of filaments that can be stacked, without noticeable deformation of the lower filaments. Ma et al. (2019) even set a requirement of at least 20 filaments per printing session, otherwise the material is not suitable for printing. The biggest issue is that good buildability properties go at the expense of the printability of the material in general (Buswell et al., 2018). For that reason, there should always be strived for an optimum between those properties.

Workability
Workability is a term that can be interpreted in multiple ways. Thinking of traditionally cast concrete, workability means that the mixture is flowable enough, can be compacted without segregation of the aggregates, and that the mixture has sufficient open time for transportation and casting. For 3DCP, workability should be interpreted more strictly. A workable concrete mixture for 3DCP is considered to be extrudable, but as soon as a filament is deposited, the desired property is that the mixture gains immediate stiffness. This is not yet possible, but the rheology of the mixture should be such, that it is both extrudable, and buildable.

2.1.3. Differences with traditionally cast concrete

Besides the fact that 3D printed concrete offers a lot of advantages and future opportunities, there are also differences compared to traditionally cast concrete. The main differences in the construction process, financial differences, differences in the mix design, and differences in anisotropic properties are described in this section.

Differences in construction process
Massive differences can be found in the procedure to design and build 3D printed structures. The use of moulds, also known as formwork, is nowadays the only applied construction method to cast concrete structures. Formwork can be made of several materials, like timber, steel, or even polystyrene panels. Which type of formwork is used, is mainly dependant on the repetition factor, which refers to the amount of times the formwork can be reused (Jha, 2012). This is not only dependant on whether the formwork is customized, but also whether the formwork can be reused or not. The use of formwork therefore also contributes to the financial differences between cast and printed concrete, because during the 3D printing process, no formwork is required. Besides the generated advantages like the use of free shapes, increasing building speed, and financial benefits, the main disadvantage of 3DCP (or challenge) is the limited shape stability of the printed filaments during the 3D printing process (Chen et al., 2019a). The deposited filament(s) should already have significant green strength to be able to bear the weight of the subsequent filaments. Some changes can be made in the mix-design, to create a non-slump mixture (Chen et al., 2017; Ma et al., 2019), but there will still be a limit to the stacking rate of the filaments. The influence of the process parameters on for example the building procedure, is explained later.

Differences from economical viewpoint
Referring to the use of formwork needed to cast concrete structures, also financial benefits can be obtained if structures are 3D printed instead of cast. According to Jha (2012), the costs of formwork are as large as 35% of the total construction costs, and the activities related to formwork consume 50-75% of the total construction time. Taking into account that formwork activities always come with labour, the over-all project costs can be decreased significantly if the use of formwork is eliminated. Jha (2012) showed that the total costs related to formwork, including the labour costs, are as much as 54% of an over-all concrete structure. These costs can be directly deduced from the costs of a 3D printed structure (Bos et al., 2016). On the other hand, elimination of formwork does not by definition lead to 54% reduction of over-all costs. The lion's share during the 3D printing process are the costs for a printable mix design, and (the operation costs of) a suitable concrete printer. The mix design is

more expensive because of the addition of admixtures to obtain a printable mixture, as explained in the next paragraph. The machinery needed for the over-all printing process, will also generate higher (renting) costs compared to traditionally cast concrete. According to De Schutter et al. (2018), the total equipment costs are very much dependant on the sophistication of the 3DCP machine, like the use of sensors for precise placement of filaments, adjustable nozzles that are suitable to use for many applications, and the use of adapted conventional construction equipment. The latter describes traditional equipment, adjusted to be used for 3DCP. Finally, topology optimization reduces over-dimensions and material waste, which leads to optimal material use (De Schutter et al., 2018). This approach can eventually save costs, but the reduction of costs is very much dependant on the type of application.

Differences in mix design
To make concrete printable, a mixture should be extrudable and buildable, which are two contradicting properties that traditional concrete does not have by definition. Traditional concrete mix designs consist of cement, water, and aggregates. By mixing these three elements in the right proportions, normal strength concrete can be obtained, if the material is well compacted. In the past, new, innovative structural designs required a new type of concrete: High performance concrete (HPC). High performance concrete, most of the time a combination of high-strength concrete and self compacting concrete (SCC), is nowadays widely applied (Boukendakdji et al., 2012; Lei and Plank, 2012). The reason that HPC is so successful, is because of the use of a high-range water reducer, also called superplasticizer (SP). In order to obtain high strength concrete, coarse aggregates are replaced by fine aggregates. All these fine particles bind water, resulting in a very high water demand in order to keep the material workable. This high water demand results in a high water-cement ratio, which decreases the mechanical performance of the material. Superplasticizer is a chemical admixture that increases the fluidity of concrete by dispersing cement particles in the mixture. The dispersion of solid particles improves the flow characteristics of concrete, resulting in the use of a lower water-cement ratio, and therefore a higher concrete strength. Lei and Plank (2012) even described the introduction of SP in engineering industries as the beginning of a new era. By using the right amount of fine aggregates in combination with a superplasticizer, even a self compacting concrete can be obtained, where deformability and segregation resistance are the most important properties (Memon et al., 2011).

For 3DCP, good flow characteristics are a must in order to create an extrudable mix design. On the other hand, this aspect is also the direct problem related to printable mix designs. Shape stability is essential when filaments are printed. A flowable mix design with a high deformation capacity is useless in 3DCP, because printed elements will not retain their shape. Where the use of superplasticizer was the beginning of a new era in the development for HPC, a Viscosity Modifying Admixture (VMA) can be the break-trough in the era of 3DCP. VMA is added to concrete mixtures to change the plastic viscosity of the mixture, because VMA has the property that it can bind water molecules to form polymer chains (Sonebi et al., 2013). Sonebi et al. (2013) concluded in their research that an increasing VMA dosage leads to higher yield stress and plastic viscosity, due to the entanglement of VMA chains and the water in the cement paste. This results in an intertwined particle structure, which gives a high shape stability. Figueiredo et al. (2019) concluded in their research to develop a 3D printable strain hardening cementitious composite, that shape stability is directly improved with increasing dosages of VMA, and that VMA can contribute positively to the development of printable mix designs.

Differences in mechanical properties
The anisotropic element properties are caused by the production process of printed elements. The 3D printer deposits filaments of concrete onto each other, layer by layer. The interface between two adjacent filaments causes deviating element properties, and the bond strength of two filaments was mentioned as a critical parameter for the characterization of the material (Wolfs et al., 2019).

Figure 2.2 shows the three directions that have, according to the literature, different mechanical properties. The figure shows two printed filaments, with an interface in between, and the longitudinal direction is also the printing direction. The perpendicular direction represents the loading direction perpendicular to the interface. The other two directions are loaded parallel to the interface, namely in printing direction (longitudinal) and width-wise (or lateral) direction.

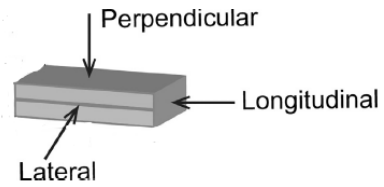

Figure 2.2: Three directions representing the different loading directions (Sanjayan et al., 2018).

Several researchers mentioned that the directional dependence of the material strength properties is due to the interface properties, i.e. the bond strength of two filaments (Nerella et al., 2019). According to Tay et al. (2019) the bond interface adhesion can be divided into mechanical interaction and chemical bonding. Where mechanical interaction is mainly dependent on good compaction, the chemical bonding mainly dependent on the state of hydration, in combination with the time interval between extrusion of the filaments. The ongoing hydration gives the printed filament a higher stiffness when time passes, due to the C-S-H being formed. Concrete that is being printed, with the same age as the earlier printed filament, has less material stiffness due to the pumping process. The shear force during the printing process breaks the C-S-H and therefore the new filament can still be extruded onto the deposited filament. The insufficient deformation capacity of a filament that is minutes to hours old, makes that the interaction between the filaments is not optimal (Tay et al., 2019). In the interface, air voids might be present, which weakens both the mechanical interaction and chemical bonding. In Figure 2.3, anisotropic properties in compression are presented, as investigated in three different articles. It can be clearly seen that samples had the largest compressive strength when loaded in longitudinal direction (X- or Par2 direction). The perpendicular and lateral loading direction showed a strength decrease.

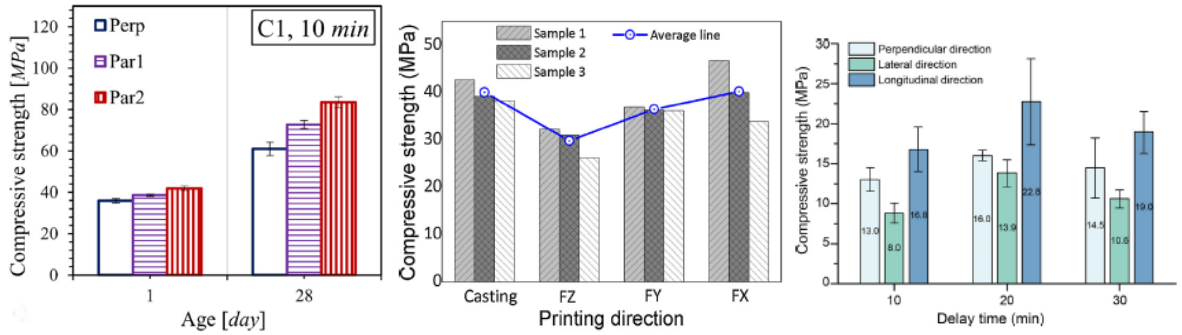

(a) (Nerella et al., 2019) **(b)** (Ma et al., 2019) **(c)** (Sanjayan et al., 2018)

Figure 2.3: Examples of anisotropic material properties in compression.

Panda et al. (2017) and Sanjayan et al. (2018) explained the anisotropic material properties because of both directional compaction during the printing process, and the self weight of subsequent filaments that was being exerted on previously printed filaments. Due to the extrusion pressure, which is probably the highest in extrusion direction, the material is best compacted in that direction. In the other directions, the pressure is less, and therefore also the compaction in that direction is not as good as the longitudinal printing direction. The layered structure of the printed elements is however unavoidable, and therefore there is a need for reliable mechanical properties for structural calculations, as also described before (Wolfs et al., 2019).

The compaction of concrete turns out to be a critical for mechanical performance. For traditionally cast concrete structures, manual compaction should be applied, and is widely used in the construction industry. For 3D printed structures however, compaction using a vibration needle is not possible. The only way the material might obtain a good compaction, is because of the high pressure in the concrete pump, and due to the weight of the subsequent filaments (Nerella et al., 2019).

2.2. Available 3DCP techniques

This section describes the available 3D printing techniques that are currently being used in practice. Also different types of printing equipment are explained, as well as the general workflow.

Extrusion-based technique

The extrusion-based technique makes use of printable concrete that is extruded through a nozzle (Xia et al., 2019). This technique is suitable to print, buildings and bridges, as also has been described in the introduction of this thesis. De Schutter et al. (2018) described Contour crafting and 3D printing as the main concrete printing techniques. Contour Crafting, developed by Khoshnevis (2004), is an automated construction process to create complete structural elements, including reinforcement, plumbing, etc. De Schutter et al. (2018) described contour crafting as a technique where the outer shells are created by extruded filaments and where the inner space is filled with conventional concrete. 3D printing differs from contour crafting in the sense that extruded filaments form the whole element, which has as main disadvantage that implementing reinforcement and plumbing is more difficult.

Powder-based technique

The powder-based technique, also referred to D-shape technology, is a 3D manufacturing technique that is specifically suitable for 3D printing of very complex shapes (Xia et al., 2019). Instead of using ready mixed concrete, a binder is precisely deposited in a powder bed. The powder will then react with the binder and eventually, when all excess powder has been removed, the desired shape remains, that was difficult to print if the extrusion based technique was used.

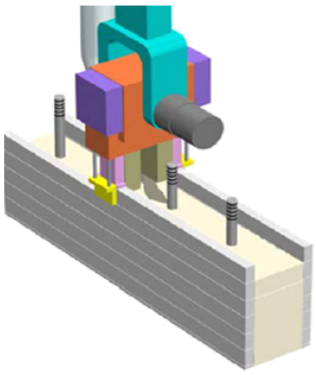

(a) Contour crafting (Xia et al., 2019)

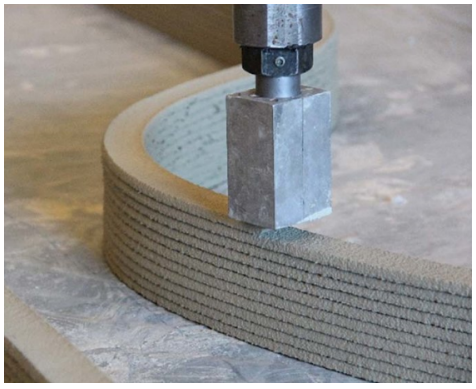

(b) Extrusion technique (Wolfs, 2018)

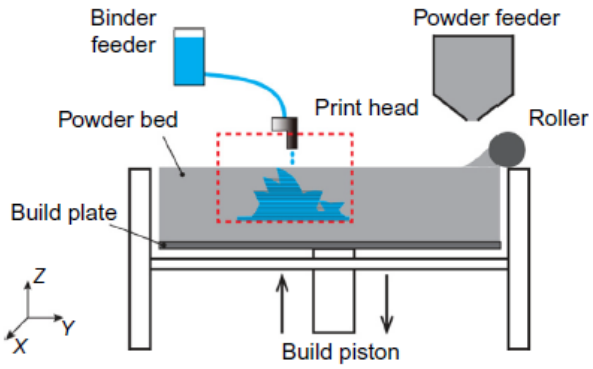

(c) D-shape principle (Xia et al., 2019)

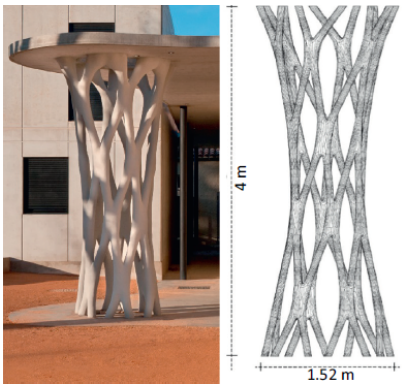

(d) D-shape example (De Schutter et al., 2018)

Figure 2.4: 3DCP technologies.

3D printing systems
Nowadays, three different types of concrete printers are available (Le et al., 2012a; Paul et al., 2018). The first system is a gantry system, which can move in X-, Y-, and Z-direction (see Figure 2.5a). An advantage of this machine is, according to Paul et al. (2018), that the height can be easily adapted and both large and small objects can be printed. The second system is a printer with a robotic arm, as presented in Figure 2.5b. This printer has full freedom in motion, because of a six degrees of freedom axis system. An advantage is thus that no extra rotating parts are needed to obtain full freedom in motion, but the main disadvantage is the size of the robot. Up-scaling is not easy with this machine, and only objects with a limited scale can be printed. Finally, the crane system is comparable to the robotic arm printer (Figure 2.5c). The only difference is that the crane has less degrees of freedom, and therefore also needs a rotating nozzle type. The main advantage of such a printing system is that up-scaling is possible, and moving the machine to a new location should be easy if a movable crane is used (Paul et al., 2018).

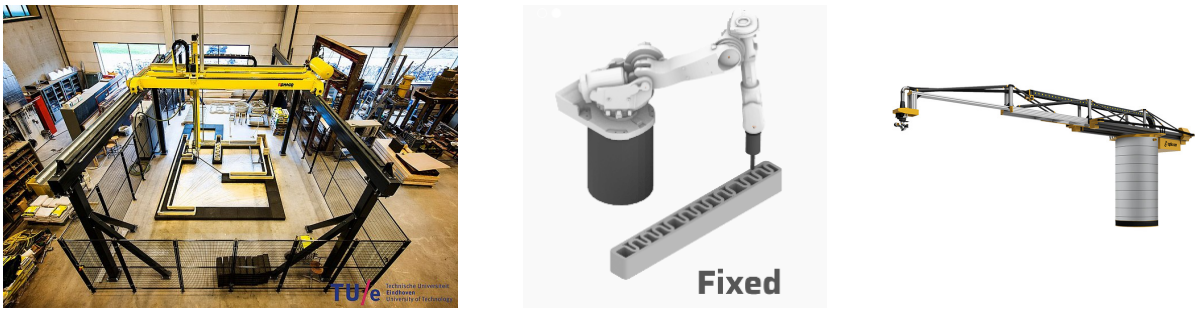

(a) Gantry system, TU Eindhoven **(b)** Robotic-arm printer (CyBe) **(c)** Crane printer (ANIWAA)

Figure 2.5: Available 3D concrete printers.

2.3. Process parameters

During the printing process, there are many parameters that may influence the structural performance of printed elements. To get an overview of all process parameters that have an influence on the mechanical properties, this section briefly describes recent research projects where process parameters were investigated. Based upon the results and conclusions of those projects, a selection of the most important parameters was further investigated in this research.

2.3.1. Time interval

The parameter that was mentioned most in almost every research is the time interval between printing two filaments. The strength reduces as the time interval increases, because of the decreasing bond strength of the interface, and an increasing amount of air voids present in the interface (Le et al., 2012b; Tay et al., 2019; Wolfs et al., 2019).

Compressive strength
For the compressive strength, no clear strength reductions were found as the time interval increased. The anisotropic properties were however present. The results of Nerella et al. (2019) showed almost no reduction of strength when samples of 1 day interval time were compared to samples with an interval time of 1 and 10 minutes. Also no clear decrease of strength can be observed in the results from Sanjayan et al. (2018). Remarkable is however, that their compressive strength results with a time interval of 20 minutes is 20% - 30% lower compared to samples with time intervals of 10 and 30 minutes. The author of this article allocated this result to surface moisture content. For the specific mix-design that was used, first no visible surface moisture was present, then surface moisture was visible due to bleeding, afterwards a decrease of surface moisture was observed. Bleeding, expelled moisture, and evaporation all played a role in the visibility of surface moisture. Therefore the somewhat strange compressive strength results can be explained anyway.

Tensile bond strength

An interesting article, where research was conducted by Tay et al. (2019), showed the effect of time intervals on the bond strength of 3D printed concrete. Direct tensile tests were performed on several samples, each with different time intervals. Samples were fully clamped in the testing device. Figure 2.6 shows a high reduction of the tensile strength within a time interval of one hour.

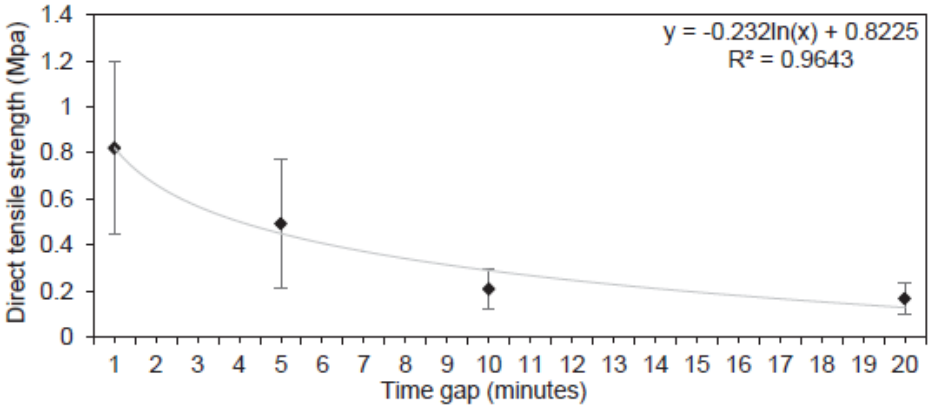

Figure 2.6: Tensile strength test results by Tay et al. (2019).

Two possible explanations for the decreasing bond strength, also concluded by Tay et al. (2019), are on the one hand the amount of air voids in the interface that become larger if the time interval increased and also the increase of stiffness of the initial filament could make the interface too stiff to mix well with the subsequent filament. Sanjayan et al. (2018) performed the same mechanical test, however with a different test setup, using hinged connections during the test. The focus in this research was the influence of surface moisture on the interlayer strength, which is discussed in section 2.3.6. The conclusion regarding interval time was that the tensile strength between 10 and 30 minutes time interval are almost identical, and are therefore in contradiction with the results of Tay et al. (2019). The same test, performed by Panda et al. (2018), shows again different results. This can be seen in Figure 2.7.

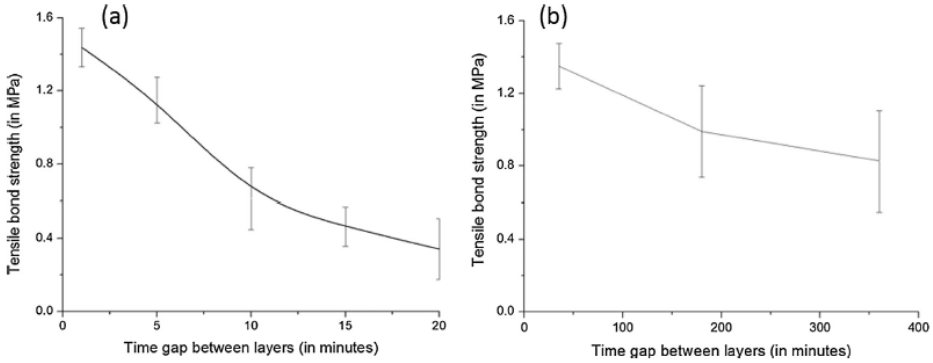

Figure 2.7: Tensile strength test results by Panda et al. (2018). The left graph shows the results using the same concrete batch for each filament, and the right graph shows results using a new concrete batch for each filament.

This test had as extra parameter the open time, i.e. the age of the concrete batch. It is noted that printing with a batch older than 20 minutes is difficult, and that new batches had to be mixed. Therefore the left graph is more related to the open time of the concrete and the right graph can be used to compare with other articles, regarding the time interval of the printed filaments.

Tensile splitting strength

Wolfs et al. (2019) performed several strength tests and found a reduction in tensile splitting strength of 21% after a time interval of 24 hours, compared to a sample with 15 seconds time interval. Up to a

time interval of 4 hours, no clear strength drop was observed. The same research was performed by Ma et al. (2019), where analysis of the results showed a decrease in tensile splitting strength of 24% to 37% in longitudinal- and lateral direction, respectively. The tensile splitting strength in direction one (perpendicular to the interfaces) was approximately the same as the reference (cast) material. These results are also shown in Figure 2.8.

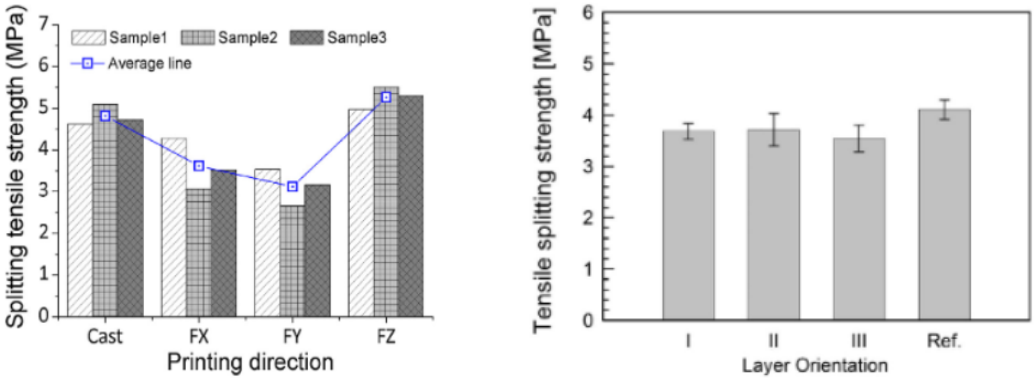

(a) Tensile splitting strength results by Ma et al. (2019).

(b) Tensile splitting strength results by Wolfs et al. (2019).

Figure 2.8: Tensile splitting strength.

2.3.2. Printing speed

The printing speed of a 3DCP machine is typically given in mm/sec. The speed should be adjusted very accurately to make sure that the concrete filament is well deposited on the substrate, and has a good compaction without being stretched after deposition. The printing speed should be determined related to the pump speed. In case the pump speed is operated separately from the printer, a balance should be found between the pump speed and the print speed of the nozzle. Le et al. (2012a) described that an improper printing speed related to the flow rate of concrete, can lead to micro voids developing in the micro-structure of the printed material. Panda et al. (2018) focused on the differences in tensile strength related to a different printing speed, using a constant pump speed. Results for 70 mm/s showed almost no scatter in the results, but for increasing printing speed, the scatter increased a lot, up to 90% strength loss. A similar hypothetical conclusion was drawn, that a too high printing speed creates air voids in the material, leading to decreasing strength properties.

2.3.3. Nozzle standoff distance

The vertical position of the nozzle with respect to the initial layer is of importance for the strength properties of the interface (Wolfs et al., 2019). Not only the interface strength properties are influenced by the nozzle standoff distance, but also the surface quality, i.e. surface roughness (Panda et al., 2018). Down-flow nozzles were used, and the default nozzle standoff distance was in both articles chosen to be equal to the height of the filament. Wolfs et al. (2019) mentioned that a nozzle standoff distance that is chosen too high, resulted in a large scatter in the results due to inaccurate positioning of the filaments. Using a small nozzle standoff distance resulted in squeezing of the filaments. Further research of the influence of squeezing on for example the compaction and air void content was however not performed. Results of this research showed no clear difference with changing nozzle standoff distance. This is in total contradiction with the research performed by Panda et al. (2018). Those results showed a reduction in bond strength of approximately 65% with 4 mm nozzle standoff distance increase, compared to the default height. It must be noted that in both researches a nozzle with vertical deposition was used.

2.3.4. Nozzle type

The geometry of the nozzle, i.e. the cross section of the nozzle opening, comes in many shapes and dimensions. A distinction can be made between nozzles where the material is extruded vertically, horizontally, or at an angle. Vertical extrusion means extrusion of the filament at the bottom of the nozzle, and horizontal extrusion means a printing process where the filament is extruded horizontally, i.e. at the back of the nozzle. A combination of the two, where the main parameter will be the angle of the deposited material, is also possible. Secondly, also a distinction can be made between a rectangular and a circular nozzle opening. Research focused on mechanical properties related to the nozzle type, was however not found. This section is based on all kind of nozzles used in multiple articles, and Figure 2.9 shows three different nozzle types.

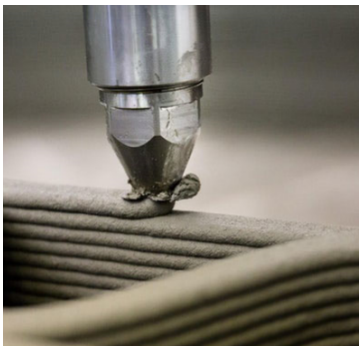

(a) Down flow, circular extrusion (3Dnatives).

(b) Back-flow, rectangular extrusion (Ogura et al., 2018).

(c) Hybrid-flow, rectangular extrusion (Rubio et al., 2017).

Figure 2.9: Different nozzle types.

2.3.5. Object geometry

The object geometry does not directly influence the mechanical properties of the material itself, but in relation with the nozzle geometry, it can be important to take care of sudden changes in print-path directions. Buswell et al. (2018) mentioned the influence of the maximum corner radius related to rectangular nozzle dimensions. A small corner radius can lead to under-fill in the outside-corner of the filament, while no problems occur at the inside of the corner. It is also mentioned, that due to under-fill, air voids appear and the density is less compared to well-compacted material.

2.3.6. Curing conditions

Dehydration of the filaments, and then mainly the surface where new filaments should be deposited on, has a great influence on the mechanical properties of the interface. Several articles mentioned this problem and pointed out possible solutions to prevent surface dehydration. Wolfs et al. (2019) made a distinction between covered and uncovered samples when testing time intervals of 4 and 24 hours. Flexural tensile strength reductions of up to 51% were measured. Sanjayan et al. (2018) recommends to do more research after finding a great influence of the present moisture level on the bond strength of two filaments.

2.3.7. General conclusions from literature

A clear conclusion of Wolfs et al. (2019) was that the process parameters could not be considered independently of the mix-design and other printing parameters, like the nozzle standoff distance and moisture/water loss of the deposited filaments. This conclusion was supported by Panda et al. (2018), who also mentioned that an optimum needs to be found between the variety of process parameters. Based on all results presented above, it must be mentioned that for every research different mix designs were used. For that reason it was hard to define a range how fast the mechanical properties change, with changing process parameters.

3

Experimental research

Experimental research requires a detailed plan to obtain the desired results. The first part of this chapter presents a research plan that is mainly based on the literature review. The second part of this chapter gives detailed information about the mix design that was used in this research for both the experimental part and the case study. The research methodology, printing equipment, and the sample preparation procedure are described in detail subsequently. Finally, the presentation of the experimental results concludes this chapter.

3.1. Research plan

The first part of this master thesis was experimental research. This experimental research consisted of 3D concrete printing of samples and testing the samples for its mechanical performance at the age of 7 days. The influence of several process parameters on the mechanical performance of the material was investigated, but due to the combination of limited time and the large number of experiments, it was necessary to limit the amount of variables during the experimental research. The experimental parameters for this research are presented in the research plan.

3.1.1. Process parameters

According to the information found during the literature review, many parameters have an influence on the final mechanical performance of printed elements. It was not possible to investigate all parameters, and therefore this research focused on only three main variables. The variables that were tested are 1) the nozzle standoff distance, 2) the time interval between the printed filaments, and 3) curing regimes of the filaments. Also the anisotropic properties of the printed material were part of this research. For the remaining parameters reasonable assumptions were made based on the information from the literature review. For every process parameter is explained whether or not assumptions were made. The choice of which parameters were relevant, was not only based on information from the literature review, but also on which parameters were absolutely necessary to further elaborate the case study.

Nozzle geometry

From the literature review, it became clear that sudden changes in direction, and squeezing of the filaments, can lead to the entrapment of air voids in the material. Horizontal extrusion was chosen to disrupt the lower filaments as little as possible. The dimensions of the nozzle opening were designed at 40mm x 12mm. This nozzle was developed at the TU Delft, and a prototype of this nozzle was 3D printed in plastic. Considering that for this research only a small quantity of concrete was printed, the nozzle-prototype was sufficient for execution of this research.

Nozzle standoff distance

It could be concluded that the nozzle standoff distance has a significant effect on the bond strength of

a printed element, but also that the decrease of mechanical properties, depending on variable nozzle standoff distance, is strongly related to the mix-design used. In this research a new nozzle type was used, as well as a different mix design, so therefore it was useful to find out if an increasing nozzle standoff distance reduces the mechanical properties of the interface and printed material in general. Also for the case study this was a useful parameter. Realizing that slump of the extruded filaments may unexpectedly occur in practice, and the nozzle standoff distance therefore increases as a consequence, it is critical to have information about the remaining strength of the specific interfaces. The effect of the nozzle standoff distance on the strength of the material was tested for <1mm, 5mm, and 10mm. Time intervals between extrusion were kept at 1 minute, to exclude the effect of increasing time intervals on the strength of the elements.

Printing speed
From several studies, it became clear that the printing speed varies in the range from 40 to 75 mm/s. For this research, the default printing speed was chosen at 60 mm/s. Before printing samples, a speed test was performed to match the pump speed with the printing speed, since the printer and the pump had to be operated separately. The settings were correct if the extruded filament was not stretched or compressed horizontally due to the speed of the nozzle. Also the shape and dimensions of the filament must have the same dimensions as the nozzle opening. Once these parameters were optimized, they were used as default printing speed and pump speed for the remaining part of this research.

Time interval
The time interval between the extrusion of two filaments has an influence on the bond strength, and therefore also on the mechanical performance of the printed elements. Literature showed that the range of strength decrease is critical, even with time intervals of only minutes. This parameter is highly dependant on the mix design, and was therefore a crucial parameter in the characterization of mechanical properties of the new mixture used in this research.

Time intervals of 20 seconds, 1 minute, 10 minutes, and 3 hours were tested in this research. These values were based on literature, choosing a reasonable range in which decreasing strength is likely to be observed. Keeping the design procedure of an emergency shelter in mind, a very basic calculation with the printing speed was made, to check whether the printing rate is suitable for printing small emergency shelters. Printing one minute with a speed of 60 mm/s gives an element length of 3,60 meters. 10 minutes gives an element length of 36 meters. For now, it was sufficient to assume that 36 meters is enough to print the outer walls of at least two emergency shelters. The 3 hour time interval was tested together with the multiple curing conditions. According to literature, significant strength decrease could be expected at a time interval of 3 hours. The strength decrease is essential to clearly observe the influence of different curing conditions on the strength of the material.

Curing conditions for the 3 hour time interval samples
Although the curing of the printed filaments was mentioned in several papers, no clear results based on different curing conditions have been presented yet. Multiple recommendations to cure filaments were collected from literature, and expanded to one set of curing conditions to test. Four curing conditions looked promising, and were compared to samples that were not cured, exposed to the air, in an indoor environment. Curing conditions to be tested were: spraying a thin layer of mist on the printed filament, using time intervals of (1) 30 minutes and (2) one hour, and covered samples using (3) a plastic film and (4) a wet burlap. It was investigated whether these curing regimes had a positive effect on the bond strength, compressive strength, and tensile splitting strength.

3.2. Background of the mix design

During this research an existing mix design was used to test for mechanical properties. The mix design was a fixed parameter and optimizing its properties was not within the scope of this research. Therefore this paragraph only describes the general aspects of the mix design. The mix design was developed by Chen et al. (2019b) at the Delft University of Technology. Parts of his PhD-research formed the starting point for this MSc-research, and therefore the most important aspects regarding the mix-design and the fresh properties are highlighted in this section.

To make the concrete more sustainable, the ordinary Portland cement (OPC) type CEM I 52.5R was partly replaced by a limestone filler (LF) and two types of calcined clay. The two types of calcined clay used in the binder of the mix contain 50% and 80% Metakaolin (MK) respectively, and are therefore called low-grade calcined clay (LCC) and high-purity calcined clay (HPCC). MK is a reactive pozzolanic material, obtained as the reaction product from the calcination of kaolinite clay (Khatib et al., 2018). Also according to Khatib et al. (2018), kaolin mines can be found in South East Asia, America, Australia, and some places in Europe. The types of calcined clay used in this research were obtained from a kaolin mine in Burgress, in the United States. The composition of three mix designs are shown in Table 3.1.

Type	CEM I 52.5R	Calcined Clay		LF	Sand	Water	SP	VMA
		LCC	HPCC					
	(kg/m3)	(kg/m3)	(kg/m3)	(kg/m3)	(kg/m3)	(kg/m3)	(kg/m3)	(kg/m3)
MIX-L	331	331	0	166	1242	248	17	2
MIX-M	331	248	83	166	1242	248	17	2
MIX-H	331	166	165	166	1242	248	17	2

Table 3.1: Mix designs developed by Chen et al. (2019b) at the TU delft.

Two admixtures were added to the mix design. A superplasticizer (SP) was added to ensure the flowability, pumpability and extrudability of the mix during the printing process. Also a small amount of VMA was added to the mixture to ensure the shape stability of the material, once the filaments have been extruded.

The three mix-designs presented in Table 3.1, were all developed by Chen et al. (2019b). In all mix designs, 50% of the OPC was replaced by calcined clay. The only difference between the three mixtures is the ratio between the HPCC and LCC, varying from 100% LCC in MIX-L (Low content), 75% LCC + 25% HPCC in mix M (Medium content), and 50% LCC + 50% HPCC in mix H (High content). However, only mix-M was considered in this research. Multiple reasons for choosing mix-M are explained below.

3.2.1. Fresh properties

The reason to choose for MIX-M was based on the fresh properties of the three mix designs presented in the research of Chen et al. (2019b). Several tests were performed on the three mix designs, including a penetration resistance test, an extrusion test, a green strength test, an ultrasonic pulse velocity test, and a compressive strength test, at an age of 1, 7, and 28 days. For this research the first three tests showed to be of great importance for the printability of the material. The latter two tests were only analyzed to ensure that the mixes have comparable strength properties based on regularly applied concrete classes.

Extrusion test

The extrusion test was used to quantify the extrusion pressure by using different ages of the three mixtures. A ram-extruder was used to perform this test. Despite the fact that in this research a screw extrusion pump was used to print the material, the results of the ram extrusion test gave a good indication of the relative differences in pressure for the different mixtures, even if a screw extrusion pump was used. The three mixtures showed stable shapes, already after the first time interval of ten minutes. However, a more detailed analysis showed that MIX-H and MIX-M have a much higher increase of the extrusion pressure in time. These mixtures also showed a greater standard deviation after the initial setting time. A clear note made by Chen et al. (2019b), is that the extruding pressure for MIX-H

becomes dangerously high, potentially even damaging the test-setup. This is one of the reasons why MIX-H was not considered as mix design for this research. The risk of damaging the concrete pump, which has a screw-mechanism instead of ram-extrusion, was too high. Any damage would directly influence the time schedule of this relatively short research project.

Green strength

The initial stiffness of the printed material, also referred to as the green strength, is of great importance once a filament has been extruded. The printed filaments need to be able to bear the load of several upper filaments that will be extruded subsequently, after a prescribed time interval. The green strength of the material should be sufficient from the moment the material is extruded, and results of Chen et al. (2019b) were analyzed for all three mix-designs. Cylindrical samples, with a diameter of 33,5mm and a height of 67,5mm, were loaded in compression. The test was load-controlled with a load rate of 0,2 mm/s, and a maximum displacement of 20 mm. The results are shown in Figure 3.1.

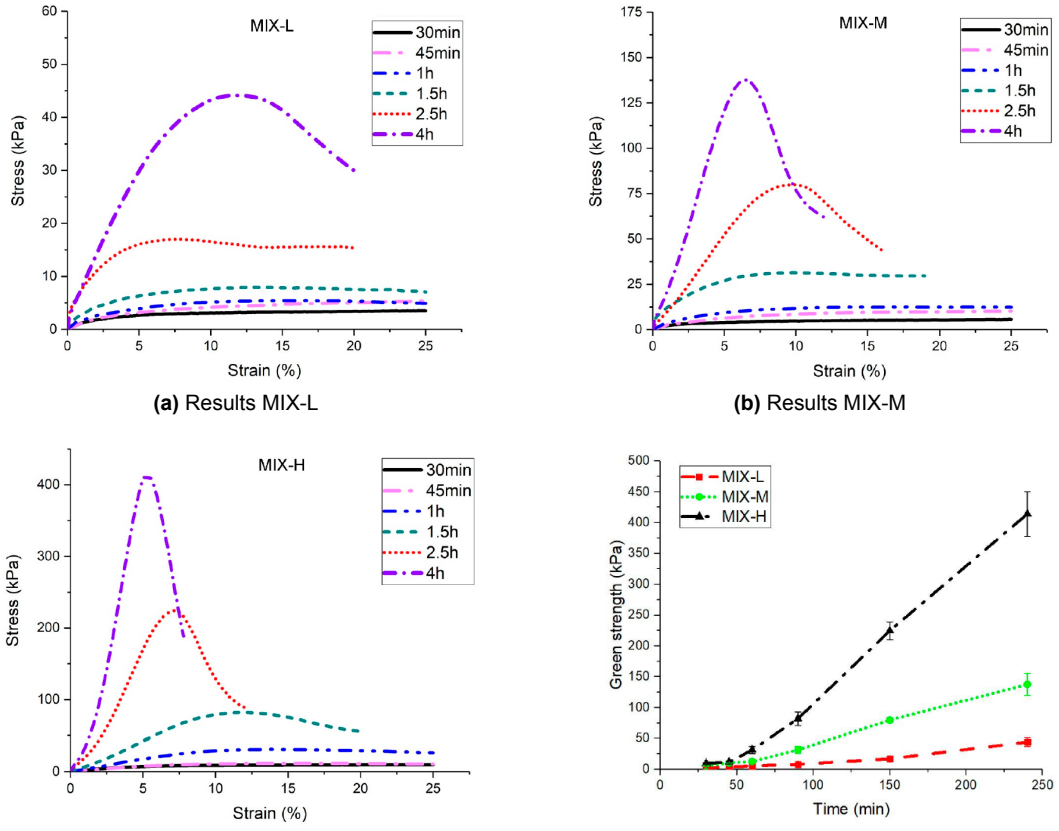

(a) Results MIX-L

(b) Results MIX-M

(c) Results MIX-H

(d) Green strength of mix L, M, and H, changing with time

Figure 3.1: Figure 3.1a, 3.1b, and 3.1c represent the stress-strain curves of mix L, M, and H respectively, tested after 30 minutes to 4 hours, obtained by a ram extrusion test. Figure 3.1d shows the green strength of the material up to four hours. Results are obtained from Chen et al. (2019b).

The green strength of MIX L, M, and H after one hour was 0 kPa, 10 kPa, and 40 kPa, respectively. After 4 hours the green strength was 40 kPa, 135 kPa, and 415 kPa for MIX L, M, and H, respectively. These values were analyzed parallel to the stiffness of the material, which can be obtained from the first three graphs of Figure 3.1. Mix-L showed no significant stiffness, even not after 4 hours, Mix-M and Mix-H showed increasing stiffness, already after 90 minutes. Since this is still the only available green strength data, also related to the buildability of the material, Mix-L was disregarded for the continuation of this research.

Compressive strength
As mentioned before, the compressive strength of the materials did not have a direct influence on the choice of mix-design for this research. However, the material must have sufficient strength to be able to use it as a structural material. For cast in-situ structures, a concrete strength class of C20/25 is most of the time sufficient for regular buildings / structural elements. The compressive strength results, that can be found in Chen et al. (2019b), showed no critical values. All mixtures had a strength of at least 25 MPa, at the age of 7 days. A note must be made that the results of Chen et al. (2019b) were based on cast samples. Eventually the material was printed and then the strength was different due to for example different compaction, and deviating interface properties.

Summary of the mixture characteristics
The mix design that was used in this research is MIX-M, based on three main arguments:

- The extruding pressure for MIX-H becomes dangerously high. Therefore MIX-H was not an option;
- MIX-M develops better green strength properties than MIX-L;
- MIX-M showed 35% and 21% higher compressive strength properties compared to MIX-L, at an age of 7 and 28 days respectively.

3.3. Research methodology

This research only focused on unreinforced concrete. For that reason the compressive strength test, bond strength test, and the tensile splitting test were the most relevant tests to perform. Flexural- and shear tests were of less importance, because in case flexural and shear stresses are governing, it is likely that reinforcement would be implemented. Based on standards like the Eurocode, NEN, and ASTM, as well as previous research articles, the background and the test-setup of each test are presented in the continuation of this section.

3.3.1. Tensile bond strength test

The tensile bond strength of the interface of a printed sample can be tested by means of a direct tensile bond strength test. For this test there was no regular norm available. However, the ASTM C1583, and several previous research articles, formed a good guideline to perform this test.

Test set-up

To perform the tensile bond strength test, a loading machine that can perform deformation-controlled tests was needed. Tay et al. (2019) used an Instron 5960 dual column machine, and for the research performed at the TU Delft by Reinhardt et al. (1986) an electro-hydraulic loading machine was used, which is in general the same setup as the Instron machine. The machine that was used for this research was the Instron 8872 universal loading machine, see figure 3.2a. The Instron is located in the Microlab of the Delft University of technology, CEG faculty. The machine has a capacity of 10 kN and can perform deformation controlled tests, where all data is being recorded on the connected desktop computer.

(a) Instron 8872 loading device

(b) Prepared sample for the bond strength test

(c) Test set-up, LVDT controlled

Figure 3.2: Reference, sample, and test set-up for the bond strength test.

Samples

To obtain accurate results, the sample size and sample preparation are very important. In the case of 3D printed elements, the cross-sectional dimensions of a filament are limited, because of the dimensions of the nozzle opening. As a consequence, size of the printed elements was limited. According to the research performed by Tay et al. (2019), a suitable dimension of the samples is 30x30x30 mm. To make sure that the obtained tensile bond strength is indeed obtained from the interface, notches were sawn around the perimeter of the sample. The notch is the line of crack initiation (Reinhardt et al., 1986). Sawing the notch was an extra complicating factor, because the notch had to be positioned exactly at the line of the interface. In this research samples of 20x20x30 mm were used, including a notch at the position of the interface. The side view of the samples is presented in Figure 3.2b.

Procedure

The tensile bond strength test was deformation controlled. This is a suitable method to obtain full load-deformation graphs of the test. The research performed earlier at the TU Delft, showed a deformation controlled test with a rate of 0,08 μm/s. A note must be made that much larger samples were used with a height of 250 mm. For the printed samples in this research the height was limited to 2 filaments. Due to the limited height, a smaller deformation rate was used of 0,01 μm/s. The samples were glued in the test set-up, to solid steel loading plates, as presented in Figure 3.2c. These steel plates were

used to prevent deformation of the test set-up as much as possible, and to obtain unbiased results. The deformation was controlled by two Linear Variable Differential Transformers (LVDTs). The LVDTs were connected to the steel bars on either side of the sample. Once the test had started, the force was measured against the known displacement. When the test was finished and the sample was broken at the position of the notch, the exact cross-sectional dimensions was measured. This information was necessary to calculate the tensile bond strength of the sample with Formula (3.1):

$$f_{tb} = \frac{F_{tb}}{A_{tb}} \tag{3.1}$$

where f_{tb} is the tensile bond strength in MPa, F_{tb} is the failure load of the sample in N, and A_{tb} is the cross sectional area of the failed section in mm^2.

3.3.2. Digital Image Correlation

To ensure that the crack initiated at the right location, at the notch, the test was monitored by a method called Digital Image Correlation (DIC). DIC is an optical tool to measure quantitatively the in-plane deformation of an object, by making close-up images of the sample during an experiment (Hild and Roux, 2006; Pan et al., 2009). A random DIC tool was used to analyze the series of images and calculate the displacement or strain of every image compared to the reference image. The only requirement was that the surface of interest had a dot pattern and the first picture should be taken in the undeformed situation in order to serve as the reference picture. Figure 3.3 shows the principle of the DIC analysis.

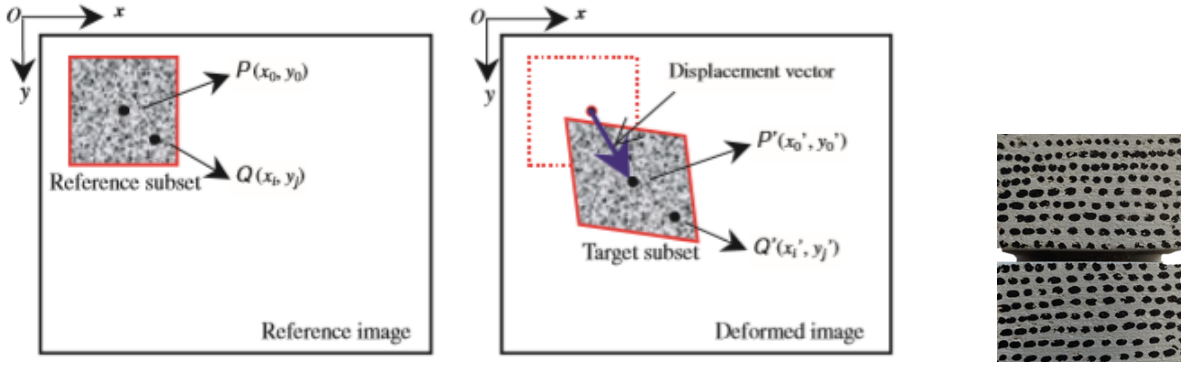

(a) DIC principle

(b) Sample for DIC analysis

Figure 3.3: 3.3a: principle of DIC analysis. The DIC-tool compares the image of the deformed sample to the reference image, and calculates the strain / deformation relative to the reference image (Pan et al., 2009). Figure 3.3b shows the prepared sample for DIC analysis in this research.

DIC is very useful to check the location of crack initiation during the experiment. Not only can the position of the crack initiation be determined, also the boundary conditions can be checked by analyzing the strain at the boundaries (Hild and Roux, 2006). In this way the complete test was monitored and served as evidence that the test was performed correctly. The equipment needed to perform this test was a high resolution camera with the ability to set predefined time intervals. The images were taken during the experiment, and were loaded into the DIC software. An available DIC-tool is the Ncorr. Ncorr is an open-source platform tool, built as a Mathlab extension (Ab Ghani et al., 2016). Also according to Ab Ghani et al. (2016) the results of Ncorr are of high accuracy compared to other expensive tools, such as a strain gauge. This software was downloaded for free. Figure 3.4 shows an example of the calculated strain by Ncorr, in three steps.

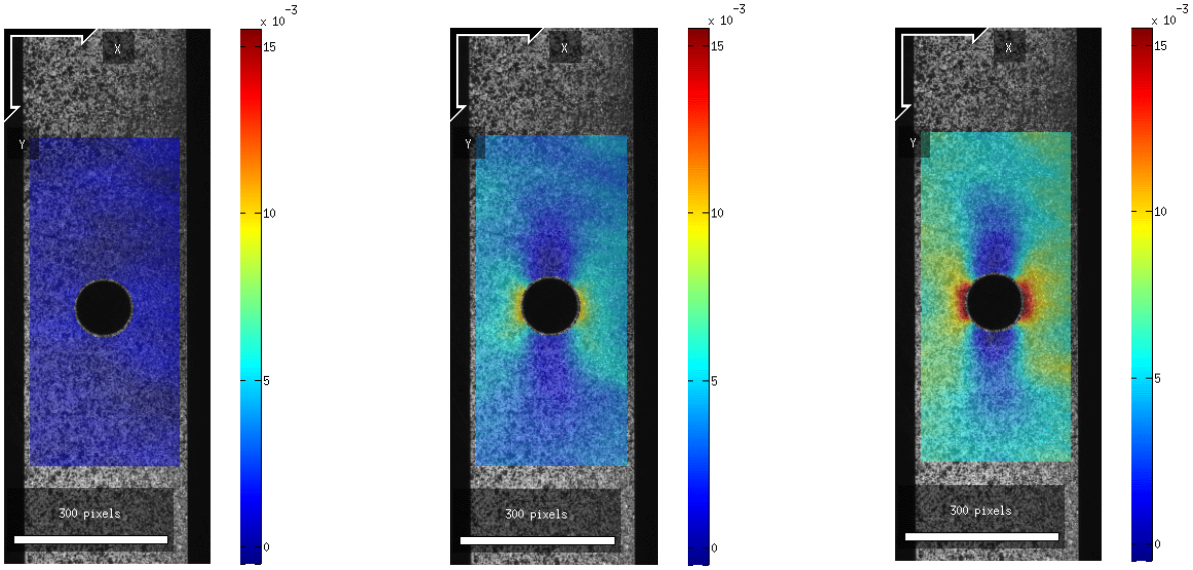

(a) Reference picture **(b)** First analysis **(c)** Second analysis

Figure 3.4: Example of a DIC strain analysis, obtained from (NcorrV1.2).

3.3.3. Splitting strength test

The second method used to test the tensile strength of the samples material, was the tensile splitting strength test. A tensile splitting strength test is a test where a line load is exerted on a sample and where the material fails by means of splitting. The failure is perpendicular to the direction of the line load. This test was important for the printed samples, because objects can be loaded in printing (longitudinal) direction, where the interfaces are parallel to the load. The tensile splitting test was conducted according to the NEN-EN 12390-1. This NEN-norm was originally written to test the splitting strength of cylindrical samples, but an appendix has been added where guidelines for cubic specimens are also presented.

Samples

According to the NEN-EN12390-6, the splitting test should be performed on samples with a dimension of 150x150x150mm. Since the printed objects had a limited dimension, this was an extra complication, because the samples would then have had interfaces in two directions, due to the small nozzle that was used. To test the splitting strength of single filaments printed on top of each other, Wolfs et al. (2019) used samples that were scaled down to a dimension of 40x40x40mm. The loading rate was calculated according the NEN-EN12390-6, which is 125.7 N/s for the mentioned dimensions.

Test set-up

From figure 3.5a, it can be seen that the sample was loaded in a loading jig where the line load was applied by a steel loading piece (3). In between the loading piece and the sample was a packing strip (2) to redistribute the load and make sure that the stresses were evenly distributed over the surface of the sample. In the ideal situation, the packing strip is made of hardboard. According to the NEN-norm the packing strip should have a width of 15 mm and a thickness of 4mm. These dimensions are however suitable for the larger samples of 150x150x150mm. For this reason the the dimensions of the packing strip were also scaled down to a cross sectional dimension of 5x2mm. This packing strip was positioned exactly on the interface between two filaments in order to get the desired interface strength properties, although miss-positioning of a few millimeters should not lead to different results, according to Wolfs et al. (2019). Figure 3.5c shows the sample including the loading strips that are used in this research. The test set-up is shown in figure 3.5d.

When the failure load was known, the tensile splitting strength of the sample was calculated using Formula (3.2):

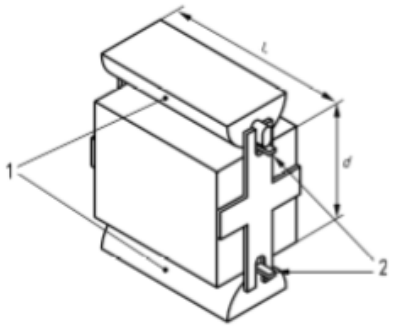

(a) 3D-overview of the test setup (NEN-EN12390-6)

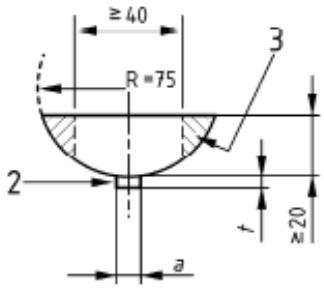

(b) Side view of the test setup (NEN-EN12390-6)

(c) Sample for the tensile splitting test

(d) Test set-up

Figure 3.5: Setup for the tensile splitting test according to the NEN-EN 12390-6.

$$f_{ct} = \frac{2 * F}{\pi * L * d} \tag{3.2}$$

where f_{ct} is the tensile splitting strength in MPa, F the failure load in N, L the length of the line load in mm, and d the cross-sectional height in mm.

3.3.4. Compressive strength test

The compressive strength of the material was tested in three different directions, because of the anisotropic material properties. For standard concrete, the NEN-EN 12390-3 can be used, where the samples must have dimensions of 150x150x150mm or 100x100x100mm. Just like the tensile splitting test, this was an extra complicating factor for 3DCP, since only single filaments of concrete were extruded on top of each other. Wolfs et al. (2019) performed also compressive strength tests on printed concrete. Their solution was again to downscale the dimensions of the samples to 40x40x40mm. Since the mix design in this research had a maximum aggregate size of 2mm, the mix-design was considered as a mortar and then the NEN-EN 196-1 complied as well.

Test set-up

The NEN-EN 196-1 requires samples of 40x40x40mm. These samples were tested using a compressive strength machine, where the sample were placed in a loading jig, as shown in Figure 3.6a. The applied loading rate, according to the NEN-EN 196-1, was 2400 N/s, and when the applied load during the test dropped 20% or more, the test was terminated. The compressive strength of the sample was

calculated according to Formula (3.3):

$$f_{cc} = \frac{F}{A} \tag{3.3}$$

where f_{cc} is the compressive strength in MPa, F the failure load in N, and A the cross-sectional area of the sample in mm.

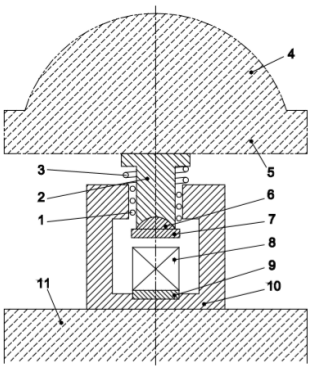

(a) Setup of the loading jig according to the NEN-EN 196-1.

(b) Sample for compressive strength test.

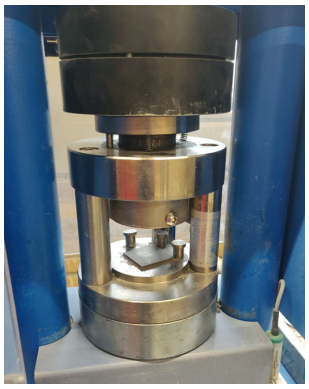

(c) Loading jig at the TU Delft.

Figure 3.6: Setup of the compressive strength test, presenting the loading jig, sample, and compression machine.

3.3.5. CT scanning

A measure to find evidence for differences in mechanical properties, is CT scanning of cylindrical samples. CT scanning stands for Computed Tomography, and is a non-destructive technique to analyze internal micro structures of materials (Vicente et al., 2017). The CT scanner uses an X-ray emitter and an X-ray detector. The emitter sends X-rays at a certain intensity through a sample and the X-rays are then detected by the detector. 2D cross-sectional images of the sample are then obtained. Gathering all the data, and using an algorithm to combine 2D images, will result in a three-dimensional data set (binary image) of the sample (Laustsen et al., 2010). This technique can be used for multiple purposes, but for this research, only the expected air voids in the interfaces and filaments were of importance. Figure 3.7 shows binary images of a concrete sample.

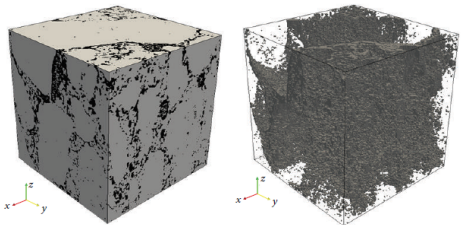

Figure 3.7: Example of a full binary image of a concrete sample (left) and the void distribution within the sample (right) (Chung et al., 2015).

.

Procedure

According to literature, it is likely that air voids get entrapped in the interfaces. To test this hypothesis, cylinders with a diameter of 24mm (2 filaments), and a height of 25mm were drilled from the printed beams, and scanned using a Phoenix Nanotom CT scanner. The sample included 2 filaments (of

12mm) and the air void distribution was of importance. The result from CT scanning was a set of horizontal slices with a resolution of 13.3x13.3x13.3 μm/voxel, and thus also a thickness of 13.3 μm. The next step was to reconstruct the slices into the three-dimensional data set as described above. To do so, the software of Poenix Datos was used.

3.3.6. Size effects

As described in the previous section, in some of the tests the dimensions of the samples did not comply with the standard dimensions for concrete samples. The sizes were scaled down compared to the standard. This was possible because the maximum aggregate size was 2mm in the printed samples. For this reason the results can deviate from 'standard results' that would have been obtained if standard dimensions were used. According to van Vliet and van Mier (2000), size effects are inevitable, and there is no unambiguous explanation for this phenomena. The authors also mentioned many possible reasons that could lead to size effects, like micro-mechanical mechanisms and the crack length relative to the structural size. By testing multiple samples in uni-axial tension, each with different scale factors, they concluded with two phenomena. The first conclusion was that for small scale samples, micro-structural effects dominate. These effects are mainly dependant on the aggregate size distribution in the critical cross section. The second conclusion was, also supported by Yi et al. (2006), that when samples get larger, the micro-structural effects average out, and the samples have a lower strength.

To be able to design structures based on the data of small samples, as was done in this research, conversion factors for strength were used. Below, a selection of tables and graphs shows conversion factors to take the size effect of samples into account. Del Viso et al. (2007) did research onto the effect of specimen sizes and shape on the compressive strength of concrete. Their findings were applicable in this research. Figure 3.8 shows the strength of samples, based on different sample dimensions.

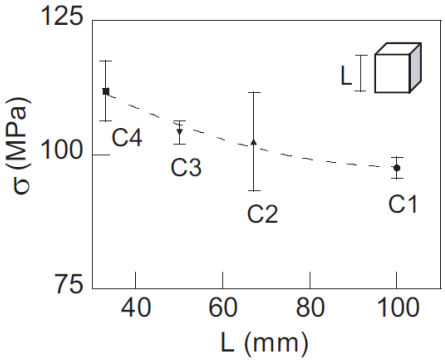

Figure 3.8: Size effects for (cast) cubes loaded in compression, by Del Viso et al. (2007).

.

Kadleček and Modrỳ (2002) did a similar research, but aimed to find size effect correlation factors for the tensile splitting strength of samples. By testing square and cylindrical samples with dimensions between 40mm x 40mm and 200mm x 200mm, the relation of the size effects was analyzed using statistical models. The results for cubes are presented in Figure 3.9. A conclusion of Kadleček and Modrỳ (2002) was that shapes of samples do not have a significant influence on the size effects. Therefore, it was possible to derive one conversion formula to calculate the size effect, see Equation (3.4):

$$R_{t,tr} = 200A^{-0.128} \tag{3.4}$$

where $R_{t,tr}$ describes the size effect in % relative to a sample with dimensions 150mm x 150mm. It was mentioned that the width of the bearing strips should be 10% of the width of the sample. The bearing strips in this research had a width of 4,5mm, and therefore the presented results were useful.

Table 1 – Cubes - factors $\kappa_{t,tr}$ for conversion into strength of standard size specimens (1)			
Edge a (mm)	A (cm^2)	$R_{t,tr}$ (%)	Values $\kappa_{t,tr,cu}$
40	16	140	0,71
70	49	122	0.82
100	100	111	0.90
150	225	100	1.00
200	400	93	1.07

Figure 3.9: Size effects for (cast) cubes and cylinders, failing in tensile splitting. By Kadleček and Modrỳ (2002).

To the best knowledge of the author, no experiments were conducted to investigate the size effects of very small samples under uni-axial tension. One article was found where samples with dimensions between 12,5mm x 12,5mm and 62,5mm x 62,5mm were investigated for size effects by means of a finite element analysis. In this article, Wang et al. (2015) preformed Monte Carlo simulations on samples with a random aggregate distribution. The maximum aggregate size was not explicitly mentioned, but the research of Kadleček and Modrỳ (2002) showed that the relative difference in the size effect between samples with aggregate sizes of 4mm to 32mm, was less than 10% in tensile splitting. For this reason, the dependence on the aggregate size was neglected in this research, and the results from Wang et al. (2015) were used to scale the results obtained in this research. Figure 3.10 shows both a graphical presentation of the results and the obtained data by Wang et al. (2015). The relative size effects of samples in uni-axial tension were calculated according to this information.

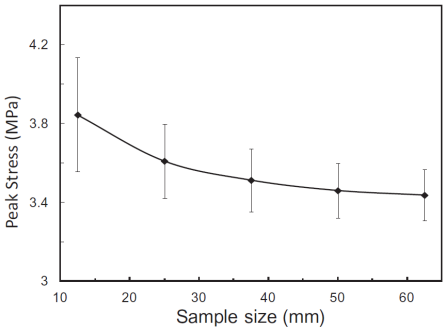

(a) Curve for size effects in uni-axial tension of cast samples.

Size L (mm)	12.5	25	37.5	50	62.5
Mean peak stress (MPa)	3.845	3.611	3.514	3.461	3.438
SD (MPa)	0.288	0.189	0.159	0.139	0.129
CoV (%)	7.490	5.227	4.528	4.021	3.765

(b) Average data

Figure 3.10: Size effects for (cast) samples loaded in uni-axial tension. By Kadleček and Modrỳ (2002).

.

3.4. The printing process

This section describes the necessary printing equipment, the printing procedure and observations made during the printing sessions. Any abnormality could have an influence on the mechanical performance of the samples.

3.4.1. Equipment

Three main elements were needed during the concrete printing process. Figure 3.11 shows the main elements needed to print concrete. The 3D concrete printer available at the TU Delft consists of a gantry system, with inner dimensions of 1,1m x 0,72m x 0,29m. Attached to the gantry is a linear-movement mechanism capable of moving in the X, Y, and Z direction. The hose of the concrete pump can be attached to the vertical element of the moving mechanism. The printer is a Computer Numerical Controlled machine (CNC), operated by G-code. G-code is a coded set of numbers for movement along axes (Shin et al., 2007). This means that the printing path that should be followed by the machine, is programmed in G-code. The second element, a concrete pump, was necessary for extrusion of the concrete through the nozzle. The pump was separately operated from the 3D printer. The pump exists of a container where fresh concrete was poured in, a pumping mechanism, and a hose to which the nozzle was connected. The concrete pump used in this research is shown in Figure 3.11b. The pump can handle a maximum aggregate size of 3mm, has a maximum pressure of 20 bar, and a capacity of pumping 20 liters of concrete per minute. This pump uses a screw mechanism for extrusion of the concrete, as shown in Figure 3.11c. The speed of the rotating screw mechanism was set manually, to obtain optimal extrusion speed and pressure, in relation with the printing speed.

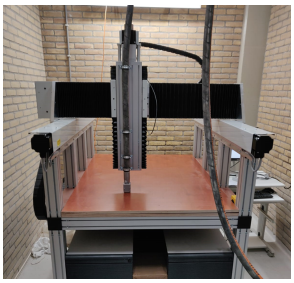

(a) CNC printer at the TU Delft

(b) Concrete pump

(c) Screw extrusion mechanism

Figure 3.11: 3D printing equipment at the TU Delft.

The last element, the nozzle, comes in multiple materials and shapes. For this research, a rectangular nozzle opening was used, as described in section 3.1. This nozzle was developed at the TU Delft and a first prototype was printed using an Ultimaker printer for plastics. Figure 3.12 shows images of the nozzle, including the connection to the hose and horizontal extrusion of concrete.

3.4.2. The printed elements

To print concrete elements, a strict procedure was followed. First the concrete pump and the 3D printer were connected via the hose. Second, the nozzle was connected to the hose. Once the computer system was ready, the machine was calibrated, i.e. nozzle standoff distance with respect to the printing table was set manually. Once the printer was ready, the concrete mix was mixed according to the applicable mixing procedure. As soon as the concrete mix was poured in the concrete pump, printing could start by starting both the pump and the 3D printer. For this research, the only printed elements that were needed were straight beams from which the samples were sawn. Based on the maximum dimensions of the printer, beams of 800mm were printed. The beams consisted of four filaments, and therefore had maximum total height of 48mm, not taking into account any slump. The width of the beams was 40mm. From these beams it was possible to saw the samples as described in section 3.3. The parameters that were tested, and most likely had an influence on the interface strength, were introduced in the second interface, i.e. between the second and the third filament. The first and third interface had default properties. The default interfaces had a time interval of one minute, and a nozzle standoff distance of < 1mm. Figure 3.13 shows the printed beams, cross section of a printed beam, and the position of the cylindrical samples for CT Scanning. Once the beams were printed, they were

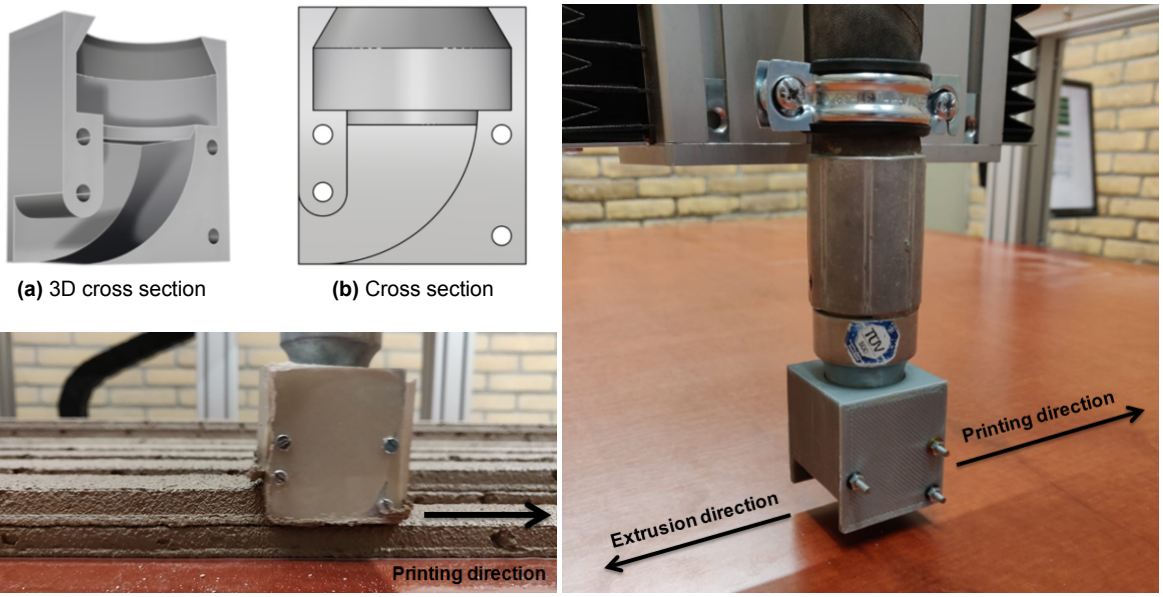

(a) 3D cross section **(b)** Cross section

(c) Horizontal extrusion **(d)** Nozzle connected to the hose

Figure 3.12: Impression of the nozzle.

immediately covered with a plastic film for the next 18-24 hours. After that time the beams were moved to a curing room with optimal temperature and relative humidity.

(a) Printed beams with 4 filaments

(b) Cross section of a printed beam (4 filaments)

(c) Position of the cylindrical samples (top view)

Figure 3.13: An impression of the beams printed for this research.

On the next page, the curing regimes of the printed samples with a time interval of 3 hours are presented.

(a) Samples without curing on the left, samples covered with a wet burlap in the middle, and samples covered with a plastic film on the right.

(b) Samples sprayed with water, every 30 minutes or 1 hour.

Figure 3.14: Curing regimes.

3.4.3. Observations during the printing process

During the printing process, multiple abnormalities were observed. This section shows all deviations that were observed during the printing process, and that possibly had an influence on the mechanical performance of the samples. See chapter 6 for a detailed analysis.

Scraping and squeezing of the nozzle

During printing, it was noticed that in some cases the nozzle standoff distance was programmed too low with respect to the lower filament. The nozzle was squeezing, disrupting the interface that was still to be printed on. Furthermore, due to the rectangular shape of the nozzle, movement of the nozzle also introduced scraping of the surface. Where possible, the beams were recollected, and used to print new beams, with an adjusted G-code. Only for the samples with 3H time interval, this was not an option. Samples covered with a wet burlap as curing condition, showed scraping between the third and fourth layer. These beams were eventually tested in compression, and therefore the results might be influenced. Figure 3.15a shows how the nozzle scrapes into the previous filament.

Slump, causing increasing nozzle standoff distance
The beams printed with 20 seconds and 1 minute time interval showed some slump. The nozzle standoff distance was only controlled by the G-code, and not by extra sensors that adjusted the nozzle standoff distance depending on the height of the previous filaments. It was noticed that the the nozzle standoff distance for the third and fourth layer showed a slight increase, but it was however not possible to exactly measure the increase, as the nozzle was still moving at a speed of 60 mm/sec. Depending on the results, it had to be determined if the unexpected increased nozzle standoff distance had an influence on the mechanical properties.

Drying shrinkage of the filaments in longitudinal direction
When uncovered beams were printed and cured in the air, shrinkage was present after 15-20 minutes. See Figure 3.15b. For the three hour time interval between the second and the third layer, possible unequal shrinkage introduced horizontal friction in the interface, influencing the mechanical properties of the interface.

Excess of material at end of printed beams
A limitation of the printing equipment was the pump had to be operated separately from the CNC printer. If the pump was stopped after printing one filament, the pressure decreased slowly over the full length of the hose. Also the extrusion did not stop immediately. For this reason, the pump was not stopped in between printing two filaments. The excess material was collected by hand, until the next filament was about to be printed. It was however unavoidable that at the beginning and at the end of the beams, excess material introduced deviating pressures on printed filaments. Also larger material quantities were present (see Figure 3.15c). The edges (10cm-15cm) were not used to prepare samples.

(a) Scraping and squeezing of the nozzle

(b) Shrinkage of the filaments

(c) Excess of material at beam end - side view

(d) Excess of material at beam end - top view

Figure 3.15: Observations made during the printing process.

Material accumulation inside the nozzle
The last observation was made after 5 to 10 minutes of material extrusion through the nozzle. Small amounts of concrete gradually accumulated on the inside edges of the nozzle. This problem led to small air voids present at the edges of the filaments. Where possible, the inner walls of the nozzle were provided with a lubricant.

3.5. Experimental results

The results of the conducted experiments are presented in this section. Each result is provided with a description that serves as a clarification of the results. Any deviation or uncertainty that was observed during the experiments, is mentioned. Later on, in chapter 6: Discussion, a detailed analysis of the obtained results and observations is presented.

3.5.1. Tensile bond strength

The tensile bond strength test was performed for all variables, including the reference material. Stress-displacement graphs were obtained from at least 3 samples per variable and the correctness of the tests was controlled by Digital Image Correlation.

Reference material

Results of the tensile bond strength test of cast samples are presented in Figure 3.16. For this parameter, 5 samples were successfully tested, and all samples showed similar behaviour. The cast samples had an average strength of 2.96 MPa and a standard deviation (SD) of 0.15 MPa, corresponding with a relative standard deviation (RSD) of 5.1%.

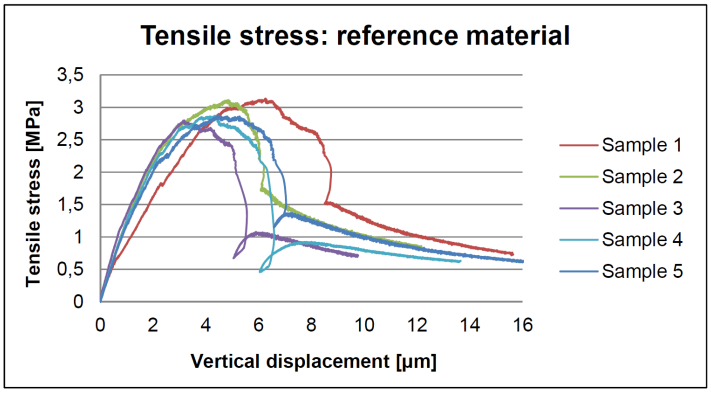

Figure 3.16: Stress-displacement graphs obtained from the direct tensile bond strength test of cast samples.

Time intervals

The results of the samples tested with different time intervals are presented in Figure 3.17. Figure 3.17a shows the average strength for three different time intervals, based on at least three samples per time interval. Standard deviations are shown in each bar. The relative standard deviation of the 20 seconds and 1 minute time interval samples were 5.3% and 3.7%, respectively. The scatter for the samples tested with 10 minutes time interval increased significantly, resulting in a RSD of 13.3%. Also the strength of the 10 minute time interval samples decreased approximately 20% relative to the samples with time interval 20 second and 1 minute. The individual results of each sample are shown in Figure 3.17. All samples showed similar behaviour, but Figure 3.17d shows that the post-cracking behaviour of the samples with 10 minutes time interval is a much shorter curve compared to the 20 seconds and 1 minute time interval samples.

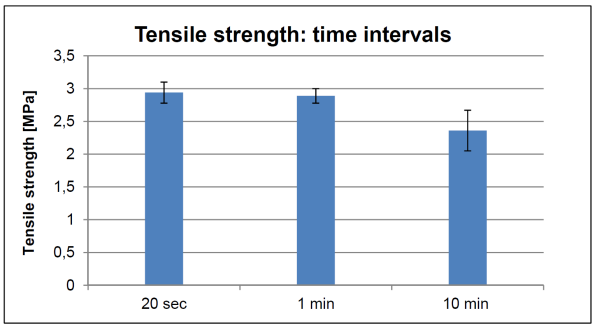

(a) Average tensile Tensile bond strength, including standard deviations.

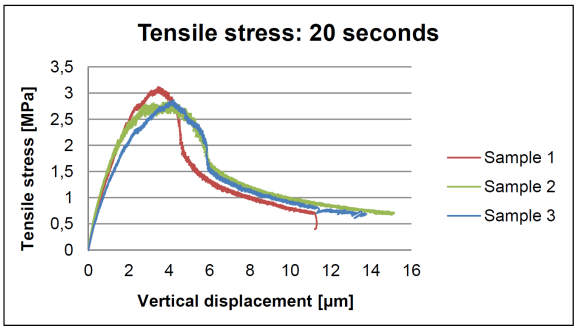

(b) Tensile stress for 20 seconds time interval samples.

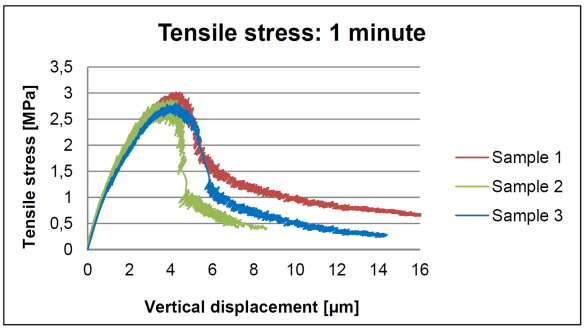

(c) Tensile stress for 1 minute time interval samples.

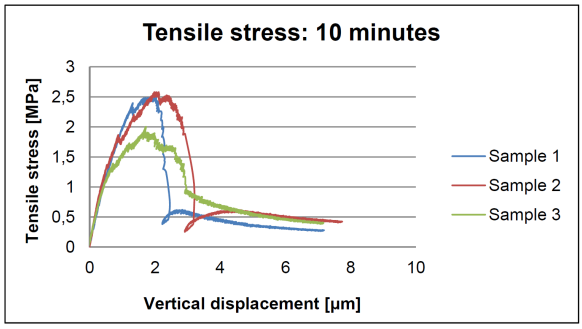

(d) Tensile stress for 10 minutes time interval samples.

Figure 3.17: Results obtained during the direct tensile bond strength test for samples printed with different time intervals. Sample size: 20mm x 20mm x 30mm with notch. Age: 7 days.

Nozzle standoff distance

Figure 3.18a shows the tensile strength of the materials with a nozzle standoff distance of < 1mm, 5mm, and 10mm. All standard deviations were below 10%, but remarkable is that no significant trend that can be observed from the three nozzle standoff distance variations, as the results from the 5mm standoff samples were significantly lower than the samples tested with < 1mm and 10mm nozzle standoff distance. However, a remark must be made about the samples that have been used during the experiment. The samples with a nozzle standoff distance of < 1mm and 10mm were printed on the same day, with an indoor temperature of 20°C. The samples with a nozzle standoff distance of 5mm were printed during a second printing session, when the indoor temperature was around 35°C. To the best knowledge of the author, both printing procedures were the same, except for the different room temperatures during the printing sessions.

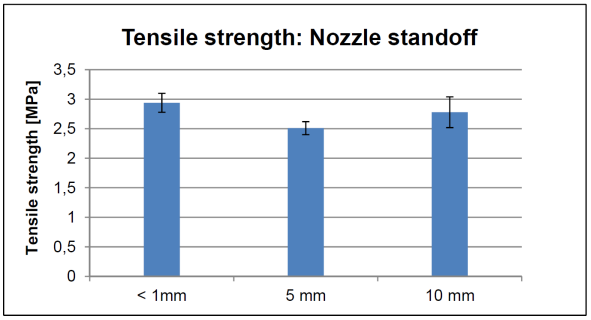

(a) Average tensile Tensile bond strength, including standard deviations.

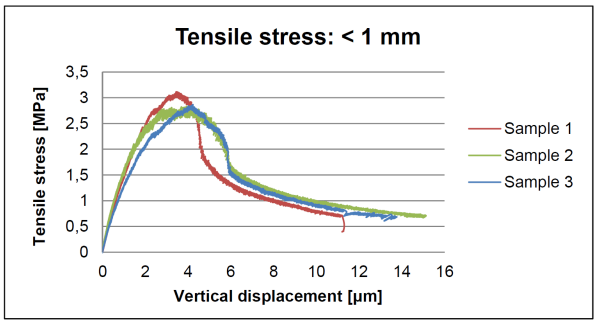

(b) Tensile bond stress for < 1mm nozzle standoff distance samples.

Figure 3.18: Results obtained during the direct tensile bond strength test for samples printed with different nozzle standoff distance. Sample size: 20mm x 20mm x 30mm with notch. Age: 7 days.

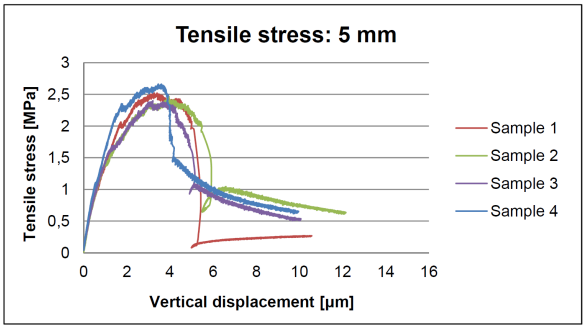

(c) Tensile bond stress for 5mm nozzle standoff distance.

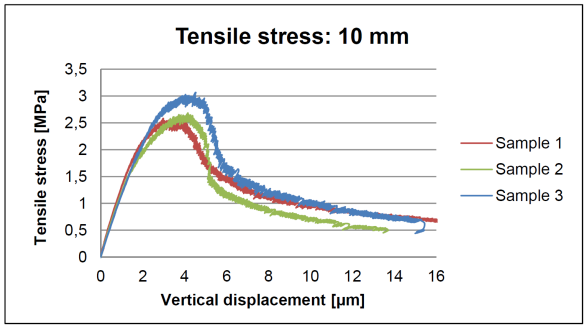

(d) Tensile bond stress for 10mm nozzle standoff distance.

Figure 3.18: (continued)

Also the post cracking curve was different for the 5mm standoff samples. This can be observed if Figure 3.18c is compared to Figure 3.18b and 3.18d. The failure of the 5mm standoff samples took place more brittle, compared to the other parameters.

Curing conditions

Finally, the tensile strength of samples with different curing conditions are presented. The first try-out of testing samples with different curing conditions (and a 3 hour time interval), showed that many samples broke during preparation of the test setup, at the position of the interface. This indicated that the strength of the samples was much weaker than the previously tested samples. For this reason the decision was made to prepare samples with dimension of 30mm x 30mm x 30mm. A larger force was needed to break the samples at the interface and it was possible to test the samples according to the same procedure used for the 20mm x 20mm x 30mm samples. Figure 3.19a shows the average results of the samples with adjusted dimensions. Large differences in strength can be observed, and also the standard deviations were between 8.8% and 26% for the samples covered with a plastic film and mist spray each 30 minutes, respectively. Based on the average results, the samples covered with a wet burlap had the highest strength, namely 1.39 MPa. If however the peak values of the standard deviations were compared, then the samples covered with a mist spray, each 30 minutes, showed also good potential. Also can be seen that samples with any type of curing, showed better results than the samples that were cured in the air for 3 hours.

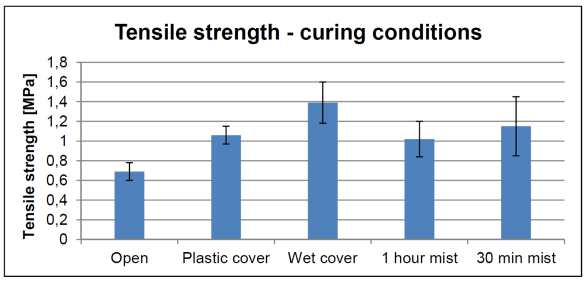

(a) Average tensile Tensile bond strength, including standard deviations.

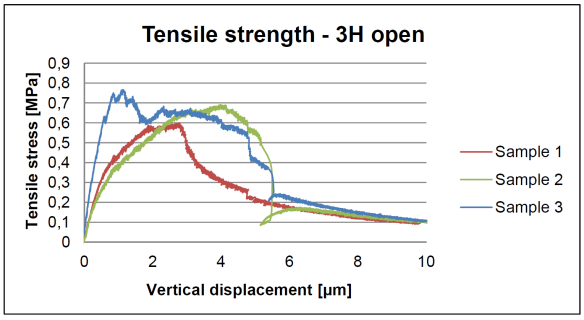

(b) Tensile bond stress for samples without curing conditions.

Figure 3.19: Stress-displacement graphs obtained from the direct tensile bond strength test. Parameters that are tested are related to different curing conditions.

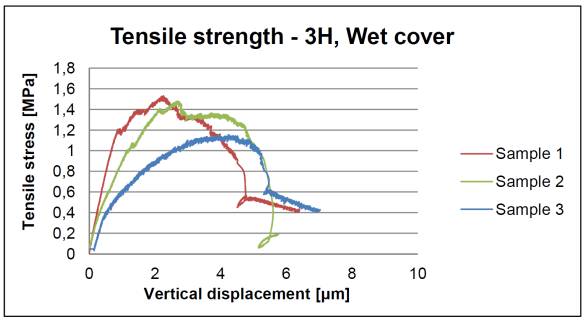

(c) Tensile bond stress for samples covered with a wet burlap.

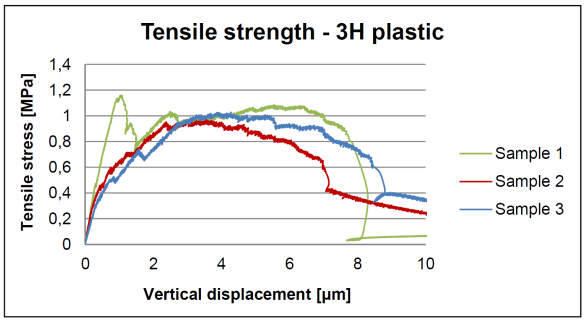

(d) Tensile bond stress for samples covered with a plastic film.

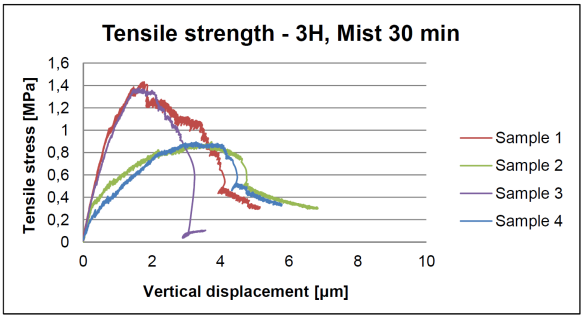

(e) Tensile bond stress for samples cured with a mist layer every 30 minutes.

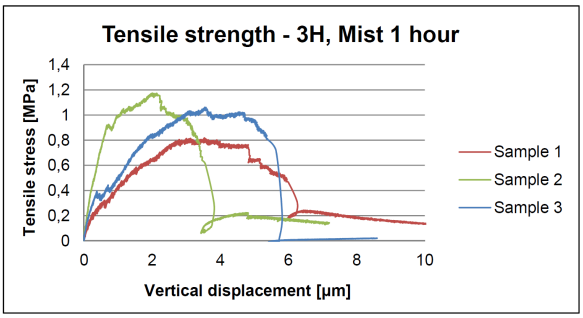

(f) Tensile bond stress for samples cured with a mist layer every hour.

Figure 3.19: (continued)

However, by looking at the individual graphs that were obtained during the tests, many differences in failure behaviour can be observed. Every variable showed two types of graphs. The first type can be distinguished by a fast increase in stress rate, up to the failure load. A short post cracking curve follows, and finally the curve fails fully at approximately a vertical displacement of 6 to 8 μm. The second type of graphs are graphs that show a cracking behaviour right from the start of the experiment. The load keeps increasing gradually up to the peak load, and the post cracking curve then decreases again gradually until complete failure occurred. The scatter in the results is thus also visible in the over-all failure behaviour of the samples. Due to the differences in behaviour, question marks could be placed by the validity of these results, and therefore a profound analysis is made, during the discussion.

Digital Image Correlation

The analysis of the digital image correlation was only made to exclude any mistakes during the experiments. The cast samples, samples with different time intervals, and samples with different nozzle standoff distance showed expected strain behaviour. Figure 3.20 shows the results of a random sample tested with a time interval of 1 minute. The boundary conditions are correct, because the boundaries show no deformation. This means that the glue did not fail during the experiment, and that the sample was not pulled out of the glue. Therefore it could be assumed that the sample remained fully clamped during loading. Looking at the four images in time, the point of crack initiation was indeed at the position of the notch, and the sample eventually failed exactly at the interface. This was also observed when the sample was disconnected from the Instron and the exact dimensions of the failed cross section were measured.

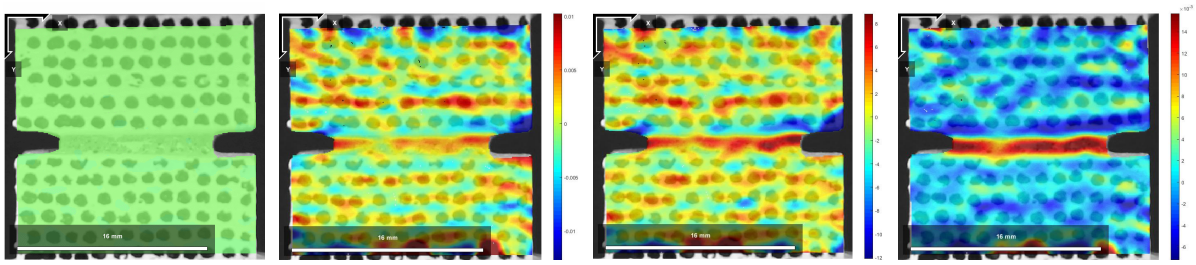

(a) Image 1 **(b)** Image 2 **(c)** Image 3 **(d)** Image 4

Figure 3.20: DIC results of a sample tested with a time interval of 1 minute. These results show no deviations in the boundary conditions and the location of crack initiation.

Samples that showed cracking behaviour right from the start of the experiment, i.e. gradually increasing stress, also showed deviating strain behaviour at the position of crack initiation. As can be seen in Figure 3.21, the position of the crack starts clearly at the right side side of the sample, indicating rotation of the sample during the tensile test. These results were obtained from one of the samples with 10 minutes time interval. Most of the samples with different curing conditions also showed this behaviour. However, the boundary conditions looked good for all samples, so the test set-up was as expected for all experiments.

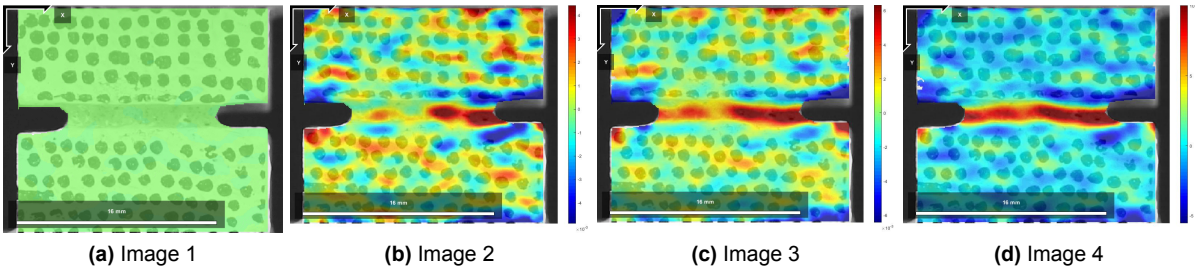

(a) Image 1 **(b)** Image 2 **(c)** Image 3 **(d)** Image 4

Figure 3.21: DIC results of a samples tested with a time interval of 10 minutes. These results show no deviations in the boundary conditions, but the crack initiation is introduced on the right side, indicating rotation of the sample.

Complementary to the results of DIC for the samples with 3 hour time interval, the displacement rate of LVDT 1 and LVDT 2 was different for the samples that showed immediate cracking. This was an indication that the sample rotated during the loading process.

3.5.2. Anisotropic compressive strength

Figure 3.22 shows all results for the conducted compressive strength tests at 7 days. Compressive strength tests were performed for the samples with different time intervals and different curing conditions, according to the methods described in section 3.3. Based on these results, no large differences were expected compared to the compressive strength of samples with different nozzle standoff distance. Also taking into account the limited time available, the decision was made not to test the compressive strength of samples with different nozzle standoff distance, and samples with 10 minutes time interval.

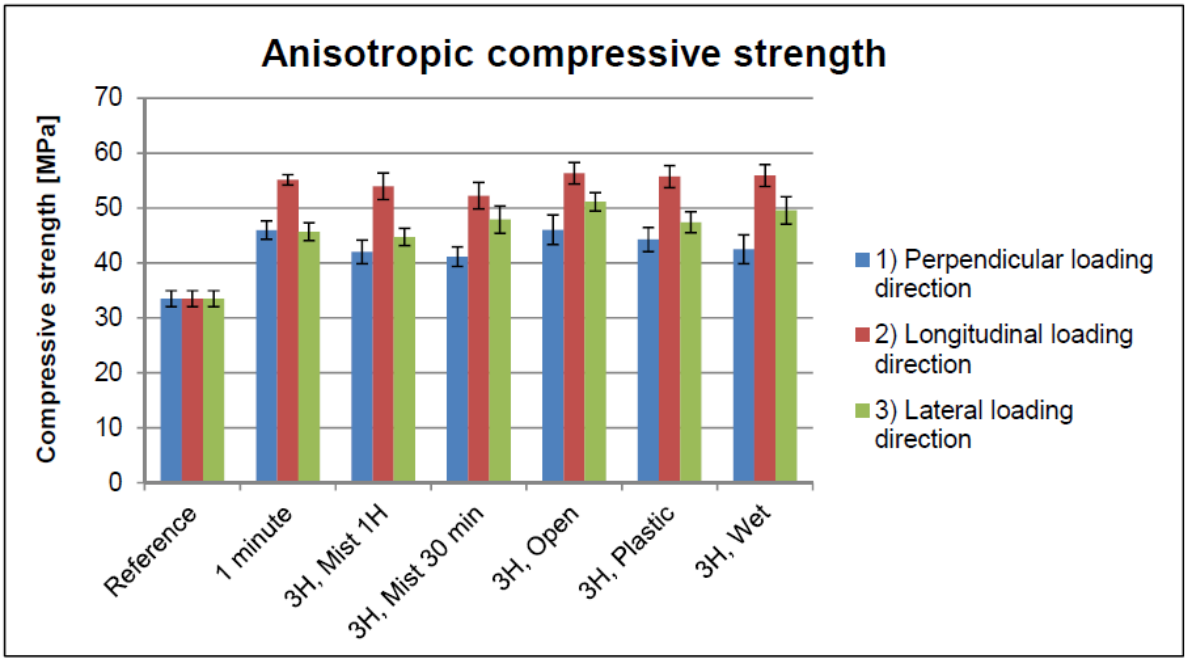

Figure 3.22: Anisotropic compressive strength of 3D printed elements, each with different parameters as shown below each chart. Size of the specimens: 40x40x40mm cubes, age: 7 days.

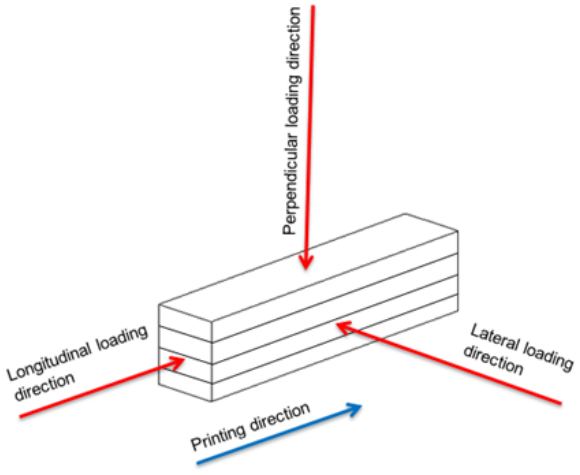

The three loading directions are shown below the figure. The loading directions correspond to the three bar charts in Figure 3.22. The compressive strength of the reference material was also added to the chart, to be able to compare the compressive strength of the printed material to the material that was cast. Standard deviations were added in the figure.

The data shown in Figure 3.22 are average values calculated from at least 5 samples. To show the scatter in the results, the Relative Standard Deviations (RSD) are shown for every bar. Calculations learned that the relative standard deviations were not larger than 6,1%, and the strength values of the samples were corrected by the exact cross-sectional dimensions of each sample.

Observations during the tests

During the tests, several observations were made that could possibly influence the outcome of the test. Before the test was started, it turned out that some samples were not perfect cubes. The bottom and top loading surfaces showed an angle relative to each other. The loading jig that was used to load the samples, contained a rotatable plate that made it possible to load the samples in a correct way. The full loading surfaces were in touch with the loading plates of the loading jig. The standard deviation in the results of samples that showed this defect, were not higher compared to samples that were perfect cubes.

Figure 3.23: Impression of the failure mechanism that was observed the most. The filaments are positioned horizontally, but not visible in this figure.

After each test, the failed samples were analyzed, and the failure mechanism was noticed. For direction 1, which is the perpendicular loading direction, all samples failed in the same manner. A clear cone shape was observed, as can be seen in Figure 3.23. It is worth mentioning that for all samples, the individual filaments were still connected, i.e. the interface was not broken. Direction 2, the longitudinal loading direction parallel to the interfaces, showed the same failure mechanism as samples loaded in direction 1. Samples loaded in direction 3, the lateral loading direction parallel to the interfaces, showed two different failure mechanisms. Samples that had a visibly flat loading surface, failed in the same way as the samples loaded in direction 1. Samples that did not have perfectly flat loading surfaces, showed a 'two-step' failure mechanism. First is was observed that the interface failed: singe filaments sheared along each other and this broke the interfaces. As the loading continued, a second failure mechanism was observed where a cone-like shape was formed as the sample collapsed. The possible influence of this failure mechanism is discussed later.

3.5.3. Tensile splitting strength

The results of the tensile splitting strength test are shown in Figure 3.24. The test was performed according to the description in section 3.3. Two directions were tested to be able to compare the splitting strength perpendicular to the interface and the splitting strength parallel to the interface. The two loading directions are shown next to the figure.

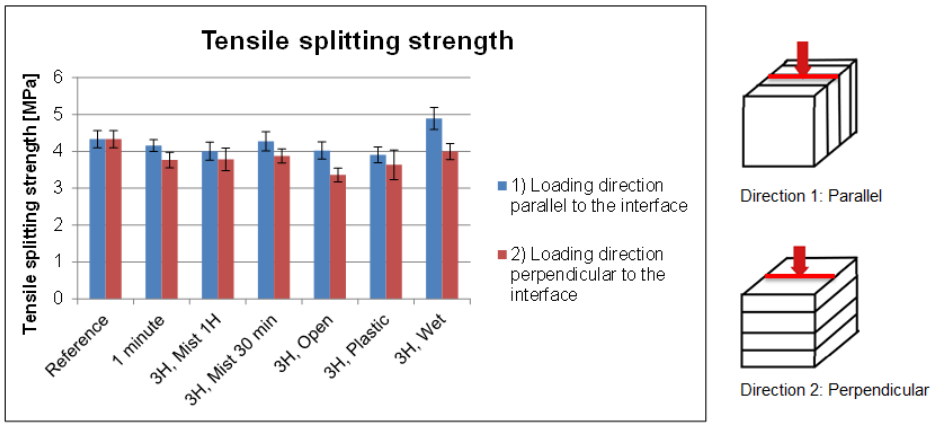

Figure 3.24: Tensile splitting strength of 3D printed elements, each with different parameters as shown below each chart. Size of the specimens: 40x40x40mm cubes, age: 7 days.

Observations during the tests

The results showed less deviation compared to the results obtained during the tensile bond strength test. According to the results presented above, the influence of the time intervals and curing conditions was almost negligible. During the tests, no clear mistakes or uncertain circumstances were observed. The test was however difficult to perform, because no standard loading jig was available for small cubic samples. The result of a tensile splitting test is therefore very much dependant on the position of the sample in the loading device. Multiple samples were prematurely broken due to inaccurate positioning in the loading device, eccentric loading of the sample, and rotation of the sample. Results of samples that showed these phenomena were not taken into account.

3.5.4. CT scanning results

The images obtained by CT scanning are presented in this section. A distinction is made between the cast samples, and samples with different time intervals, curing conditions, and different nozzle standoff distance.

Cast samples

Figure 3.25 shows the porosity of the samples that were cast. The samples were cast according to the procedure as described by Y. Chen. No compaction was applied, because the material should be self-compacting.

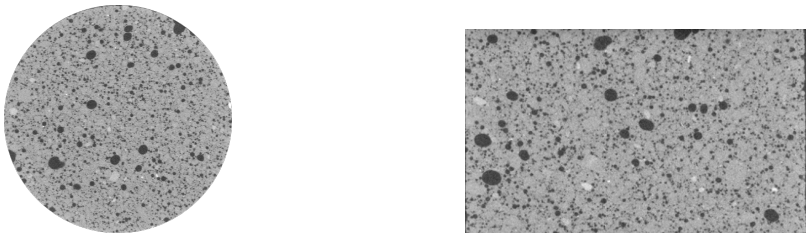

(a) Horizontal cross section

(b) Vertical cross section

Figure 3.25: CT scanning result showing the porosity of the cast sample.

The results clearly show the presence of air voids in the micro structure of the sample. Both small and large air voids can be seen, in a random orientation.

Different time intervals

The results of the samples printed with different time intervals are presented in Figure 3.26. A clear difference in porosity can be observed in the horizontal cross sections of the interface and the filaments. The filaments all seem to have a visibly good compaction, while the interfaces have large air voids, increasing from 20 seconds to 10 minutes. The vertical cross sections clearly show the position of the interface between filament two and three, and even complete filaments of air are visible in Figure 3.26i.

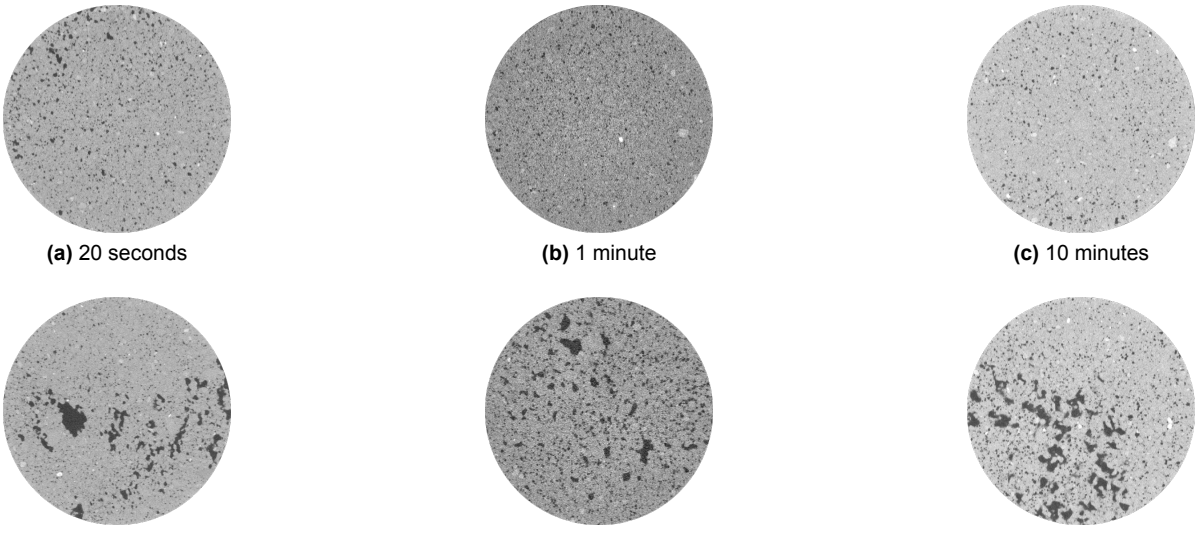

(a) 20 seconds **(b)** 1 minute **(c)** 10 minutes

(d) 20 seconds **(e)** 1 minute **(f)** 10 minutes

Figure 3.26: CT scanning results showing the porosity of the samples with different time intervals. First row: horizontal cross sections taken in the middle of the filament. Second row: horizontal cross sections taken in the interface. Third row: vertical cross section taken in the middle of the sample, showing filament number two and three.

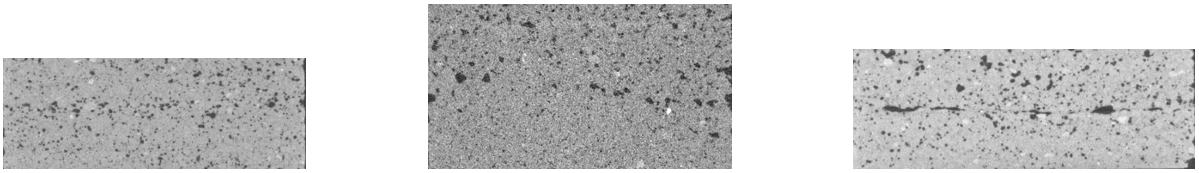

(g) 20 seconds **(h)** 1 minute **(i)** 10 minutes

Figure 3.26: (continued)

Different nozzle standoff distance

The filaments of the samples with different nozzle standoff distances seem to be homogeneous without the presence of visible air voids. However, the samples with 5mm nozzle standoff distance contain much more (and larger) air voids compared to the <1mm and 10mm nozzle standoff distance. This is in accordance with the results of the tensile bond strength test, presented before. Also the interface seems to have more air voids in the horizontal cross section. In the vertical cross section it can be seen that the samples with a nozzle standoff distance of 10mm have much more air voids distributed in the filaments as well.

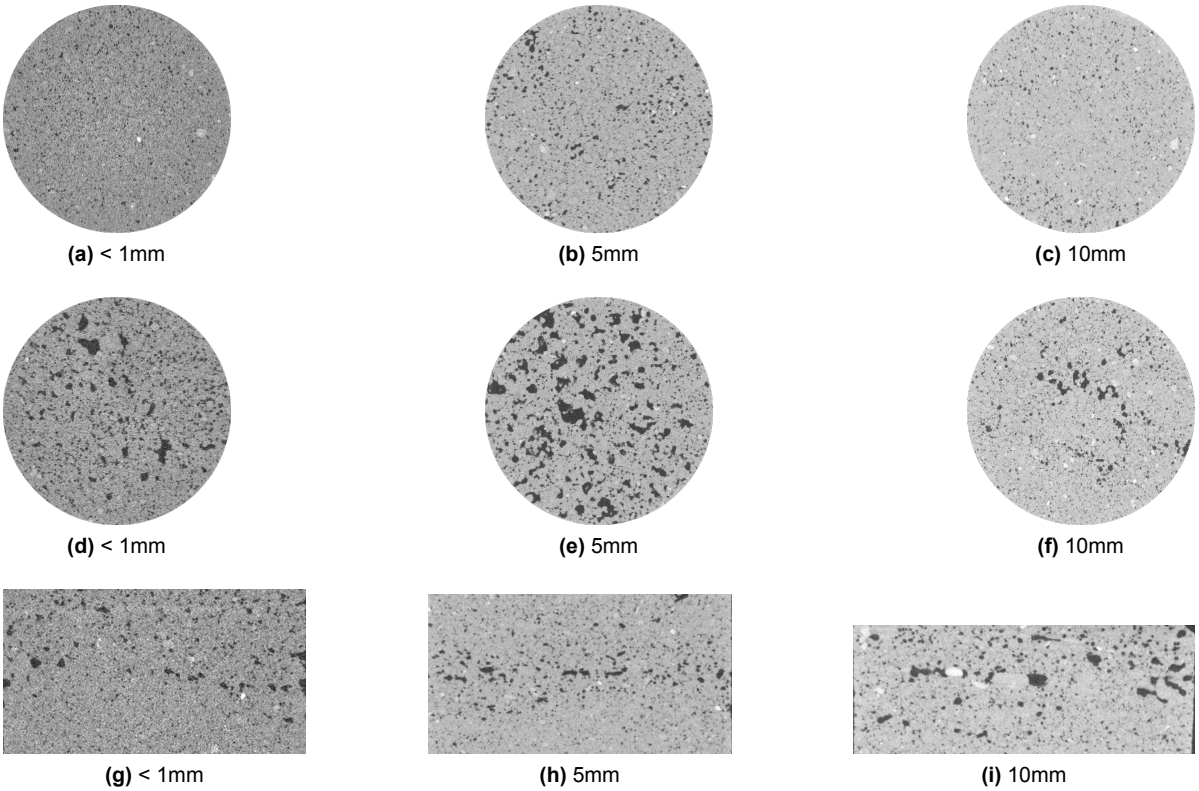

(a) < 1mm **(b)** 5mm **(c)** 10mm

(d) < 1mm **(e)** 5mm **(f)** 10mm

(g) < 1mm **(h)** 5mm **(i)** 10mm

Figure 3.27: CT scanning results showing the porosity of the samples with different nozzle standoff distance. First row: horizontal cross sections taken in the middle of the filament. Second row: horizontal cross sections taken in the interface. Third row: vertical cross sections taken in the middle of the sample, showing parts of filament 2 and 3.

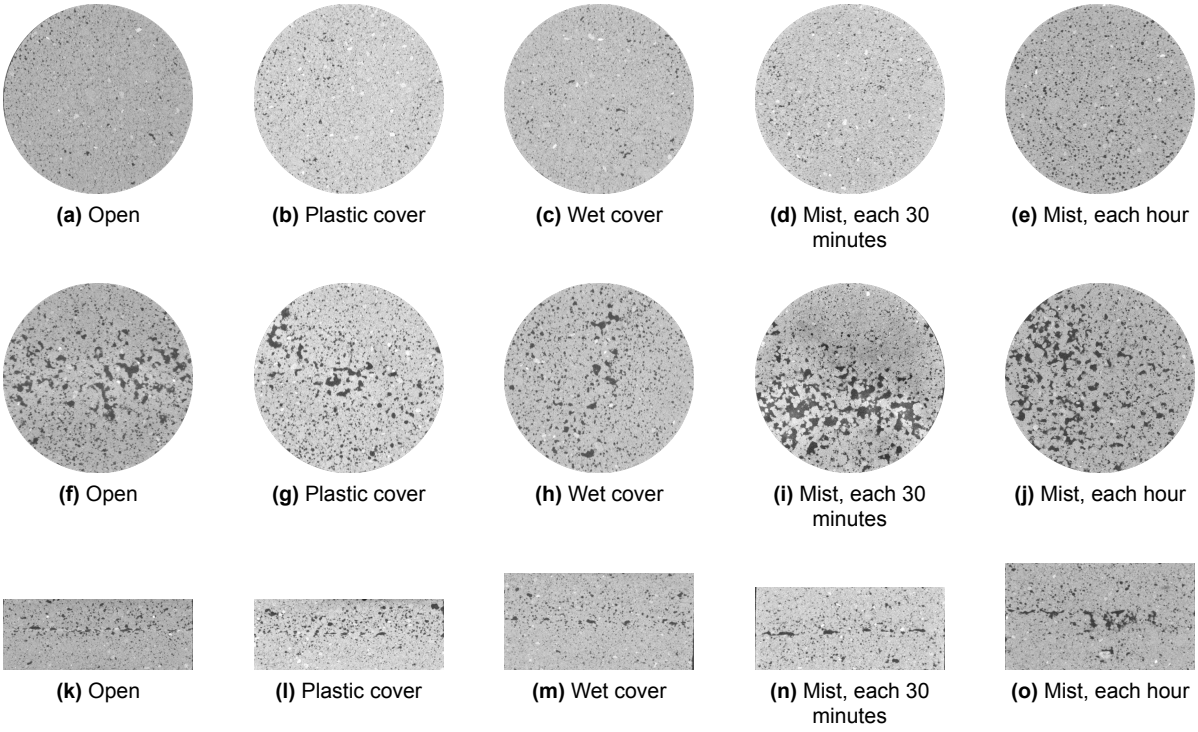

Figure 3.28: CT scanning results showing the porosity of the samples with different curing conditions, and a time interval of 3 hours between printing filament two and three. First row: horizontal cross sections taken in the middle of the filament. Second row: horizontal cross sections taken in the interface. Third row: vertical cross sections taken in the middle of the sample, showing parts of filament two and three.

Different curing conditions

The results for the different curing conditions, presented in Figure 3.28, show approximately similar compaction of the filaments for all samples. Also no great differences can be observed when the horizontal cross sections of the interfaces are compared. The amount of air voids is much higher compared to the samples with different time intervals and different nozzle standoff distance, which might explain the decreasing bond strength. A thorough analysis of the results is again presented in the discussion.

4

Numerical material model

Due to the anisotropic element properties of 3D printed concrete, the use of numerical material models in finite element analyses are still a rarity. This chapter was written to show the step-by-step development of a numerical material model in DIANA, to verify the results of the experiments presented in chapter 3. With this model, it was possible to further develop and verify the structural design of 3D printed concrete structures, which was in this thesis the design of an emergency shelter.

4.1. Relevance of new material models

As explained in the introduction of this thesis, the research on 3D concrete printing was experimental research, focusing on the mechanical properties of printed elements. The structures (houses, bridges, etc.) that have already been printed were most of the time only verified by means of a load test. The lack of standard material models and calculation procedures makes that printed structures are nowadays most of the times only experimentally tested for their capacity. This process takes time, costs extra money and causes an unnecessary environmental impact. The next step in the design procedure of 3D printable structures are numerical calculations. If the structural behaviour of printed elements can be predicted using finite element analyses, then structural designs can be optimized for their shape, and big steps can be made in terms of design speed, and complexity of structures.

This chapter describes the step-by-step approach for the development of the material model for printed elements with a 10 minute time interval. This time interval was chosen because the first impression of the strength of this material showed good potential for use in the industry. The slump will probably be negligible because of the relatively large time interval, and a maximum of six filaments can be printed per hour. The decrease of tensile bond strength was only 19% compared to samples with filaments printed each 20 seconds, still corresponding to 6% of the compressive strength of the tested samples. The material model was created using a finite element (FE) program. The FE program used in this thesis is DIANA. This program uses Finite Element Analysis (FEA), and is based on numerical calculation methods.

4.1.1. Simulation of material behaviour

To start developing a material model, it was necessary to make assumptions for the information that has not been obtained during experimental research. During the experimental research, only printed elements (including both filaments and interfaces) were investigated. However, based on the literature review, the assumption was made that the filaments are heterogeneous, where the anisotropic properties of a complete printed element are due to the layered structure, i.e. the presence of interfaces. For this reason the material was modelled as follows; the heterogeneous filaments were modelled as normal concrete phases, and the interface was modelled as interface elements with deviating mechanical properties. The filaments were assigned with standard concrete properties with a strength class

corresponding to the compressive strength of the tested samples in longitudinal direction. In longitudinal direction, the load was applied parallel to the interfaces and therefore the interfaces most likely do not have a great influence on the compressive strength. The material properties for the interface were however not known yet. Based on the experimental data, the behaviour for the interface was 'guessed'. The input for the interface is a multi-linear traction-displacement diagram which can be adjusted manually to create the desirable over-all element behaviour.

4.1.2. Simulation of tensile bond strength test

The tensile strength test, as performed during the experimental research and described in section 3.3.1, was simulated in DIANA. The results of the simulation in DIANA were compared to the average curve of all curves obtained during the experiment. After comparison, curve fitting was used to match the results of the numerical simulation to the experimental results. This was a trial and error process and required several steps to match both graphs. A step-by-step explanation is presented below for the development of the material model in tension.

Step 1: Numerical samples

The first step of the material model was to create an object that has the same shape and dimensions as the samples used during the experiments. Figure 4.1 shows the sample created in DIANA.

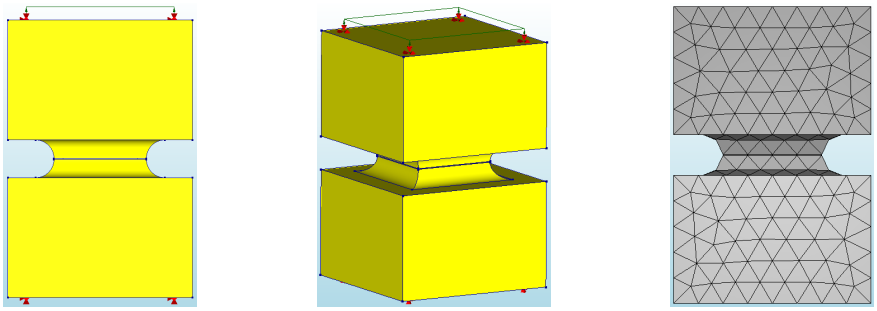

(a) Front **(b)** 3D image **(c)** mesh

Figure 4.1: Sample created in DIANA FEA for the simulation of the tensile bond strength test.

The sample consists of two solid blocks and an interface. Each block represents a filament, and was later assigned with standard concrete properties, corresponding to C55/67. The dimensions of this sample were 20x20x30mm, where the notch was 5 mm in depth and 3 mm in height. The cross-sectional area of the interface was 10x10mm. The interface is presented in the figure with the black line between the two yellow blocks. In the figure it seems that the interface has a physical height, but this is only to show the presence of the interface. The interface is dimensionless in Z-direction. To make the notch as realistic as possible, a notch with curved edges was modelled, which approached the real situation as close as possible. The mesh size of the sample was chosen at 2.5 mm. This was optimal to both get accurate results and save computational time. The mesh shape is triangular, so around the curved notch the mesh is still divided well over the area.

Boundary conditions and loads

During the experiment, the sample was glued to (almost) undeformable steel plates. This means that the sample can be considered fully clamped. To simulate the experiment, the sample has supports at the bottom and at the top and these supports were fixed for X, Y, and Z translations. The experiment was deformation controlled, so the numerical simulation was also deformation controlled, to obtain a stress-displacement graph. The deformation that was applied to the sample is 0.02 mm, which is 20 micrometers. To be able to apply a deformation to an element in DIANA, the sample needed a support at the position of the applied deformation, and the support was then displaced. This is also visible in Figure 4.1.

Step 2: assigning material properties
The next step was the assignment of material properties to both the interface and the heterogeneous concrete filaments.

Filament properties
As observed during the experiments, the interface failed and the filaments showed no clear failures. This was supported by the digital image correlation. The filaments were assigned with concrete C55/67 properties, corresponding to the compressive strength of the samples in longitudinal direction, which was approximately 56 MPa. DIANA has a material-library available, including concrete C55/67. All properties were assigned accordingly. Below, Table 4.1 shows the material properties of concrete C55/67.

Concrete parameters	
Concrete type	Normal weight
Concrete class	C55/67
Aggregate type	Quarzite
Cement type	Class N
Model parameters	
Youngs modulus	38214.2 N/mm^2
Poisson ratio	0.2
mean uniaxial tensile strength	4.214 N/mm^2
mean compressive strength	63 N/mm^2

Table 4.1: Assigned filament properties.

Interface properties
The interface properties were still unknown. Several models were available to assign to interface elements. To be able to assign specific multi-linear traction-displacement graphs for the tensile behaviour of the interface, interface elements with non-linear elasticity were chosen. The global stress-displacement behaviour of the printed elements was known, so these values could be used to create a normal traction - relative displacement diagram in DIANA. The normal traction is the quantity for the allowable tensile stress of the interface, which should correspond to the tensile stress of the samples during the experiment. The relative displacement of the interface was the unknown factor and needed to be found by means of an educated guess and a trial and error process. This is because the total deformation of the sample was measured, and includes both the strain of the filaments and (plastic) deformation in the interface. As a starting point, the average stress-deformation curve was scaled to get a stress-strain curve, and the strain was multiplied with a factor 10. This curve was entered as input in the interface model as a first try. For the compressive behaviour of the interface, no input was needed yet, because this was a tensile test. The input for the interface in compression was assigned later, in section 4.1.3, where the compressive tests were simulated. Figure 4.2 shows the graph that was assigned to the interface. The numerical values are presented in Table 4.2. The modulus of elasticity used for the non-linear elasticity model was 43600 N/mm^2, based on the angle of inclination of the stress-displacement curve.

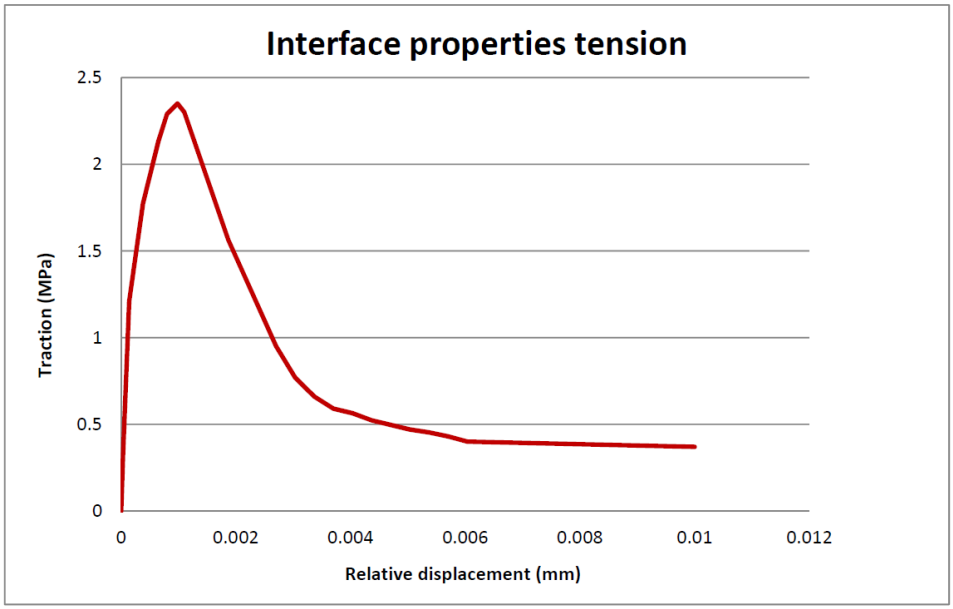

Figure 4.2: Multi-linear graph for the interface elements.

Multi-linear interface properties

Relative displacement [mm]	Traction [N/mm^2]
0	0
0.000033	0.326667
0.00014	1.21
0.00038	1.77333
0.00065	2.13333
0.0008	2.29
0.00098	2.35
0.0011	2.3
0.001866667	1.5633333
0.0027	0.95
0.003033333	0.77
0.003366667	0.66
0.0037	0.59
0.004033333	0.56333333
0.004366667	0.52333333
0.0047	0.49666667
0.005033333	0.47
0.005366667	0.45333333
0.0057	0.43
0.006033333	0.4
0.01	0.37

Table 4.2: Interface properties for the simulation of the tensile bond strength test.

Step 3: analysis

DIANA can perform multiple types of analyses. A stress-displacement curve was needed to verify the material behaviour with the experimental data. The obtained stress-displacement diagram was non-linear. Therefore the analysis performed by DIANA was also non-linear; the structural non-linear analysis. The essence of this analysis is that the deformation was applied in small steps, and that according to the deformed sample, a force was found via the assigned traction-displacement diagram. An appropriate mesh- and step size led to convergence of the numerical analysis. Specific data for the analysis is shown in Table 4.3.

Analysis properties		
Analysis type	Structural non-linear	
	Non-linear effects	Physically non-linear
Load steps	200 x 0.005	
	Max. number of iterations	25
Iteration method	Newton-Raphson	
	First tangent	Tangential
Convergence norms	Displacement + Force	
	Convergence tolerance	0.01

Table 4.3: Analysis properties.

Step 4: results
When analyzing the results of the analysis, three checks were important to verify the material behaviour:

- *Reaction force of the sample*
  The reaction force of the sample was analyzed, together with the vertical displacement. To get the tensile bond stress curve of the interface, the total reaction force was divided by the cross-sectional area of the interface, in this case 10x10 mm. By plotting the simulated stress-displacement graph together with the experimental stress-displacement graph, the results were compared. Figure 4.3 shows both graphs.

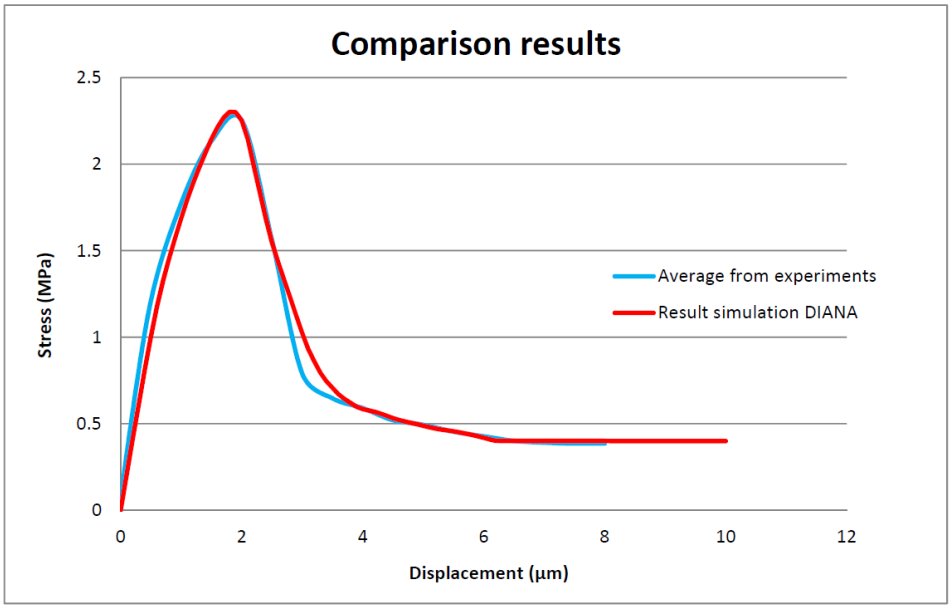

Figure 4.3: Comparison of the average results obtained during the experimental tensile bond strength tests and the simulation of the same test in DIANA. The results are given in MPa, where the obtained reaction forces have already been divided by the cross-sectional area.

This graph was obtained after several iteration steps in adjusting the input data for the interface behaviour in tension. The simulation and the experimental data match almost exactly, and could be used for the tensile properties of the interface.

- *Development of stresses*
  An important aspect is that the highest stresses developed in the interface, and that the filaments did not fail. The failure should take place in the interface, which was observed during the experimental testing. This can be seen in Figure 4.4.

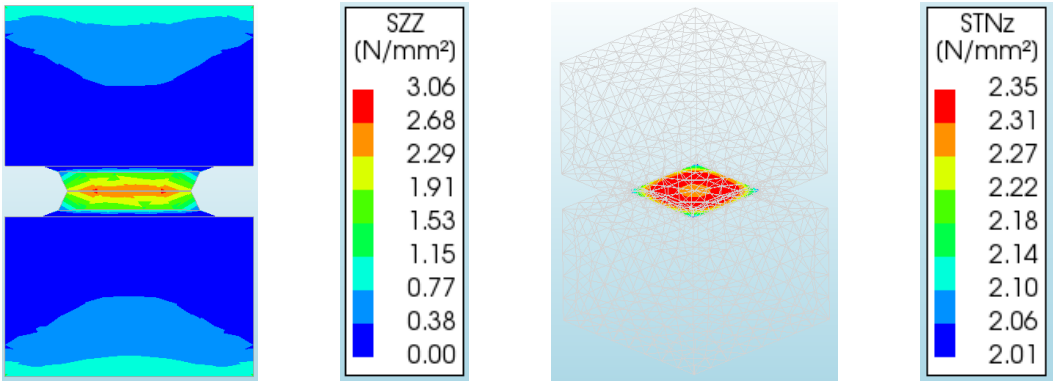

(a) Over-all failure **(b)** Legend sample **(c)** Failure interface **(d)** Legend interface

Figure 4.4: The stresses in the sample, shown at the load step of the largest reaction force (1,8 μm). This figure shows that the failure indeed occurs at the position of the interface.

- A final check included the development of stresses in the interface. These stresses should not exceed the maximum strength of 2.35 MPa. The legend in Figure 4.4 also complies for the images shown in Figure 4.5. As can be seen, the maximum stresses did not exceed the specified value of 2.35 MPa. The over-all stress-displacement graph looked good, which is the most important.

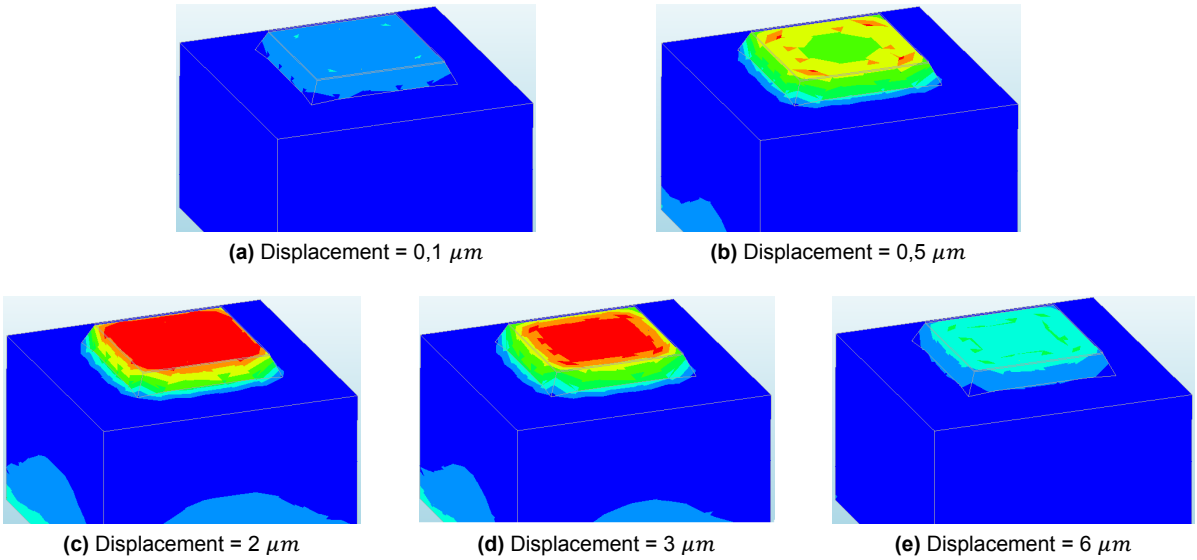

(a) Displacement = 0,1 μm **(b)** Displacement = 0,5 μm

(c) Displacement = 2 μm **(d)** Displacement = 3 μm **(e)** Displacement = 6 μm

Figure 4.5: Stress development in the sample, showing different load steps corresponding to different displacement values.

4.1.3. Simulation of compressive strength test

To be able to perform structural calculations correctly, it was important that the anisotropic compressive strength was modelled accordingly. Therefore, the compressive strength test were also simulated in DIANA. However, the obtained results from the experimental compressive strength test were only the specific strength values of the samples. No stress-displacement curves were available. For this reason the compressive strength of the interface was based on the compressive strength of the samples tested in perpendicular direction. The ratio between the tensile strength and the compressive strength is 46/2.35=19.5. This ratio differs from cast / bulk concrete, where the ratio is approximately 16-18. The difference is related to the decreasing tensile strength with increasing time intervals. Again curve fitting was used to match the material properties. Below, the step-by-step approach for the development of

the 10 minute time interval material model is described.

Step 1: Sample in DIANA
The samples that were modelled in DIANA were 40x40x40mm, including both filaments and interfaces. Four filaments were modelled, where the inner two filaments had a thickness of 12 mm and the outer filaments were 8 mm thick. This was also the the case during the experiments. Due to the sample preparation, the outer filaments were sawn to 8 mm thickness, to make the sample exactly 40x40x40 mm. The interfaces were again dimensionless in perpendicular direction with respect to the interface. Figure 4.6c shows the sample including the interfaces, where the yellow filaments were modelled as solids. The mesh size was chosen at 5 mm. Translations of the bottom surface were completely fixed in X, Y, and Z direction, the top surface was completely fixed in X and Y direction. The load was applied at the top surface in Z direction. Fixing translations was a realistic assumption, because the sample was clamped between the (undeformable) steel loading plates, where the friction between the sample and the plates makes that the sample behaves fixed. This means that the support could be regarded as completely fixed.

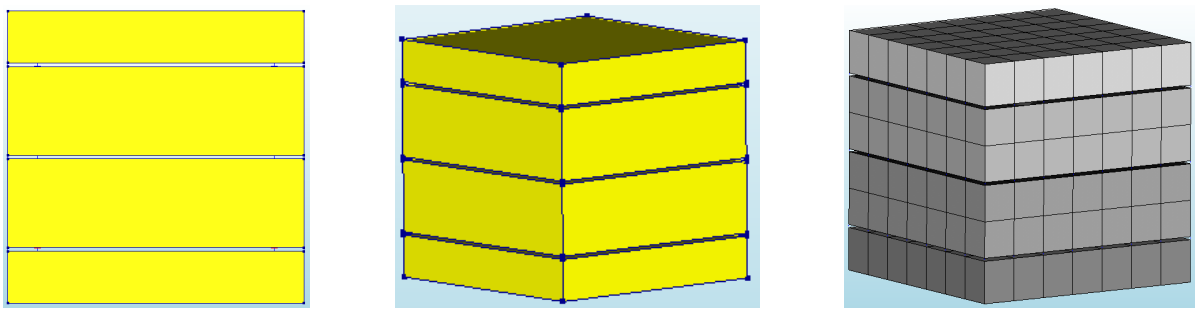

(a) Front **(b)** 3D image **(c)** mesh

Figure 4.6: Numerical samples for compressive test simulation.

The moment that the sample would fail during an experiment, DIANA should diverge and stop the calculation. By checking the reaction force, and divide the total reaction force by the cross sectional area of the sample, the strength was calculated. The strength should be close to the mean compressive strength of the material, and the results could then be compared to the the experimental results.

Step 2: Material and interface properties
The material properties for the filaments and the interfaces were kept the same as for the tensile bond strength test simulation. The only parameter that was added is the compressive strength diagram for the interface. This partial traction-relative displacement curve was extrapolated from the linear part of the tensile stress-displacement graph. This is shown in Figure 4.7. The start of the horizontal line is the compressive strength in perpendicular loading direction.

Step 3: Analysis
The analysis-type used for the simulation of the compressive strength test was a non-linear analysis, loaded step wise until failure occurred. The parameters for the non-linear analysis were the same as used for the simulation of the tensile bond strength test, the only difference was that the simulation that was force controlled instead of deformation controlled. This means that the load that was applied on the sample was applied in steps of 0,5 kN per step, up to a maximum load of 120 kN. The sample should however fail before reaching the final load.

Step 4: Results
The results of the compressive strength calculations were verified by two checks.

- *Verification of the reaction force*
  The reaction force should match the strength of the material closely. Figure 4.8 shows the reaction forces of the samples tested in two different directions. It can be seen that the reaction force of the sample is 73.4 kN and 93.8 kN for the perpendicular and longitudinal loading direction,

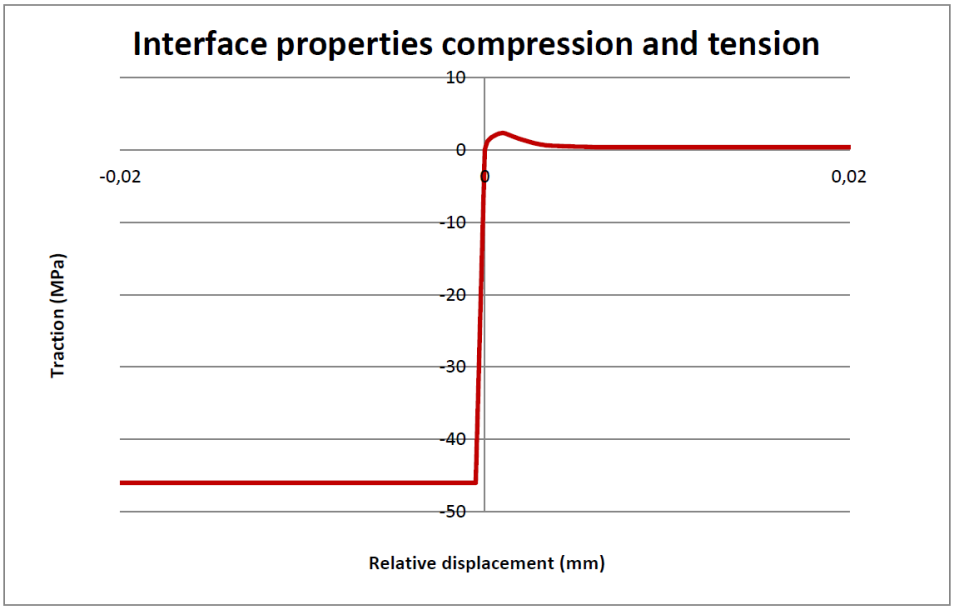

Figure 4.7: Multi-linear input for interface in compression (including tension).

respectively, corresponding to 46 MPa and 58.7 MPa. Comparing direction 1, the perpendicular loading direction, the strength of the material matched the experiment exactly, since the interface properties were governing in this direction. The simulation of direction 2, the longitudinal loading direction, showed a small difference compared to the experiment, where the average obtained value was 56 MPa. This difference can be allocated to the assigned concrete strength class C55/67, as default material for the filaments. The sustainable concrete used in this research did not completely match with these properties, since this was a newly developed material. The consideration was made to choose for a standard material according to the Eurocode, because all properties assigned to that material are known, and no uncertainties about the material properties would appear afterwards. The small difference was taken for granted.

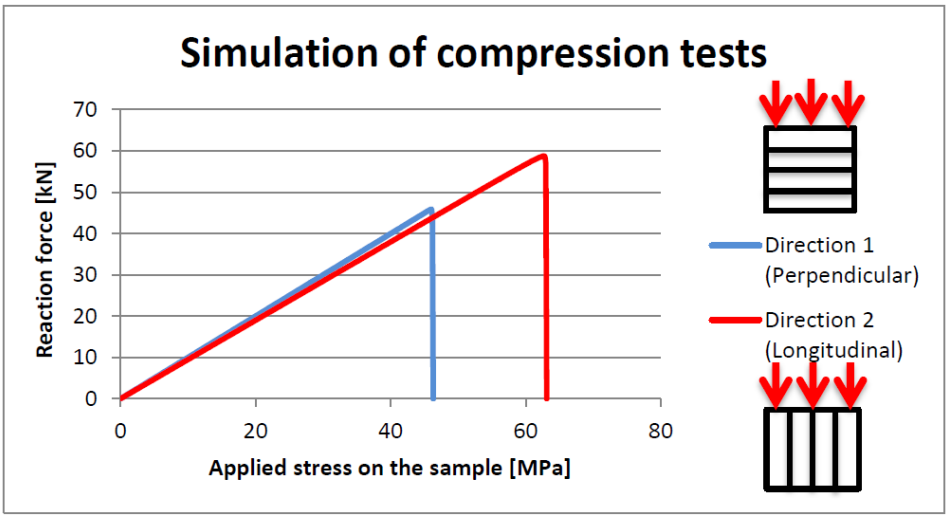

Figure 4.8: Graph showing the different reaction forces in perpendicular and longitudinal loading direction, obtained during simulation of the compressive strength test.

- *Verification of the failure mechanism*
  During the tests it was clear that a cone shape remained after failure of the sample. This cone shape can be visualized in DIANA by showing the strains in perpendicular direction, compared to the loading direction. Figure 4.9 shows the that cones remain when the sample fails.

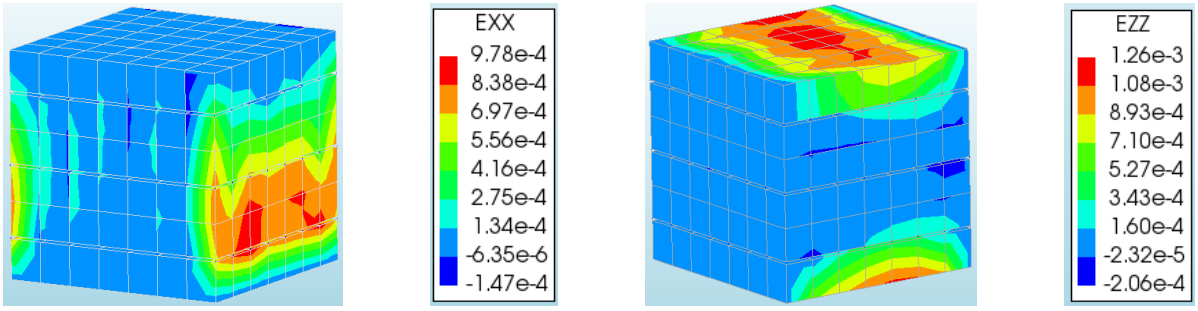

(a) Perpendicular loading direction

(b) Legend perpendicular

(c) Longitudinal loading direction

(d) Legend longitudinal

Figure 4.9: Images of the failed samples in DIANA. The cone shapes are visible, as was also observed during the experiments. Figure 4.9a shows the failed sample in perpendicular loading direction (direction 1). Figure 4.9c shows the failed sample in longitudinal loading direction (direction 2).

Simulation of the third loading direction
During the numerical research, the sample was also tested in lateral loading direction, because the experimental results showed that the compressive strength in the third (lateral) loading direction was significantly lower than the the second (longitudinal) loading direction. However, numerical simulation showed no difference between these two loading directions. Possible explanations and conclusions for this modelling aspect are presented in chapter 6: Discussion.

Reference cube
The final step was comparison between the numerical results of a reference cube without interfaces and the printed samples tested during the experiments. A standard cube without interfaces and normal concrete properties was modelled. Concrete C55/67 was chosen accordingly. The dimensions were 40x40x40 mm and the load was again applied step-wise, in a non-linear calculation. The applied load was 120 kN, loaded in steps of 0.5 kN per step. A mesh size of 5 mm was chosen and the boundary conditions were the same as described for the printed samples. Figure 4.10 shows the sample that was created in DIANA.

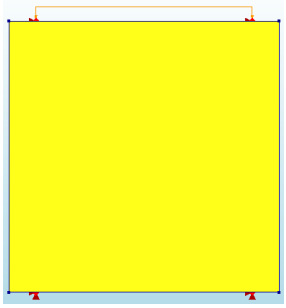

Figure 4.10: Sample used for a reference calculation.

Figure 4.11 shows the strain of the non-linear calculation of the reference sample in compression.

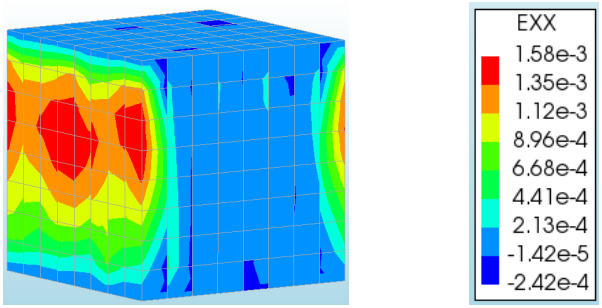

Figure 4.11: Strain of the cast reference sample without interfaces. The failure pattern is similar to the samples with interfaces.

The maximum reaction force of this sample was 98.3 kN. The compressive strength of the material was therefore 98270/(40x40) = 61.4 MPa. This value corresponds more or less to the mean compressive strength of the material, and therefore could be concluded that the this way of modelling was correct. If this results is however compared to the simulated sample with interfaces loaded in longitudinal direction, it can be observed that the strength of the reference cube was higher, approximately 2.7 MPa. This difference can be allocated to the presence of the interfaces and the sample failing in tensile splitting, perpendicular to the interfaces. A more extensive explanation for these results is given in chapter 6.

4.2. Size effect correlation factors

To be able to use this material model in practice for the calculation of structures, it was necessary to take the size effect into account. The information found on size effects in section 3.3.6 was used to apply size effect correlation factors. The strength of the samples was related to cubes of 150x150x150mm. The correlation factor was calculated based on the difference in strength between samples of 40x40x40mm and 150x150x150mm in compression and 10x10mm to 150x150mm in tension. This means that the strength of the material decreases.

Tension

In tension, the results from Wang et al. (2015) were used to determine the correlation factor that had to be applied in order to use the concrete in printed structures. Based on the values presented in figure 3.10, the tensile strength correlation factor between cross-sectional areas of 12.5x12.5mm and 62.5x62.5mm is 0.89. Given the fact that the graph is almost horizontal for cubes of 62.5mm, the assumption was made that the size effect difference between cubic samples of 62.5mm and 150mm is negligible, and that the correlation factor of 0.89 had sufficient accuracy.

Compression

The size effect correlation factors found for cast samples loaded in compression can be read from Figure 3.8. With a cube size of 40 mm, the compressive strength was approximately 108 MPa. Standard cubes of 150mm had a strength 96 MPa. The correlation factor for compression is: 96/108 = 0.89. Since this was high strength concrete with a higher compressive strength then the material used in this research, a second calculation was performed according to the data from Yi et al. (2006). The graph from this research was not directly applicable, because the cube strength was related to concrete cylinders, which gives larger correlation factors. From the raw data, a simple calculation was made. Cast samples with a cube size of 50mm had an average compressive strength of 36.2 MPa, samples with a cube size of 150mm had a compressive strength of 33.4 MPa. The correlation factor is 0.92. The cube size of 50mm did not exactly match the cube size of 40 mm used in this research. For that reason, the correlation factor of 0.89, the same as samples loaded in tension, was used for the compressive strength. This was based on the assumption that the correlation factor for smaller cubes becomes larger.

Application on filaments and interfaces
The correlation factor of 0.89 was applied to both the filaments and the interface, in tension and compression. For the filaments, the concrete strength class of C55/67 (mean strength 62 MPa) was decreased to C45/55, with a mean compressive strength of 53 MPa. The interfaces were adjusted by hand, and the graphs were multiplied with the correlation factor. Figure 4.12 shows the tensile properties of the interface before and after multiplication with the size effect factor. In compression the same variation was applied, but not shown in this graph.

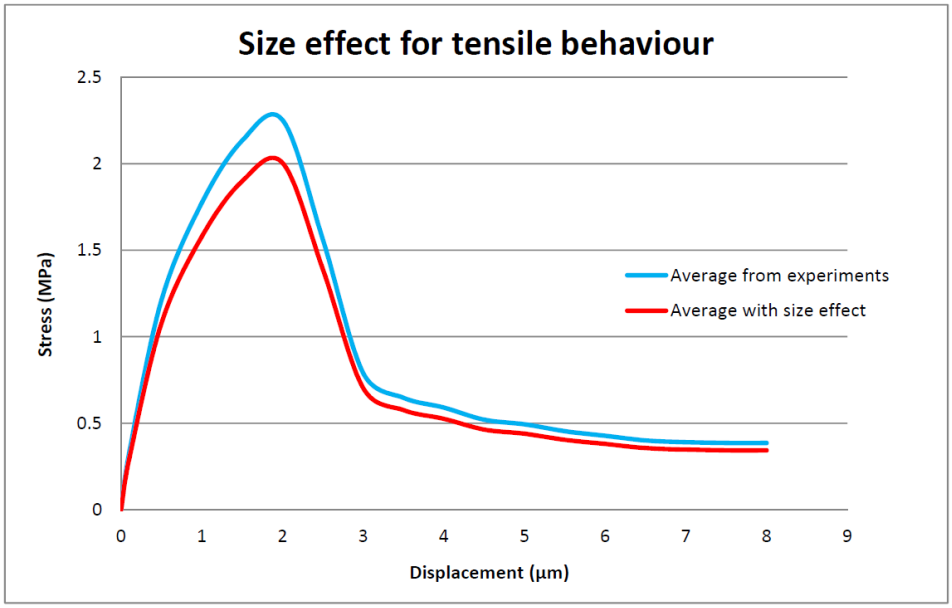

Figure 4.12: Graphs showing the influence of the size effect correlation factor.

4.3. Random variation in interface properties

During the experiments it became clear that minor differences in for example the open time of the mixture and time intervals between printing two filaments, led to a significant standard deviation of the material properties in tension and compression. The standard deviation for the direct tensile bond strength test was 13% and the standard deviation in compression in the perpendicular loading direction was 11%. These differences could be allocated to the variation in interface properties.

When a structural application is modelled, it is desirable to take these variations into account, to obtain results that are close to reality. In DIANA there was no specific function to include a standard deviation for interface elements, especially because the interface was modelled as a multi-linear graph which was fully assigned by hand. A more complicated way to assign a random factor to the assigned interface properties, is via the use of a script, using Phython or MathLAB. Using these programs, it should be possible to build a wall, layer by layer, using a unique random variable for every interface. In this way the scatter can be approached. For the continuation of this thesis however, where only simple walls were modelled, random factors were applied by hand to the assigned multi-linear curves for the interfaces. In Figure 4.13 below, eight variations of the multi-linear interface curve (tension part only) are presented and were assigned manually to all interfaces present in the wall. The standard deviations for tension and compression, served as upper and lower- bound for the variation in the results. Although full randomness can only be obtained if a random-function in Python or MathLAB is used, for the calculation of the walls, this variation was sufficient to approach the real situation for a simple structure.

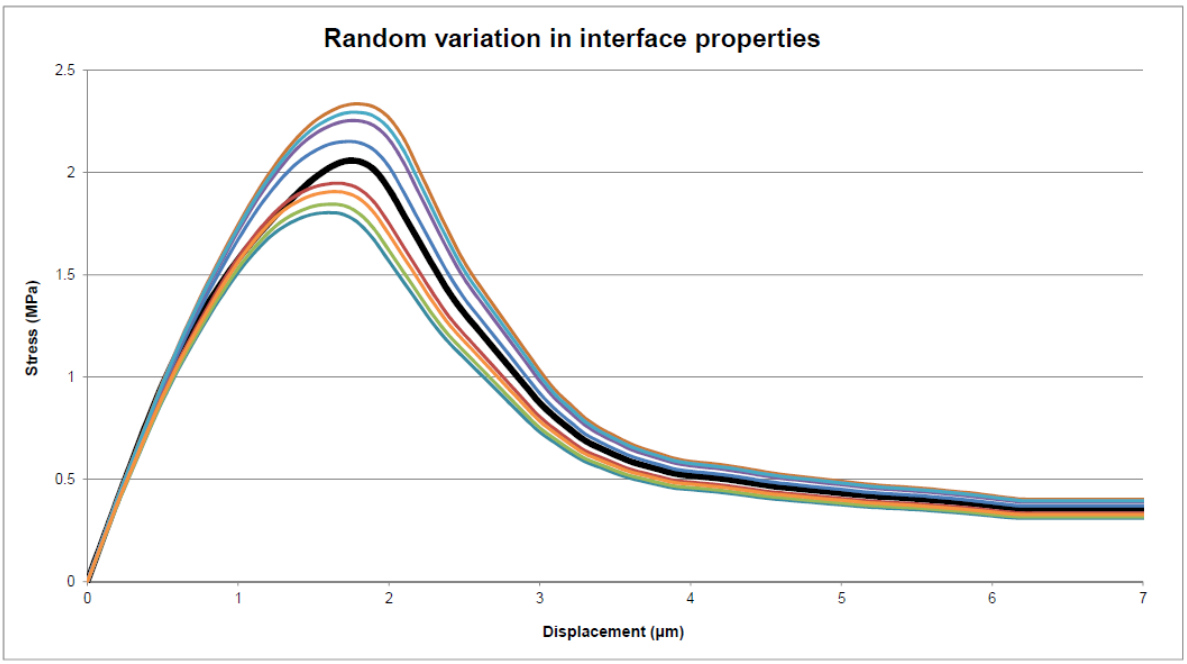

Figure 4.13: DIANA simulations for the variations of the interface properties, based on the average stress-displacement curve with a size-effect factor. The tensile strength of the material lies within 1,825 MPa and 2,375 MPa, which corresponds to the standard deviation of 13% for tension.

5

Case study

The final part of this thesis was the elaboration of a case study. Making use of the experimental results and the gained knowledge of the printing process, a simple design of an emergency shelter is presented in this chapter. Besides that, structural verification was performed by numerical analysis, to show the substantiation of this project.

5.1. Introduction

In cities, countries, or even complete continents, poverty and homelessness is every-day's business. Whether the origin of the problems are poverty, the aftermath of natural disasters, or homelessness in suburbs or slums, 3D concrete printing can be an easy and cheap solution to these problems in the future. The ease, speed and low costs of printed concrete are a good starting point for the development of simple but robust shelters, and even permanent housing. This section describes the development of a simple emergency shelter design, based on the information obtained during the experimental and numerical research.

5.2. Shelter solutions

Nowadays several organizations, like the Red Cross, UNHCR, Shelter Centre and others, are specialized in arranging emergency shelters for the humans that really need it. Where the UNHCR especially focuses on refugees, the Red cross and the Shelter Centre focus also on natural disasters, like earthquakes and floodings, but also poor people in developing countries. These organizations have several standardized shelter types available, varying in dimensions and complexity. The choice to choose for a specific shelter mainly depends on how many people at once need immediate shelter, and the perspective of how long people are expected to live in an emergency shelter or temporary housing. In case of a disaster, a large amount of tents is quickly built, but after weeks, when first shelter is arranged, the work switches to build long term shelters together with reconstruction of neighborhoods.

According to Bashawri et al. (2014), four shelters categories can be distinguished. These four categories are: 1) emergency shelters, 2) temporary shelters, 3) temporary housing and 4) permanent housing. The Red Cross defined seven shelter categories, and added transitional shelters, progressive shelters and one-room shelters to the ones mentioned before. The difference between these seven categories is the time people are expected to live in the shelter. An emergency shelter is only for very short time periods (only days), providing life-saving shelter. Temporary shelters are still for short-time use, but people can survive for several weeks to months in these kind of shelters. Temporary housing allows people to continue their daily activities, and permanent housing should in the end be resistant to hazards and disasters.

The three extra categories proposed by the Red Cross are steps in between temporary housing and permanent housing, and are also more related to natural disasters. A transitional shelter is a shelter that is mainly built by victims of disasters themselves. These shelters are built such that they can later form part of a permanent house, on a permanent location. A progressive shelter is a shelter that is first build as a temporary shelter, but can be upgraded later with extra parts and structural components to serve as a more permanent house. Also a one-house shelter is built to serve as a permanent house in the future, including plumbing, heat, and safety. In Figure 5.1, a selection of standard emergency shelters is presented, to show the types of shelters available for multiple stages after a disaster.

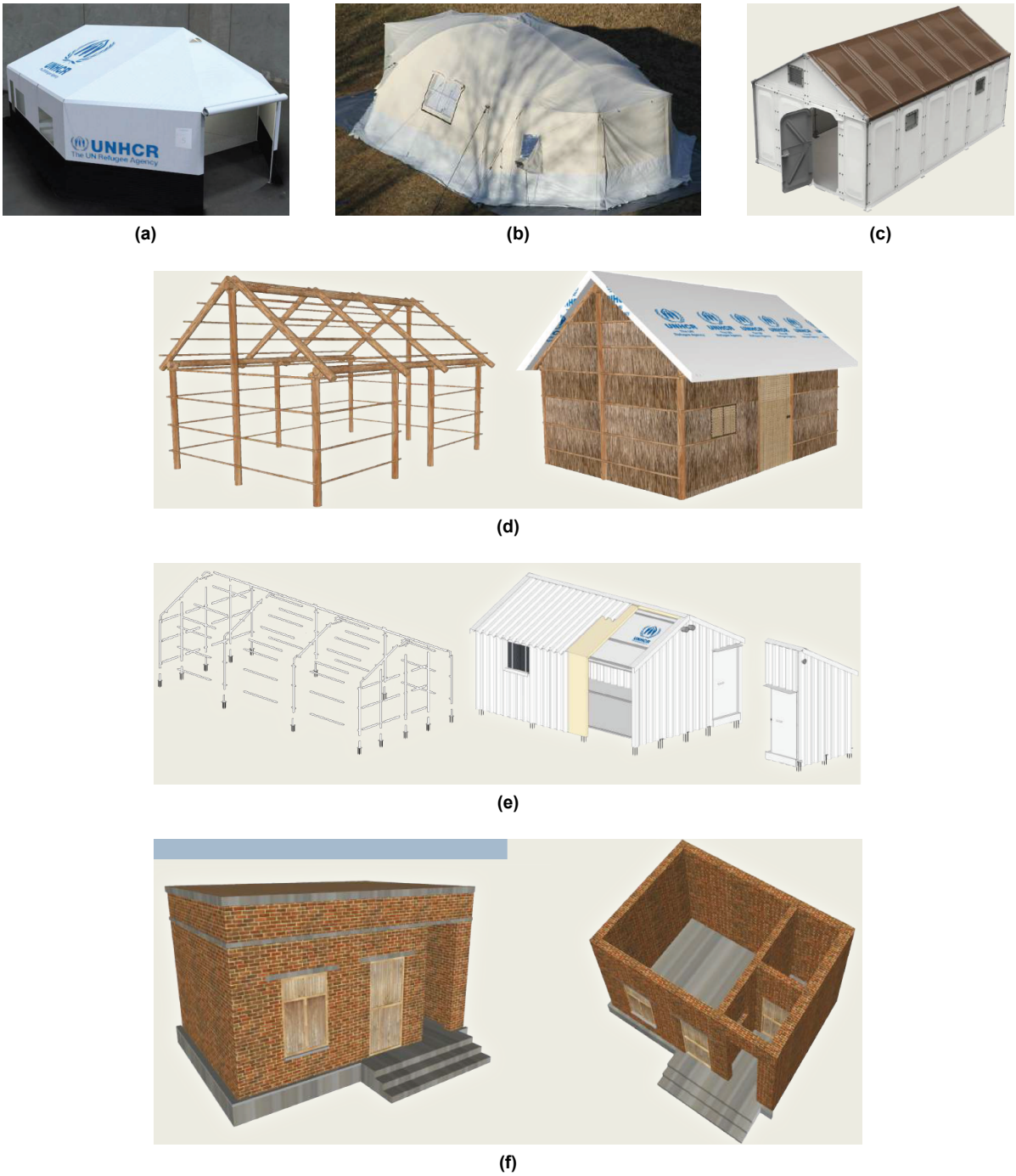

Figure 5.1: Examples of commonly used emergency shelters and temporary shelters.

Figures 5.1a, and 5.1b show the most simple type of shelters, that can be built anywhere within one

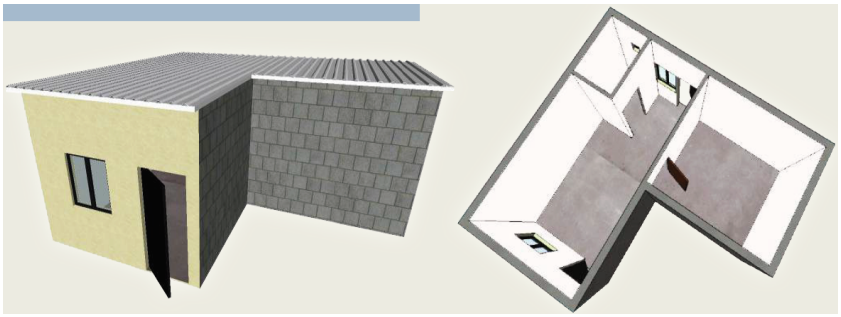

(g)

Figure 5.1: continued

hour. The tents provide only very limited insulation and are only meant for the first days of shelter after a disaster. The shelter shown in Figure 5.1c is made of plastic, and also provides very limited insulation. The prices of these type of shelters are not known. Shelter 5.1d and 5.1e were really meant as transitional shelters and temporary housing. Prices vary between €650 and €3200. These shelters have good insulation properties and people are expected to live in these shelters from months to years. The shelters presented in Figure 5.1f and 5.1g, were meant as progressive shelter, which can be used as permanent housing in the future. Prices of these type of shelters vary between €1900 and €8200. The last two types are mainly used for development of poor countries.

5.2.1. Future of shelter possibilities

Combining the information of upgrading temporary shelters to permanent housing and considering the knowledge about the 3D concrete printing process, the idea has risen to develop a multi-functional printable shelter that fulfils several requirements in multiple situations. The first situation is an emergency situation. It must be possible to build this shelter within two to three days for situations in which they are really needed, like disaster areas. The 3D printing technique has the advantage that with a few people, a complete, decent, shelter can be built in a short time period. On the other hand, in poor countries where homelessness is a problem, like suburbs of cities, or even slums, the two-day printed shelters should have the possibility to be upgraded to (almost) permanent housing, including a decent roof, doors and a pleasant indoor climate. The construction time is in that situation less critical.

5.2.2. Why 3D concrete printed shelters?

Still the question rises why 3D printed concrete shelters can be an alternative to traditional shelter options. A lot of simple reasons might keep people from using the printed shelters in the future. The building process takes much longer than an hour to build standard tents and simple shelters, so a large quantity of simple shelters will still be necessary in emergence situations, that conclusion can be drawn prior to any research. Also the costs will be considerably higher than simple shelters where the walls consist of straw, cladding or plastering, that are all locally available and producible. The time to build a simple shelter like 5.1d and 5.1e is also quite similar, and the indoor climate will not differ much much because of the good insulation properties of the natural materials used. So why 3D concrete printed shelters?

The reasons to choose for printed shelters include long term arguments, but mainly have to do with arguments related to health and well-being of humans in the need of (emergency) shelter. People need to be convinced of the advantages of 3D printed shelters. Three main advantages outweigh the mentioned disadvantages and possibly let people realize that the investment in concrete printed shelters is feasible.

The first argument, and maybe the most important, is a psychological argument. Living in a tent, or a very simple shelter with walls of straw or cladding, brings a feeling of uncertainty and un-safety. People do not feel at home, and every day is fight to survive. A decent shelter with solid walls, in this case concrete printed walls, contributes to the well-being of the people living in a shelter. It makes those people feel more at home, and makes it possible for them to focus at more important things, like their

family, and reconstruction of their permanent shelter. Also privacy created by the solid walls is an advantage that cannot be measured, but nevertheless contributes to the well-being of people. The mass of the walls provides better sound insulation, and also the air tightness of the walls is better than walls consisting of natural local materials, and therefore provides a better indoor environment as well.

The second argument is related to the possibilities to upgrade the shelter design to more permanent structures and the costs of the shelters. The two-day solution can provide life-saving shelter, but will definitely be more expensive than a simple shelter. On the other hand, if the short term solution can be extended to a long term permanent shelter, like a normal one- or two-person house, the costs are of less importance and this solution might suddenly be much cheaper than building a traditional permanent shelter. Exact costs were not yet known at this preliminary design stage, and are hard to predict because of different material costs in different countries. Together with the uncertain labour costs and supporting works, the final price of a printed shelter will very much depend on the area, repetition of the printing process and the material costs.

The last argument is about the health of people living in shelters. People that live closely together, whether it is in large groups, in tent camps or in slums, the chance of an epidemic to occur is large. The chance of infection decreases if people live in decent accommodation. If people do get ill, the chance of recovery is bigger in decent shelters than in tent camps. Also the right medical health care is often not directly available, so people often have to take care of themselves and relatives.

5.2.3. Possible locations for printed shelters

The hypothetical location where the shelter can be build was based on four criteria. It was first of all necessary to choose only locations where the concrete can be made from local materials, and can therefore be produced cheap. This means that in areas where the shelter is about to be build, Meta Kaolin should be widely available. Figure 5.2 shows the global distribution of kaolinite clay in the top- and subsoil. It can be seen that the kaolinite clay is mainly available around the equator, in the middle part of Africa, the north part of South-America and parts of Asia including the Philipines and Indonesia.

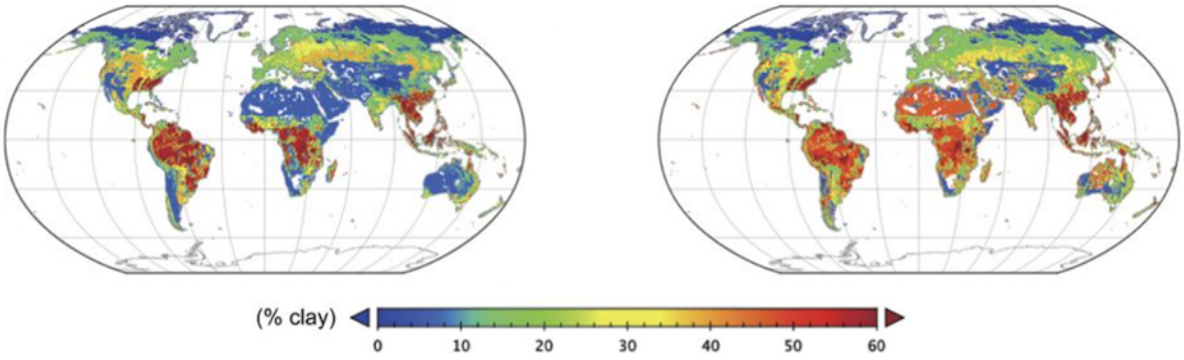

Figure 5.2: Global distribution of kaolinite clay according to Ito and Wagai (2017). Left: percentage of kaolinite clay in the topsoil, near the surface and easy to extract. Right: Percentage of kaolinite clay in the subsoil.

The second location-criteria for this study was that the main focus is on poor countries, where a substantial part of the population lives in extremely poor conditions, without decent shelter. According to the World Poverty Clock, 588 million people live in extreme poverty, which is 7.7% of the world population. The current rate of people escaping from extreme poverty is 0.5 people per second and this will lead to a situation in 2030 of still 479 million people that live in extreme poverty, corresponding to 5.8% of the world population by then. This problem is so huge that any solution, and any innovation, is very much needed to stop poverty. Time is here not as critical as directly after an emergency situation, and the focus can also be on building a pleasant neighborhood of printed shelters, thinking already of the future. However, the same design can of course also be used after disasters, when the reconstruction work has started. Figure 5.3 shows the locations in the world where people live in extreme poverty. In the red marked countries the poverty is rising, and in the green marked counties the poverty is slowly

decreasing.

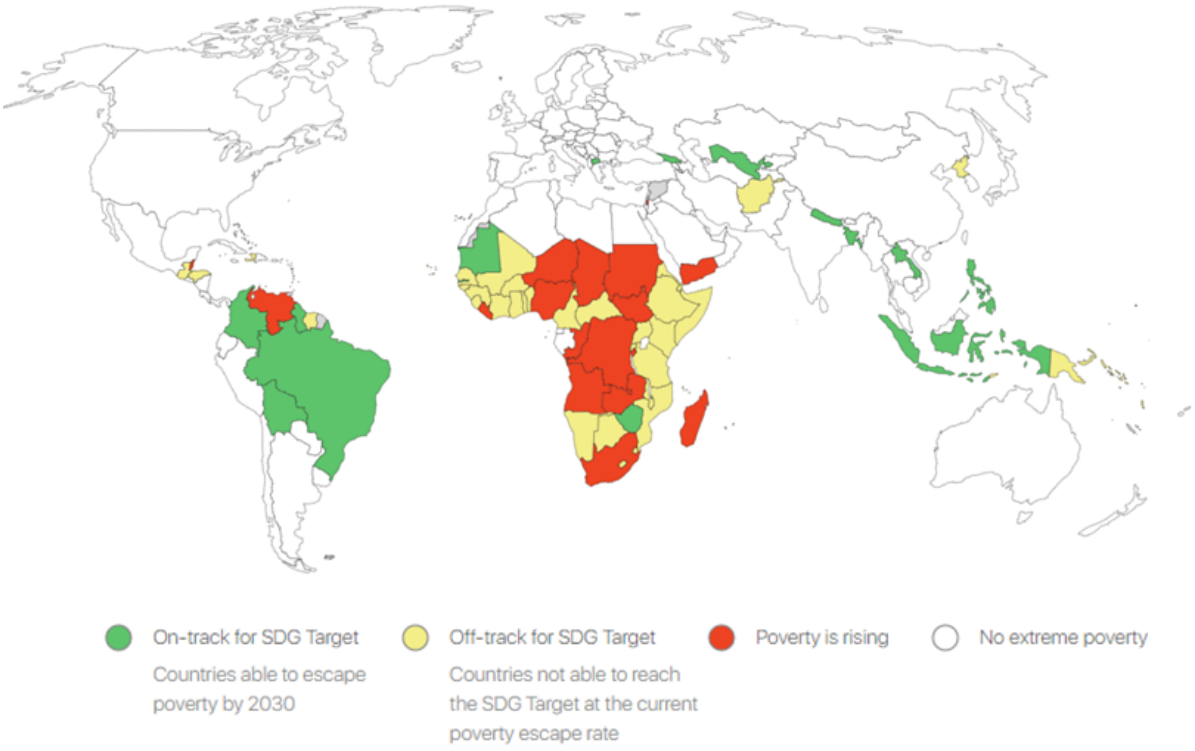

Figure 5.3: Global distribution of poverty (World Poverty Clock).

The third point of attention for determination of the location is a general overview where people were

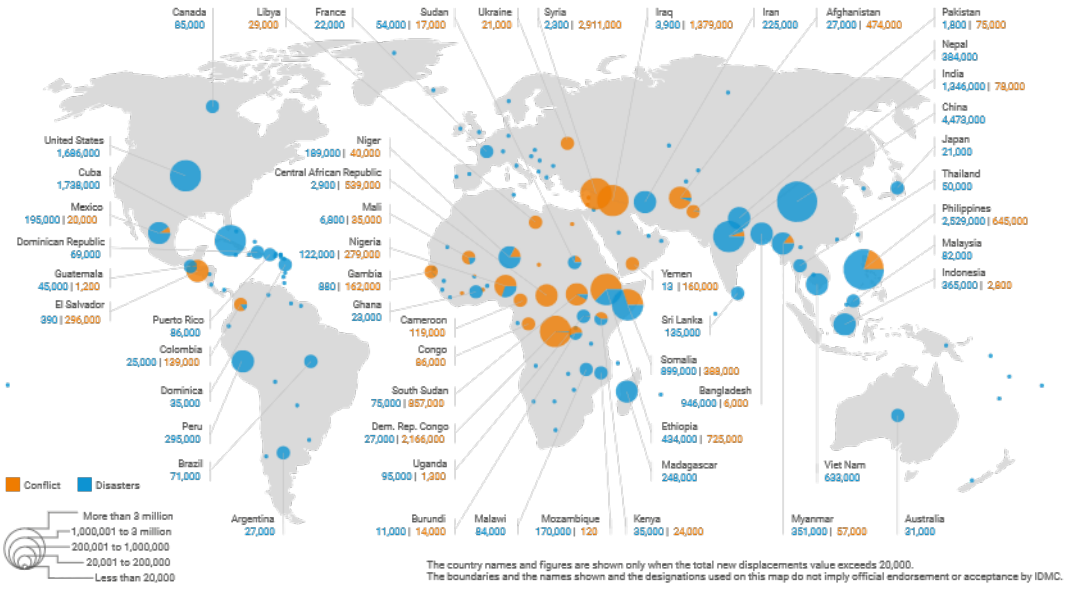

Figure 5.4: Global map presenting locations where people were displaced from their homes, cities, and countries due to conflicts and disasters (iDMC).

displaced on a national or international scale and had to leave their homes, due to poverty, disasters and conflicts. The International Displacement Monitoring Centre (iDMC) monitors the global distribution of the people that were displaced and have to find shelter elsewhere. According to the iDMC, a total of 28 million people were displaced worldwide in 2019: 10.8 million due to (political) conflicts and 17.2 million due to disasters. Figure 5.4 shows the regions where people are displaced, and gives a good overview where emergency shelters are needed.

The Final point of attention was the climate where the shelters can be built. Although the climate was not a very strict criteria, it is desirable that the shelters are build in a climate where temperatures are not extremely cold. It seems strange to mention this criteria, but the samples for the experimental research have been printed in summer with a temperature between 20°C and 35°C, and a relative humidity of around 80%. The relative humidity will not cause direct problems, because curing can also be controlled during printing by spraying a mist layer at the concrete filaments. Changing the temperature in an outdoor environment however, requires printing in heated tents, which can be a problem in poor and devastated areas. An other solution is to add chemical accelerators in the mix design to print at low temperatures. The influence of printing at very low temperatures was not investigated, but temperatures below zero, probably causes the individual filaments to freeze which will influence the mechanical properties of the interface, and therefore the mechanical performance of the complete structure.

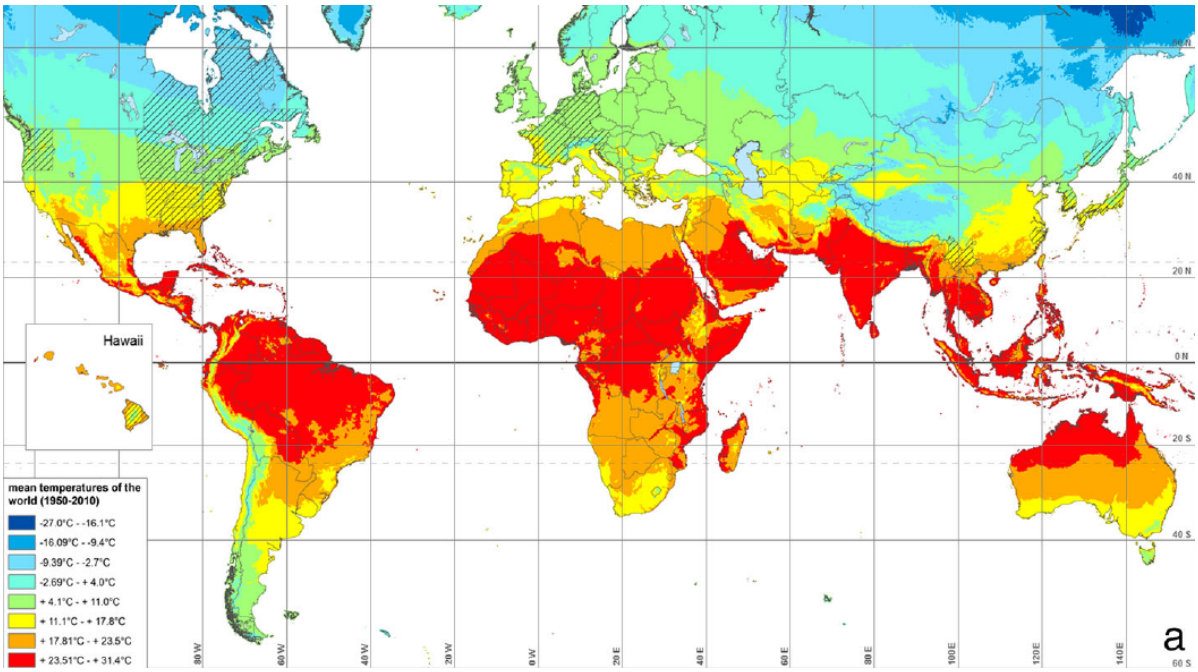

Figure 5.5: Mean temperatures of the world (Melaun et al., 2015).

5.2.4. Arguments for the location

Comparing the four global maps, each indicating a parameter of interest for this research, the location was determined. Based on the available kaolinite clay in the topsoil, the location should be around the equator. Given the distribution of poverty in the world, Africa shows the largest number of countries where poverty is rising and where people thus need help in finding shelter. The locations where people were most displaced from their homes, are widespread around the world. A high concentration of displaced people was however again in Africa, due to the poor conditions and civil wars. Also in parts of the USA people had to leave their homes, but here mainly because of natural disasters, like the hurricanes in the area of Miami. In the middle east, the people left most because of ongoing civil wars. The map showing the mean temperatures worldwide, had no influence on the choice of location, because the areas are mainly located around the equator, where very cold temperatures are not common.

For the continuation of this research, the location of the shelter was chosen in Africa, because of the poor conditions and the many displaced people. The climate is favourable for construction, and the kaolinite clay is widely available. The choice of this location does not mean that the shelter cannot be located elsewhere, but for the structural verification, the regular loads applied in Africa were used for further structural verification of the shelter.

5.3. Design aspects and shelter design

This section presents both design aspects, and a partially 3D printable shelter design, that can be printed in two to three days. The design was based on traditional emergency housing projects, and new design aspects related to 3DCP, all with the aspect of simplicity kept in mind. The design in this study is only suitable as a temporary shelter where people can live for several weeks to months. This limit was based on the simplicity of the shelter, the improvised roof and only minimum safety due to door- and window openings. In a future elaboration of this case study, measures could be presented to upgrade the two-day shelter solution to a permanent shelter. The main adjustment should then be related to the roof, comfort of living in the shelter and safety. In the next paragraph, minimum requirements for emergency shelters are presented, according to the UNHCR.

5.3.1. Minimum requirements for emergency housing

The UN Refugee Agency (UNHCR) is one of the international agencies with a lot of experience in providing emergency shelter. Their focus is especially on refugees, but their knowledge about emergency housing is applicable to anyone who needs immediate shelter. Therefore they developed an Emergency Handbook, describing the needs of people in emergency situations. The requirements for emergency housing describe for example the minimum floor area people need to be able to survive in emergency situations. Although these requirements are the very minimum, and not obliged by law, they served as a guideline for the design in this study. The main requirements are the following:

- In warm climates, people need at least 3.5 m^2 of living space per person. Cooking facilities are not included and are assumed to take place outside the shelter. The same holds for showering and personal care. Since the decision was made to focus on the continent of Africa, and other countries with the same climate, 3.5 m^2 of living space per person will serve as a guideline in this study. For cold climates the minimum living area increases to 4.5 m^2 per person, but this includes kitchen and showering facilities inside the shelter.
- The minimum height of an emergency shelter is 2 meters at the highest point. On the other hand, a larger height is not desirable because of the large area that has to be heated in case of cold weather.
- Any opening in the shelter, doors and windows, should be closed by panels, plastic, or other materials, in order to keep the indoor climate warm. Heat can be provided by a 5 to 7 kW stove, which can also be used for cooking indoor or outdoor.
- For long term use, no requirements were presented, but it was highly recommended to take into account that the requirements presented are the bare minimum, and that for long term shelter, people should look at the standardized shelter options, as presented in Figure 5.1.

5.3.2. Construction and Buildability

Before designing a floor plan for a 3D printable concrete shelter, it was necessary to consider the printing procedure, buildability of the concrete, and the number of shelters that can be printed at once. The floor plan should be designed together with the buildability- and print speed calculations. The first step was determination of the buildability of the filaments. The buildability is dependant on the green strength of the printed filaments and the weight added by the subsequent filaments. The green strength development of the filaments was determined according to Figure 3.1b, presented in the literature review. This graph shows the stress-strain graphs of the material that was 30 minutes to 4 hours old. According to Chen et al. (2020 (submitted), who did a similar calculation, 5% strain is a reasonable value to set as limit for the allowable strain. By creating a graph of the 5% stress-strain values, the green strength development can be visually checked in Figure 5.6, which is presented by the black graph. The other data shown in Figure 5.6 is the weight acting on the first printed filament, depending

on the amount of filaments printed subsequently. The weight per filament was calculated per mm^2. To calculate this stress, the dimension of the nozzle had to be determined first. The stress was calculated based on a nozzle dimension of 120x30mm, three times larger than the nozzle dimension used in the experimental research. This dimension has been chosen for the following reasons: 1) it was chosen to design the shelter with solid walls, because the material has not been tested for hollow wall elements, i.e. with rotatable nozzle parts, and thus also horizontally curved filaments. It is plausible that horizontally curved filaments have significantly lower mechanical properties; 2) since printed walls are solid, the walls had to be designed with a significant wall thickness. In the regular building industry, walls thicknesses between 100mm and 150mm are commonly used, like masonry and limestone brick walls; 3) according to Mechtcherine et al. (2019), it is possible to print with up-scaled rectangular nozzles. Several nozzle types were tested, each with a different scale factor. The largest dimension is 150x50mm, and printing of concrete at this scale, showed no difficulties.

The stress that one filaments exerts on other filaments was calculated as follows:

Volume of 1 mm^2 of filament	= 1mm x 1mm x 30mm	= 30 mm^3
	= 0.001m x 0.001m x 0.03m	= $3x10^{-8}$ m^3
Volumetric weight of concrete	= 25 kN/m^3	
	= 25000 N/m^3	
Weight of 1 mm^2 filament	= 25000 x $3x10^{-8}$	
	= 0.00075 MPa	
	= 0.75 kPa	

With the stress of one filament known, the graphs representing the buildability of the material were created (see Figure 5.6). In order to print a buildable wall, the buildability graphs should lie below the black graph, representing the strength of the green concrete. For the determination of the buildability of the walls, only the gravitational weight of the filaments was taken into account. Buckling of the walls, or eccentric loading due to inaccurate positioning of filaments, were not considered.
Figure 5.6 shows both the green strength of the concrete and the stress on the first filament, depending on the number of printed filaments. The presented time intervals are 1) 20 seconds, which is unrealistic for printing elements and unfavourable for the buildability of printed elements; 2) 1 minute; could be realistic for printing elements, but the buildability is still unfavourable, and 3) 10 minutes, the time interval from which no problems are expected, also with continuous printing. The expected strain of walls printed with 10 minutes time interval is even lower than 5%, because the buildability curve is not even close to the maximum allowable stress. Printing with smaller time intervals is possible, but then people that are printing need to take into account that they have to stop after 7 filaments when printing with one minute time interval. The work can then for example continue after 3 hours, and at that time the strength properties are also known. For the continuation of this study, filaments printed with a time interval of 10 minutes were considered for further calculations.

When filaments are printed with a time interval of 10 minutes, it is possible to print 36 meters of concrete, assuming a similar print speed of 60 mm/s. This speed was used during the experimental research. Assuming that two shelters are printed at the same time (one completed filament, for two shelters, in a 10 minute time interval), the available print-path length for one shelter is approximately 16 meters. The assumption was made that the printer needs one minute move to the next shelter.

Determination of the floor plan
With a length of 16 meters of continuous printed filament available for one shelter, the following dimensions are suitable to print:

- 4m x 4m (16 m and 16 m^2)
- 3.5m x 4.5m (16 m and 15.75 m^2)
- 3m x 5m (16 m and 15 m^2)
- 2.5m x 6m (17 m and 15 m^2)

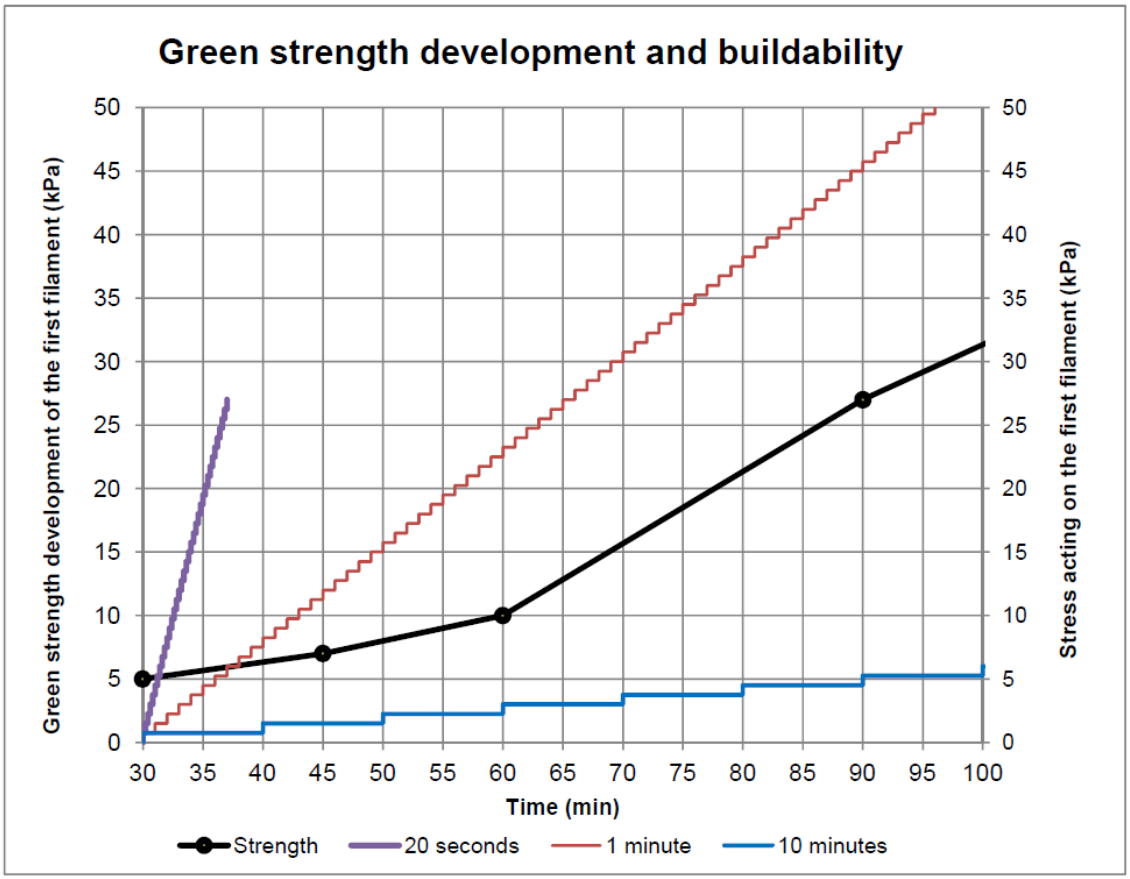

Figure 5.6: Multi-purpose graph showing the buildability of the material (MCC), and also the stresses acting on the first printed filament depending on the tine interval. The buildability can be verified if the tresses acting on the first filament remain below the green strength at any time.

These dimensions are based on outer walls only. This decision was made because in emergency situations, having a decent shelter is more important than having multiple rooms. The floor plan is chosen at 3m x 5m, because the length of the shelter creates possibilities to separate the floor area in usable space, which is more important than the total floor area available. Future research should focus on the interior design of the shelter, and was not considered in this research.

5.3.3. Design considerations

Designing 3D concrete printed structures requires knowledge about the printing process, knowledge about the critical design aspects, but more important, knowledge about the limitations of this construction method. In this section the main points of attention are presented, especially focused on the shelter design and construction aspects.

Foundation and ground floor

An essential aspect for the printing process is a good foundation. During construction, the quality of the foundation determines the quality of the walls, because any irregularity in the foundation is directly visible in the stacked filaments. The foundation should therefore be perfectly flat. The foundation can be cast on well compacted sand. Reinforcement for the foundation and the floor slabs were not considered, because of the small loads and the expected issues installing reinforcement takes with it in poor and devastated areas. Since only a one storey shelter was designed and the loads are equally distributed over the foundation, no large differences in settlement were expected. Figure 5.7 below, shows a 3D view of the foundation. The construction of the foundation is the first step in the construction process.

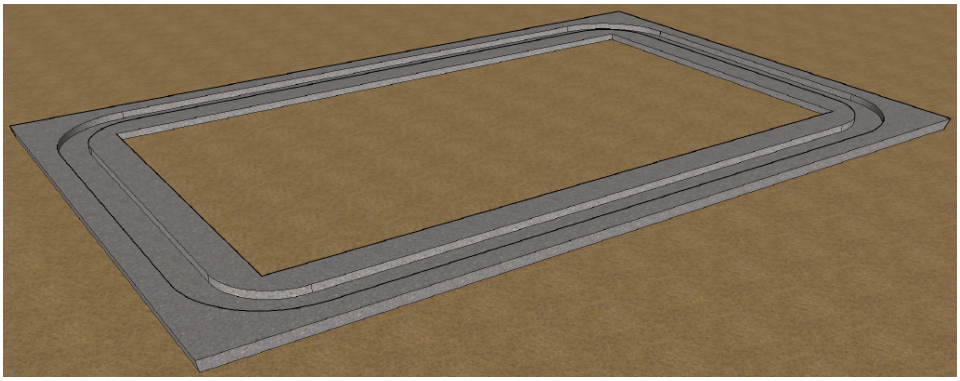

Figure 5.7: 3D view of the foundation.

There are no special requirements for the bottom side of the foundation and the floor slab. The sand should be digged out by hand or by a small excavator, after which the soil can be compacted manually. Figure 5.8 shows a dilatation at the connection between the floor slab and the foundation. Since the foundation bears much more loading compared to the floor slab, differences in settlement can be expected here. Cracks are likely to occur at this position, because of the absence of reinforcement. Therefore the floor and the foundation should be separated by a dilatation. The foundation can then settle separately from the ground floor. Finally, to prevent differences in height between the foundation and the floor slab, the ground floor can best be cast when the walls are printed. The largest settlement has then already occurred.

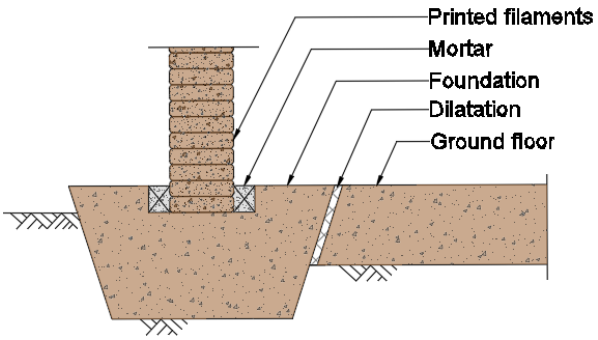

Figure 5.8: Foundation detail.

A critical aspect regarding the load distribution of the walls, has to do with the connection of the walls

to the foundation. In other words, if the walls are printed on a flat concrete slab, the walls have no horizontal connection to the foundation. This means that all lateral loads need to be transferred to the foundation by means of friction only. To ensure lateral stability of the walls in extreme loading situations, a precaution should be taken in the form of a gutter that can be created in the foundation. This principle can also be seen in Figure 5.8. The first filaments of the walls should be printed in the gutter. When the first filaments have hardened, it is possible to cast the remaining area of the gutter to fix the filaments in horizontal direction. Because no reinforcement is used, this connection should still more or less serve as a hinge. This gutter can be crated by applying a styrofoam or polystyrene panel before casting the concrete. By removing these panels afterwards, the gutter remains.

Walls

Printing the walls is the second step in the construction procedure. One of the main difficulties with 3D printed concrete, is that one layer for the wall should be designed as one continuous filament. If this is not the case, there will be weak spots in the walls, because there is no reinforcement present. Furthermore, at some positions the volume of printed concrete is affected because of the stopped, started, or interrupted material flow. This has an effect on the nozzle standoff distance, affecting the mechanical properties of parts of the wall, and therefore the quality of the complete structure. A 3D printable design should therefore be such, that the floor plan can be printed continuously, without interruptions. This is one of the reasons that the shelter has only outer walls. Designing with inner walls as well, is difficult if solid walls are used. The inner walls should be connected to the outer walls by other mechanical measures, which will probably require skilled people to install. A different wall system can also be used, and is explained further in the discussion of this thesis.

Corner radius

As mentioned during the literature review, changing the printing direction with a rectangular nozzle, can lead to an excess of material in the inner corner, and to an under fill of material in the outer corner. For the shelter, the the corners of the walls are designed with a significant radius, to prevent difficulties during printing. The radius is 0.5 meters. This decision was not based on any research. The walls are shown in Figure 5.9.

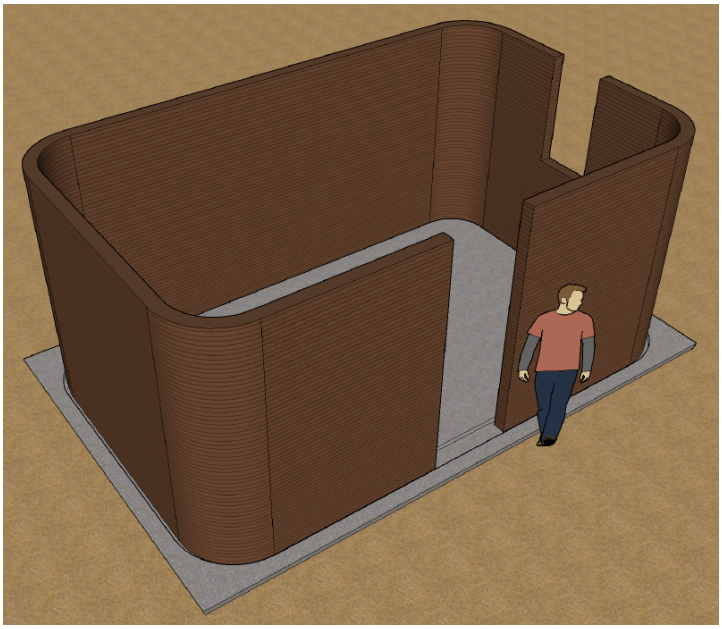

Figure 5.9: Door and window openings created all the way to the top of the walls. Also the corner radius of the walls is visible.

Doors and windows

Although doors and windows are not desirable for a continuous printing process, a minimal amount of

daylight and ventilation, as well as an entrance, are unavoidable in the shelter design. To minimize the extra activities to create windows and doors, filaments should not be printed above the door and the windows. Above the door, a window can be installed. The window was designed all the way to the roof. The main advantage of this solution is that no support beams are needed to support printed filaments above wall openings. This speeds up the printing process. Figure 5.9 shows the door and window openings.

Roof design
The final step of the shelter design was the design of the roof. This paragraph therefore presents three possibilities for the roof design of the shelter. A concrete printed roof, a timber roof and a sprayable styrofoam roof were all investigated.

3D printable roof
3D printing a concrete roof seems with the current technology not yet feasible. When considering a horizontal roof, formwork and reinforcement are still needed. Also taking into account that the construction procedure should be as simple as possible, printing a horizontal concrete roof was not considered. An alternative solution is to print concrete arches. The main advantage of arches is that most of the stresses in an arch are compressive stresses. The only problem is that the lateral forces from the arch should then be taken by either the walls or a tensile element connected to the arch ends. These principles are shown in Figure 5.10.

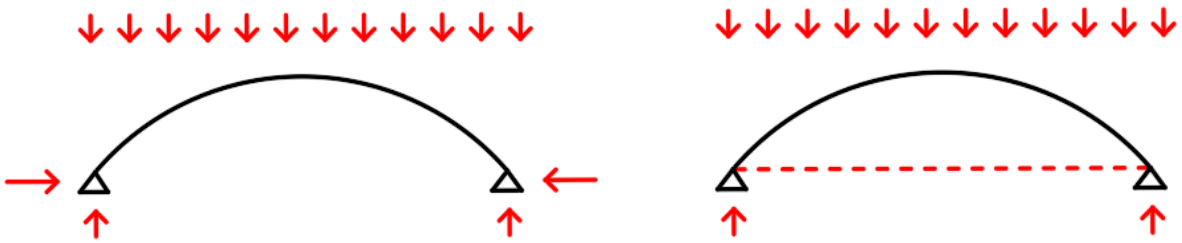

(a) Arch exerting horizontal forces on the walls

(b) Arch where horizontal forces are taken up by a tensile element (red dashed line)

Figure 5.10: Principle of forces introduced by arches.

This roof design also has disadvantages. Printing a dome or arch-like structure is for example possible using a robot printer and an air cushion to print on. However, the construction process is then critical. Also printing the arches on the ground floor, on their side, is not a possibility because then the arches need to be lifted on the walls, requiring either a crane, or a lot of people. The chance of breaking the unreinforced arches is therefore dangerously high. For this reason the design of a printable roof was not considered for the further elaboration of the shelter design.

Sprayable styrofoam roof
The second option was a hypothetical roof design, namely the construction of a sprayable, styrofoam roof. This idea is a variant of emergency shelters constructed in the past, in for example Turkey and Japan. The shelters in Turkey were built in the days after a devastating earthquake in 1970, in Gediz. The shelters were called igloos because of their dome shape. They consist of a 10 centimeter thick styrofoam shell only (Mitchell, 1976). Expandable styrofoam was sprayed on an inflated balloon and a door was cut afterwards. These shelters were intentionally built for several months after the disaster, but in 1973 the igloos were still intact and undamaged. See Figure 5.11a.

The styrofoam houses in Kyushu, Japan, are shown in Figure 5.11b. The shelters were built on a larger scale, and the construction method differed from the shelters in Turkey by the fact that prefabricated styrofoam panels were used to construct the house. The thickness of the panels was variable, where the thickest section, a roof section, had a thickness of about 450mm (i-domehouse). This seems thick, but considering the span of about 6 meters, for a material that has not been used as a structural material before, this is still a remarkable solution.

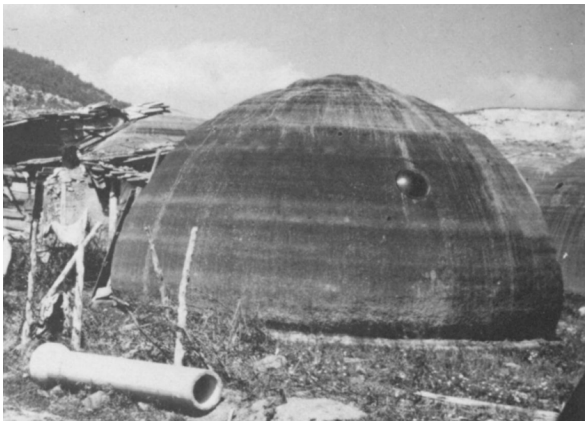

(a) Gediz, Turkey (Mitchell, 1976)

(b) Kyushu, Japan (i-domehouse)

Figure 5.11: Two examples of styrofoam shelters / houses.

The idea was to design a dome-shaped sprayable styrofoam roof. An air cushion can be inflated inside the constructed walls of the shelter, and the styrofoam can be sprayed over the inflated balloon. The connection of the roof to the walls can be made by inserting metal anchors in the top filaments, at which the styrofoam will automatically connect with when the styrofoam is sprayed over the anchors. An impression of this solution can be seen in Figure 5.12

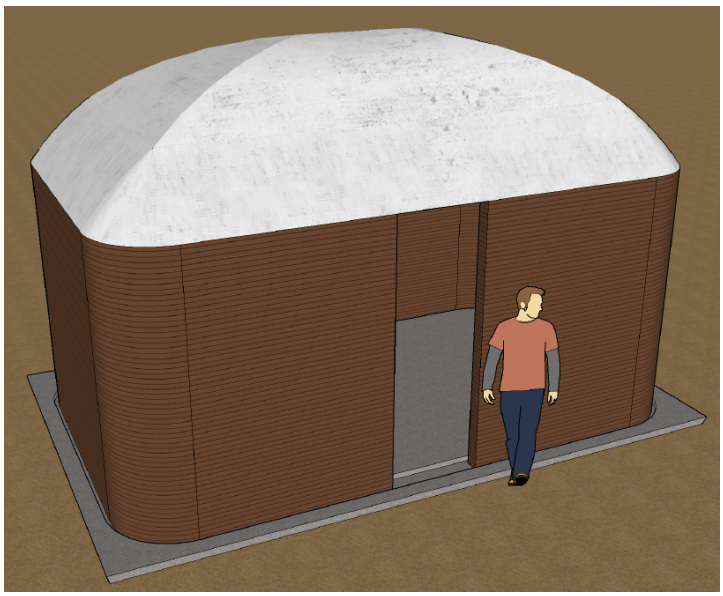

Figure 5.12: 3D impression of a sprayable styrofoam dome roof.

At last, a remark must be made about the sustainability of this roof solution. Styrofoam cannot be considered as a sustainable solution, because the material is not naturally degradable and a lot of harmful substances are emitted when the material is recycled. On the other hand, one may ask the question if sustainability should be a decisive argument in case of an emergency situation, because with this roof solution, the shelter design is buildable within two to three days. Structural verification of the styrofoam roof was not further considered in this study.

Timber roof

The last possibility for the roof design that was considered in this study is the use of timber. Timber is a commonly used construction material for simple roofs. The material is cheap and CO_2 neutral.

To simplify the roof design, to save costs, and especially to save time, trees without treatment can be used. As long as all the branches of the bark are removed, the stem of trees can be used as a structural beam for the roof. A mono-pitched roof, with a slope of around 15 degrees, is a good option. This roof type has as advantage that the windows for the shelter can be positioned in the vertical part of the roof, instead of in the printed walls. Especially the printing process can be simplified with this decision. Figure 5.13 shows a 3D overview of the timber roof, and the possible position for the windows in the vertical part of the mono-pitched roof.

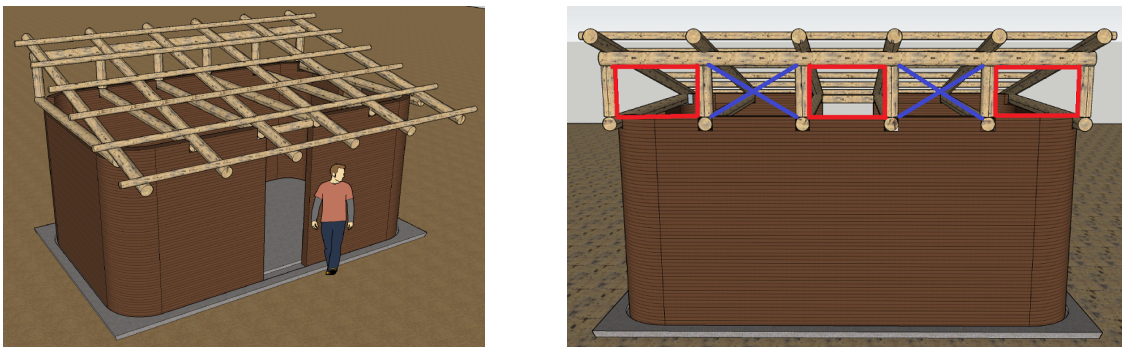

(a) 3D view of the timber roof option.

(b) Windows in the vertical part of the roof.

Figure 5.13: Overview of the timber roof option.

Anchoring of the roof

Because of the high wind loads that might be exerted on the shelter, the roof should be anchored. Anchoring the roof to the walls is possible, but the walls are unreinforced and the upper filaments will be loaded in pure tension when strong winds hit the shelter, and try to lift the roof. For this reason, the roof should be anchored to the foundation. The self weight of the foundation and the walls should provide enough counter weight to anchor the roof safely. Anchoring the roof can be done by means of simple steel cables, connected to both the foundation and the timber trusses. Steel anchors need to be cast in the foundation to connect the cables to the timber trusses. When the roof is finished, steel cables can be connected to both the roof and the foundation. These cables are visible outside the shelter.

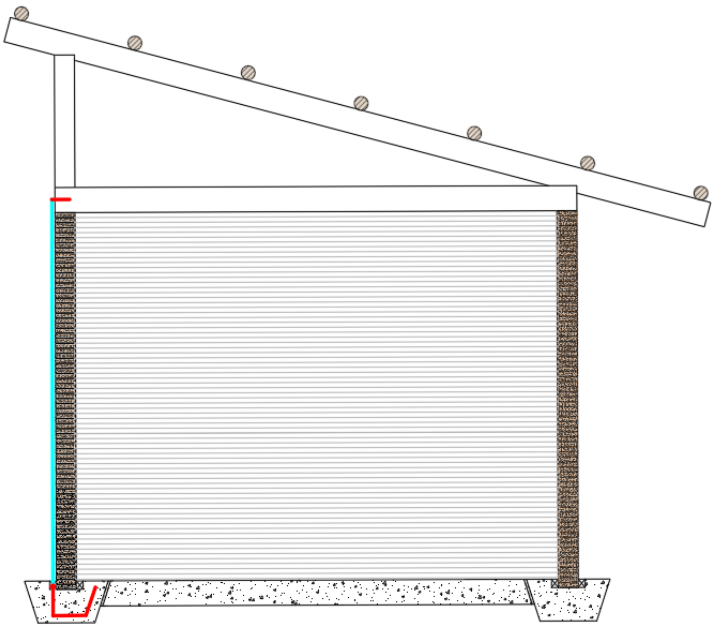

Figure 5.14: Anchoring of the timber roof.

Choice of the final roof design
Based on the three possible roof designs presented before, the timber roof design was chosen for further structural verification of the shelter. Not because this solution shows the best potential, but because this solution can be made in practice without a doubt, and the loads on the roof can be determined according to the codes.

Construction procedure
The construction procedure of the shelter was already partially mentioned during the previous paragraphs. Two shelters will be constructed at the same time, and in order to do so, the shelters should be located next to each other. The printer can be located on a rail system and can move from the first to the second shelter within a minute. In Figure 5.15 below, the rail system and the two shelters are shown. the rail system can be extended in order to print the next two shelters the other day. The rail system should be installed on a well compacted soil, in order to prevent settlement of the rail system and the printer. Settlement will lead to differences in the nozzle standoff distance, causing an inaccurate printing process if the nozzle standoff distance is not calibrated for every filament.

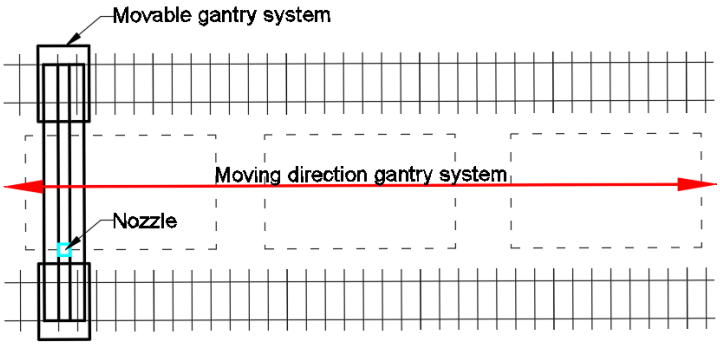

Figure 5.15: Principle of the movable gantry system.

5.3.4. Shelter design

The final design is presented in this section. Simplicity was key during the design procedure, since the construction process should be as short and as simple as possible. The design is shown based on the timber roof solution, because for now, this is the most detailed solution. A 3D view and the 3D intersection are shown below.

(c) 3D view of the printable shelter.

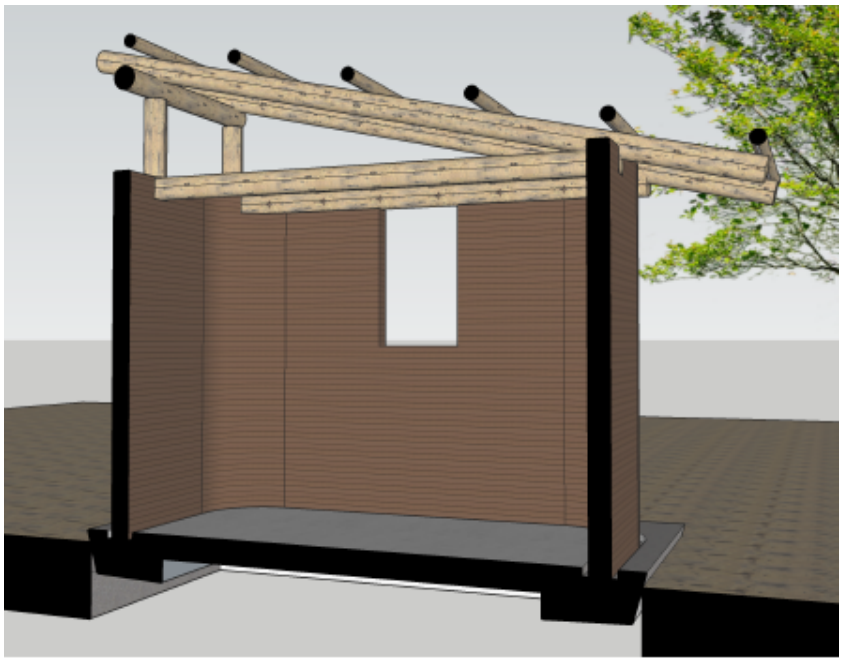

(d) Intersection of the printable shelter.

Figure 5.15: 3D intersection of the shelter design.

5.4. Structural verification

The final section is a continuation of the finite element analysis. Based on the material model that has been created, a structural verification of the shelter was performed on the shelter type with the timber roof option. The verification was performed in two steps. The first step was the verification of one small wall element, with a width of 50 centimeters. With this calculation, an indication of the structural performance of the wall was obtained fast. If this calculation showed that the wall was too weak, adjustments in the wall design could be easily made. The second step was the verification of the complete shelter. The main difference between the two verifications, is the mechanical system. The wall element was modelled as a wall supported by hinges at the top and bottom, so the interfaces cause failure of the wall. The complete shelter had no support at the top, because the over-all stability of the shelter is guaranteed by the perpendicular walls. The exact failure mechanism was not known for the final analysis. Before any calculation was performed, the loads were determined, according the African design codes.

5.4.1. Load cases

The loads that were exerted on the building were determined according to the national guidelines governing for the region where the shelters can be built. In this case study, the area of interest was chosen to be Africa. The loads that were taken into account for the shelter were vertical loading and wind loading only. Snow was not considered. The guideline for designing structures in most of the counties in Africa, is based on the Eurocode. The main differences are related to the partial safety factors and country related loads, like wind. The South-African National Standard provides all necessary information regarding the permanent and variable loading.

Vertical loading

The vertical loading consists of the self weight of the roof only. Variable loading is not applicable if maximum wind loading is assumed. The following loads were applied:

Load type	Characteristic load [kN/m^2]	Partial safety factor	ULS load [kN/m^2]
Selfweight	0.7	1.2	0.9
Total load ULS			0.9

The loads were exerted on the walls as if it is a line load, instead of six different point loads. This simplification was made because the loads will spread to the foundation. The span of the roof is 3 meters, and taking the cantilever part into account (=0.8m), the load acting on the wall is (1.5 + 0.8)m x 0.9 kN/m^2 = 2.0 kN/m. The self weight of the wall was also taken into account.

Lateral loading

Lateral loading is introduced by the wind. The windloads were calculated based on the peak wind speed governing in the specific area. Since the shelter can be positioned anywhere in Africa, the maximum wind speed was determined based on the wind speeds in Mali. Mali is the country with the highest wind speeds in Africa, namely 69 m/s as peak wind velocity. This data was obtained from the Shelter Research Unit from the International Federation of Red Cross. In this document all wind speeds in most of the countries on the world are presented, based on the Eurocode. Calculations according to the South African National Standard showed that the maximum characteristic value of the wind pressure is 2.97 kN/m^2. After applying partial safety factors, the walls should be able to resist 3.86 kN/m^2. This means that the resistance of the wall should be more than 3.86 kN/m^2, based on the wind loading. The complete calculation of the wind loading on the walls, is presented in Appendix C.

5.4.2. Numerical analysis of a wall element

The first finite element analysis was performed on a simple wall element. The wall element is simply supported with hinges at the top and at the base. Both a reference wall element without interfaces and a printed wall element were modelled, to see if the printed wall showed similar behaviour as a cast, non-reinforced, wall. Figure 5.16 shows the model made in DIANA. The height of the walls is 2.4m, the width of the walls is 0.5m and the thickness of the walls is 120mm.

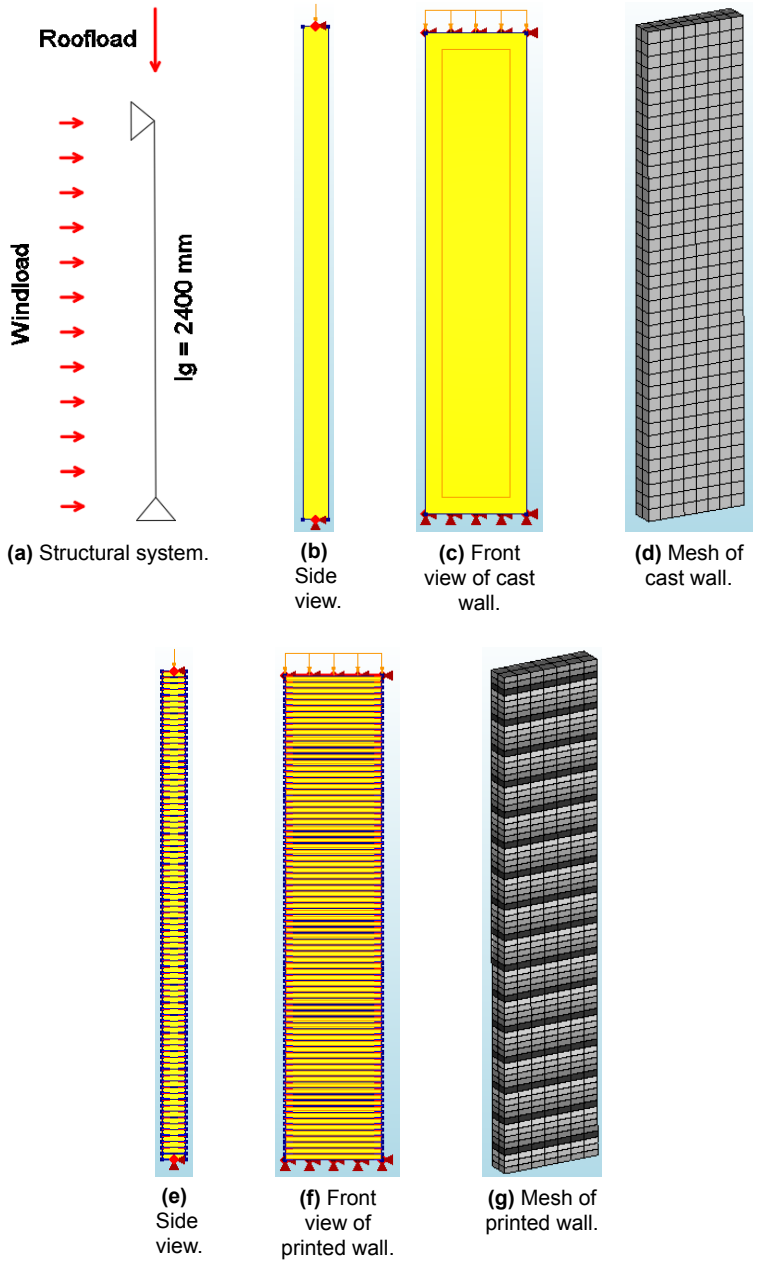

(a) Structural system. **(b)** Side view. **(c)** Front view of cast wall. **(d)** Mesh of cast wall.

(e) Side view. **(f)** Front view of printed wall. **(g)** Mesh of printed wall.

Figure 5.16: Wall elements in DIANA.

loads on the wall

The vertical and horizontal loads were applied on the wall. A distinction was made between the horizontal loading and the vertical loading. The vertical loading was applied first, in 20 steps. The horizontal loading was applied second, but this load is much higher than the calculated wind load. This was done on purpose, to calculate the failure load of the walls. The wind load was applied in small steps, until failure of the wall occurred. When the horizontal failure load was known, the ultimate wind load was calculated, and should be higher than the ULS wind load.

Results

The analysis of the results was performed based on the horizontal deformation of the wall and the vertical stresses in the wall/interfaces. These results are shown in Figure 5.17.

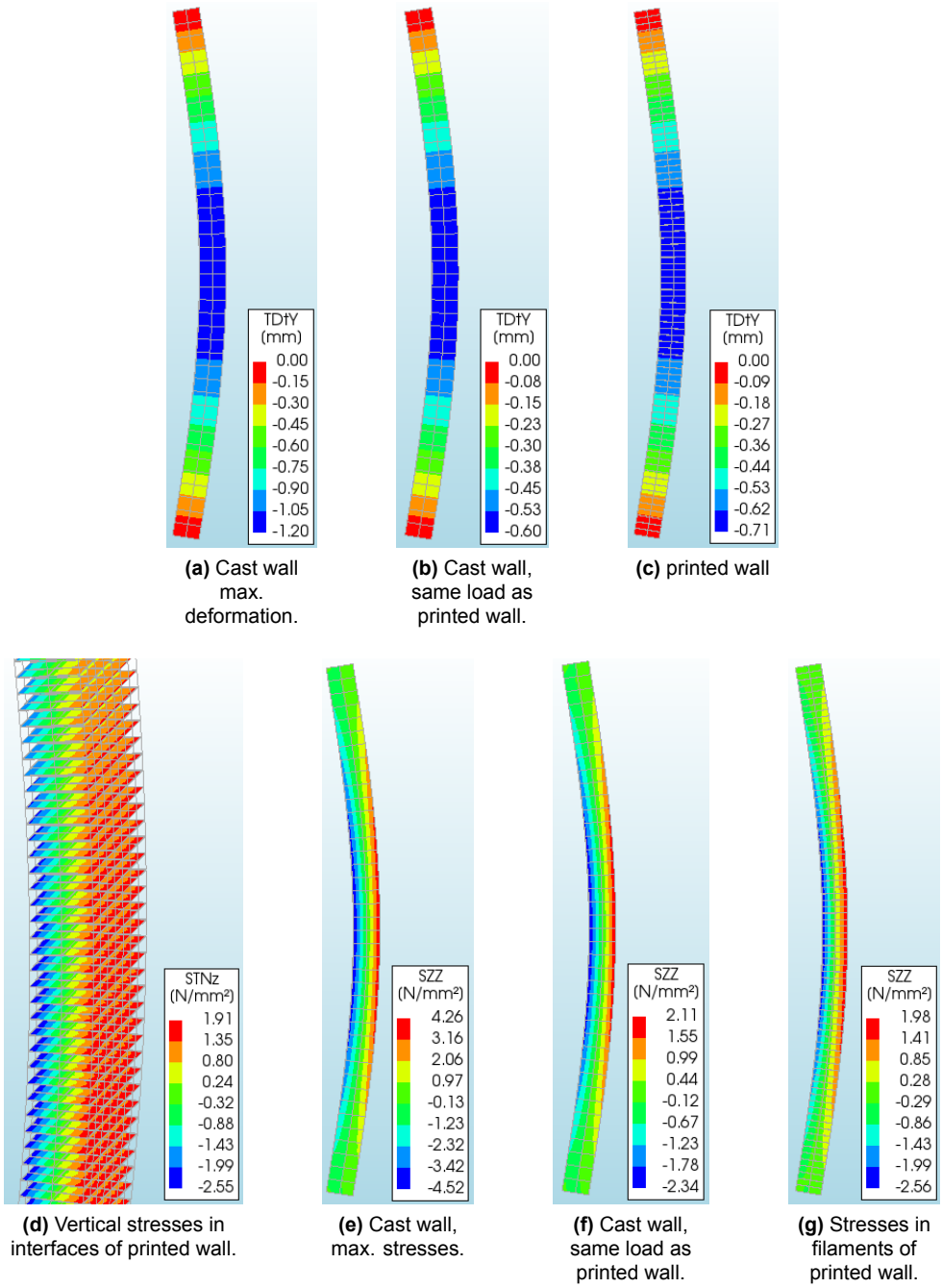

(a) Cast wall max. deformation.

(b) Cast wall, same load as printed wall.

(c) printed wall

(d) Vertical stresses in interfaces of printed wall.

(e) Cast wall, max. stresses.

(f) Cast wall, same load as printed wall.

(g) Stresses in filaments of printed wall.

Figure 5.17: Results of the finite element analysis for the wall elements. The horizontal deformations and vertical stresses are presented.

A comparison of the results showed that the deformation of both the printed wall and the cast wall showed almost similar deformation and stresses. Small differences could be allocated to the fact that the compression behaviour of the interface was not exactly known, and to the fact that the interface deformed more than cast concrete. The vertical loads were applied on the walls without any problems. The walls failed due to the step-wise wind loading. The printed wall failed at a wind load of 7.4 kN/m^2, and the cast wall failed at a load of 14.7 kN/m^2. This simplified calculation showed that the cast wall has significantly more capacity. On the other hand, when the maximum load of the printed wall was verified with the minimum wind load that it should be able to resist, then there was no problem, and both walls complied with the code. A more detailed model could thus be made, without any modifications to the wall dimensions.

5.4.3. Numerical analysis of the complete shelter

With the knowledge that a simple wall element complies with the code, a more sophisticated analysis was performed. The walls of the complete shelter were modelled without supports at the top. As mentioned before, the perpendicular walls provide the over-all stability of the walls. The material model was kept the same, and the interfaces were varied according to chapter 4.3. The model is shown in Figure 5.18.

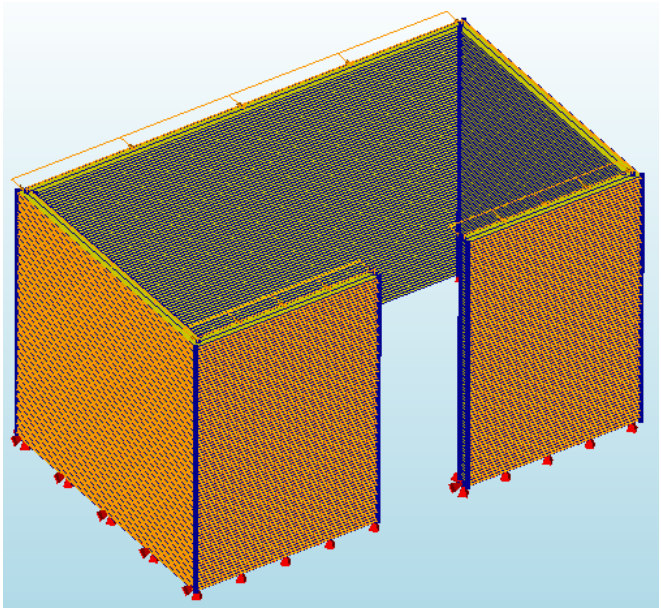

Figure 5.18: Model for numerical calculations, including the loads and supports.

The curved edges were not modeled. The self weight of the roof was kept the same as for the wall element, but the wind loads were more extensive for the complete shelter. On all walls exerted a wind load, and internal pressure coefficients were also taken into account, this is presented in appendix C.1. Three calculations were performed. The first two directions varied in wind direction. The difference is a positive or negative internal pressure coefficient, based on the location of the large door opening. The third calculation was based on no internal pressure coefficients. It is plausible that windows or doors are opened or removed, so the structure should be able to resist the wind loads, if no internal pressure is exerted on the walls. The results of the full calculations are shown in Figures 5.19, 5.19, and 5.20. Both the global deformations, and the stresses in the filaments and interfaces are shown, in the governing directions.

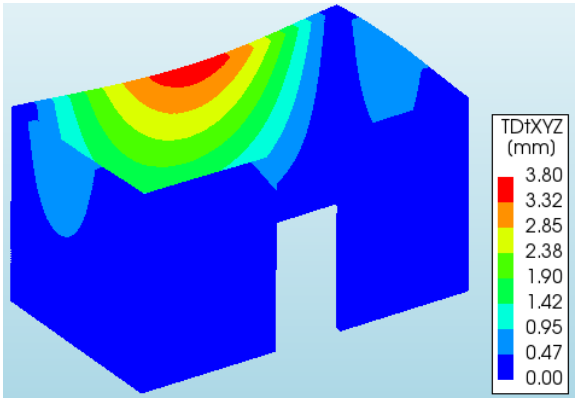

(a) Global deformations.

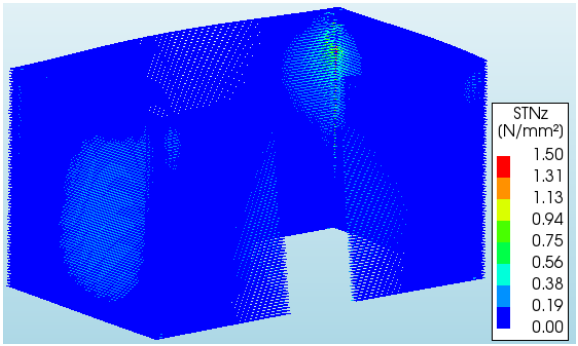

(b) Stresses of the interfaces in Z direction.

Figure 5.19: Results of the shelter where the windload is calculated with a negative internal pressure coefficient.

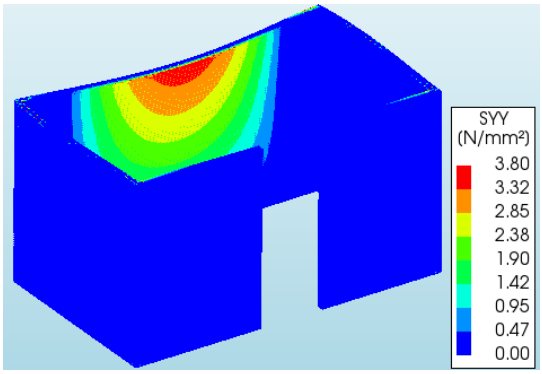

(c) Stresses of the filaments in horizontal direction (1).

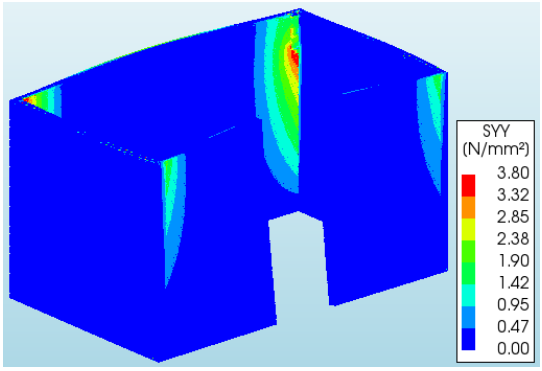

(d) Stresses of the filaments in horizontal direction (2).

The failure mechanism differs from the simple wall element that was modelled before. With the wall element, the failure took place at one or more interfaces that failed due to insufficient tensile capacity. The failure mechanism that can be seen for the complete shelter, with the first wind load combination, is horizontal buckling of the walls, at the top edge of the 5 meter wall. The tensile strength of the filaments, in longitudinal loading loading direction caused the failure. The mean tensile strength of the filaments is around 3.7 MPa in longitudinal direction. The interfaces, on the other hand, have sufficient capacity. Bending around the a horizontal axis, which leads to tensile stresses in the interfaces, did not cause failure of the walls. The tensile stress in the interfaces is around 1.5 MPa, and is more than sufficient, as can be seen in Figure 5.19b. The failure of the shelter takes place at an external pressure of 5.4 kN/m^2. The wind load in the ULS is, after application of the the partial safety factor of 1.3, 4.15 kN/m^2. Which is more than the ULS design load.

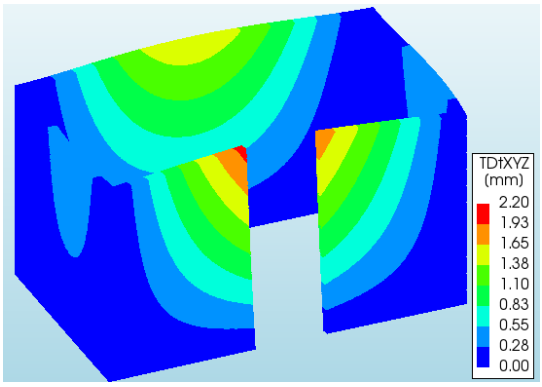

(a) Global deformations.

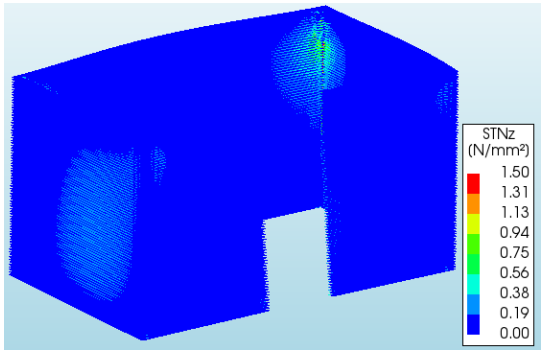

(b) Stresses of the interfaces in Z direction.

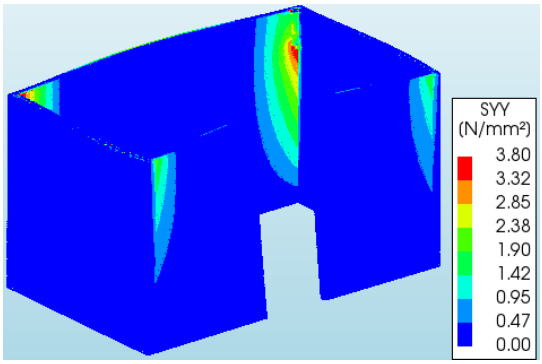

(c) Stresses of the filaments in horizontal direction (1).

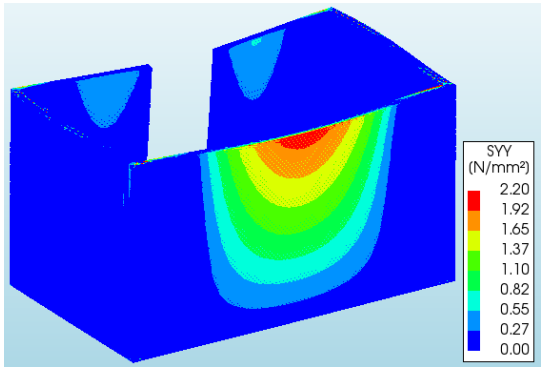

(d) Stresses of the filaments in horizontal direction (2).

Figure 5.19: Results of the shelter where the windload is calculated with a positive internal pressure coefficient.

The second wind load combination included wind loading with a positive internal pressure coefficient. The main difference is that the wind can come from the other side, causing over-pressure in the building if the door is opened. The failure occurred at the closed wall of 5 meters, where both the internal corners and the mid-part of the wall fail due to large horizontal stresses. The stresses in the interfaces, in vertical direction, were again not significant, and thus safe. The failure load of the wind is 4.5 kN/m^2, which is 3.46 kN/m^2 in the ULS. This means that the capacity of the structure is not sufficient according to the code. Discussions about this results follow in chapter 6.

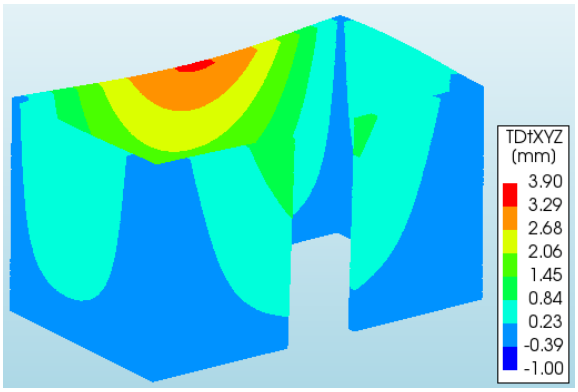

(a) Global deformations.

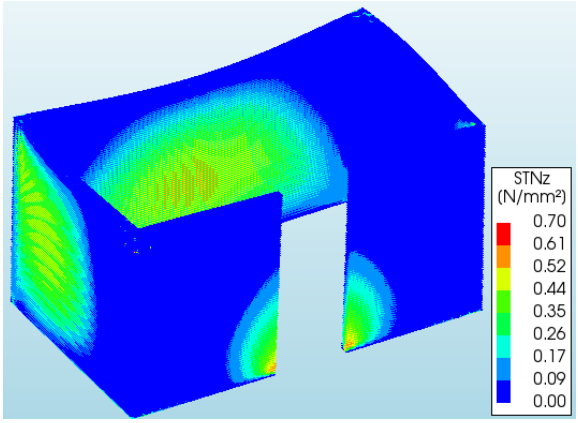

(b) Stresses of the interfaces in Z direction.

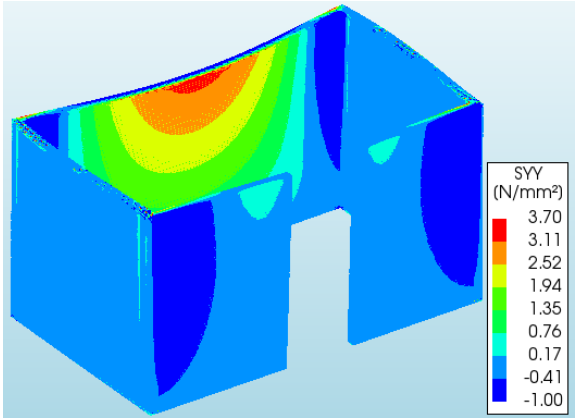

(c) Stresses of the filaments in horizontal direction (1).

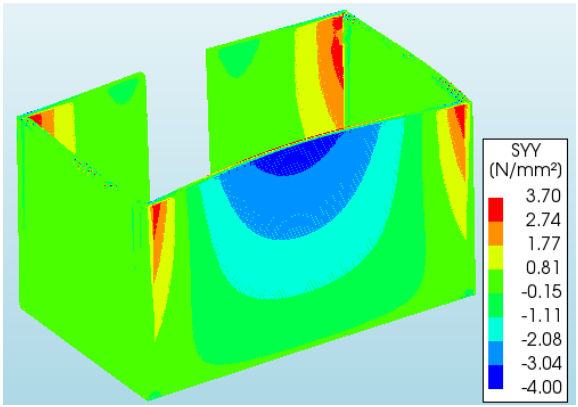

(d) Stresses of the filaments in horizontal direction (2).

Figure 5.20: Results of the shelter where the windload is calculated without internal pressure coefficients.

The last load combination, without any internal pressure coefficients, also fulfilled the requirements. The maximum windload that can be exerted on the shelter, assuming no internal pressure, is 6 kN/m^2. After deviding by the partial safety factor of 1.3, the ULS wind load is 4.62 kN/m^2, which means this load combination resulted in the highest capacity of the structure.

6

Discussion

The gained knowledge about the printing process, and the possibilities for the use of the 3D printing technology in practice, is critically analyzed in this chapter. The experimental results are analyzed, compared to literature, and judged for their correctness. Finally, the feasibility of the emergency housing project is reconsidered.

6.1. Experimental part

6.1.1. Anisotropic compressive strength

The anisotropic strength of printed samples was observed during the compressive strength tests. The strength in perpendicular loading direction was between 16.3% and 24% lower compared to the strength in longitudinal loading direction. The lateral loading direction was between 8.3% and 17.1% lower than the strength in longitudinal loading direction. These results are in accordance with the results found by Nerella et al. (2019), and Ma et al. (2019). The material properties of the tested material and the material used in these articles, were comparable for their strength, but the extrusion direction of the nozzle was different, i.e. a nozzle with down flow, exerting some vertical pressure on the printed filaments. Also the flow rate was different and the mix design could not be compared. The results of Sanjayan et al. (2018) were however somewhat contradicting to the results found in this research. The longitudinal loading direction showed the highest strength, but the lateral direction was up to 50% weaker compared to the longitudinal direction. Differences could be explained by different dimensions of the samples (50x25x30mm).

Reference material

The reference material was cast to compare the printed samples to samples that were cast. The result was that cast samples have a compressive strength that was at least 18.5% lower than the weakest printed samples, in perpendicular loading direction. The reason for this was the degree of compaction of the materials. The cast samples were not compacted at all, because for the printed samples also no manual compaction was applied. However, due to the addition of VMA in the material, the rheology of the concrete decreased significantly, which changed the self-compacting properties of the concrete. Although the printed samples were not compacted, the pressure and friction in the hose led to some compaction of the material. The degree of compaction was not quantified, only visually observed. This conclusion is supported by the CT-scanning results, where the cast samples showed much larger and much more voids than the filaments of the printed samples, as can be seen in Figure 6.1.

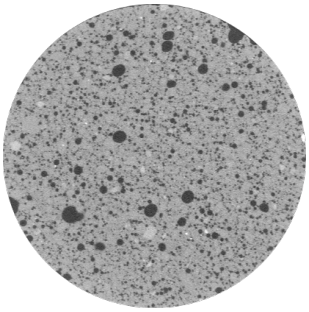

(a) Horizontal cross section of the cast samples

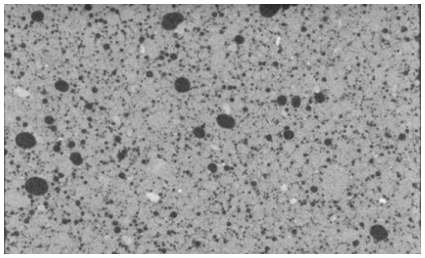

(b) Vertical cross section of the cast samples

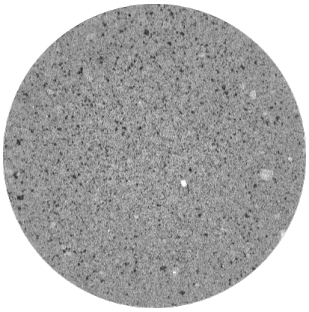

(c) Horizontal cross-section of printed sample, 1 minute time interval

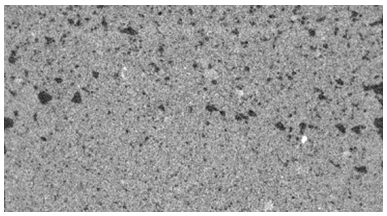

(d) Vertical cross-section of printed sample, 1 minute time interval

Figure 6.1: CT scanning results showing the difference in porosity between the printed and cast samples.

Results of printed samples

The results of different process parameters were not significant (direction 1, 2, and 3, respectively, compression only). On the contrary, the compressive strength did not decrease at all, with increasing time intervals, and different curing conditions. The only outliers were the samples printed with three hour time interval, cured with a layer of mist. The same phenomena was observed by Sanjayan et al. (2018), where the compressive strength decreased dramatically when a thin water layer was visible at the printing surface. From this, the conclusion could be drawn that when the samples are cured with a mist layer, it is important that the mist is fully dried when the next filament is printed, in order to prevent large void filaments between the filaments. During printing of the samples, the printing surface seemed almost dry, but still some shimmer was visible at the printing surface, which could have led to larger voids in the interface.

Curing of the samples

A remarkable result was visible for the samples with 3H time interval, with the different curing conditions. The samples that were air cured, i.e. were left open for the time between printing the subsequent filament, had the highest compressive strength of all samples, in all directions. The strength was comparable to the one-minute time interval samples. A hypothetical reason for this result could be that the samples remain fully untouched. The surface texture was not changed, or wiped out, by a plastic film, a wet burlap, or a mist layer. The subsequent filament may have the best mechanical interaction with the printed filament compared to the cured samples, so interlocking of the aggregates of the subsequent filament could be the best.

Voids at the interface

As mentioned during the literature review, the interaction between two concrete filaments depends both on mechanical interaction of the aggregates, and the chemical bonding of the cement with the aggregates. The mechanical interaction between aggregates turned out to be essential for the compressive strength of the sample. Loading the samples in perpendicular direction, led to the lowest strength val-

ues observed. At the same time, the CT scanning results showed a layer of voids representing the interfaces, also perpendicular to the loading direction. No mechanical interaction was possible at the location of the voids. In other words, no interlocking of the particles was possible at the location of the voids, leading to early failure of the samples loaded in perpendicular loading direction.

Samples loaded in longitudinal direction have the interface, and thus the layer of voids, parallel to the loading direction, and the concrete in loading direction is not interrupted by a layer of voids. Therefore, the strength in longitudinal direction is higher than the strength in perpendicular loading direction. However, this cannot be directly related, because it is possible that the filaments fail by means of tensile splitting. To test the influence of the interfaces parallel to the loading direction, the same sample with exactly the same compaction, should be tested without interfaces. This is not an easy task, as the cast material had a completely different compaction. Differences in the size of voids can be visually observed in the CT scanning results, but can not clearly be related to the compressive strength of the material, since no large differences were observed in compressive strength between samples printed with different parameters, other than the case reference samples.

Anisotropy
Based on the geometry of the sample, the longitudinal and the lateral loading direction were the same. The load was applied parallel to the interfaces in both directions, and the filaments were assumed to be heterogeneous, and therefore the observed differences in strength between the longitudinal and lateral loading direction were in contradiction with the expectations. On a micro-scale, multiple reasons can be thought of for the differences between the longitudinal and lateral loading direction:

- The first reason, the most obvious one, is sample preparation. During the experimental research, some samples were hard to prepare for the lateral loading direction. The width of the nozzle opening was 40mm, resulting in beams with a width of approximately 45mm, after some slump occurred. To prepare samples of 40x40x40mm, the samples were sawn. Changing sample dimensions by only a few millimeters is difficult. The sample moved during sawing, due to the lateral pressure of the sawing blade, and the sawn surface was not perfectly flat. This was observed for a few samples. If these samples were loaded, the stress concentrated on the protruding parts of the sample surface, leading to early failure of the whole sample. On the other hand, the relative standard deviations for the lateral loading directions remained below 5.2%, indicating that the samples were tested properly. Furthermore, several articles showed the same decrease in lateral loading direction (Ma et al., 2019; Sanjayan et al., 2018), where the samples were prepared properly. From this could be concluded that there must be other explanations for the lower strength in lateral loading direction, compared to the longitudinal direction.

- The second possible explanation for the lower strength of the lateral loading direction is, supported by Panda et al. (2017), directional compaction in the direction of extrusion. This phenomena has not been investigated further, but can possibly be researched by microscopy. By measuring the distance between the aggregates in multiple directions, the dependence of the extrusion direction on the compaction could be determined.

- A third explanation could be drying of the samples from the longitudinal edges. The samples were printed as beams of 800mm. This may have resulted in un-even drying of the sample from the longitudinal edges and the top surface. Figure 6.2 is added to explain the influence of the drying samples.

- The final explanation could be related to the material age and the printing speed. Although the printing speed was kept the same for all samples, the pump speed was manually set for every printing session. Minor differences in the pump speed could lead to stretching or compression of the filaments during extrusion. Also the pump speed was not adjusted related to the open time of the material, and the changing pumpability properties. Only at the beginning of each printing session, the pump speed was set manually, based on visual inspection of the printed filaments. Concrete of one hour old behaves stiffer than the same material of ten minutes old. This indicates that for a constant material flow, the pump speed should be constantly adjusted to keep the extruded material quantity the same. The limits for this process should then be the

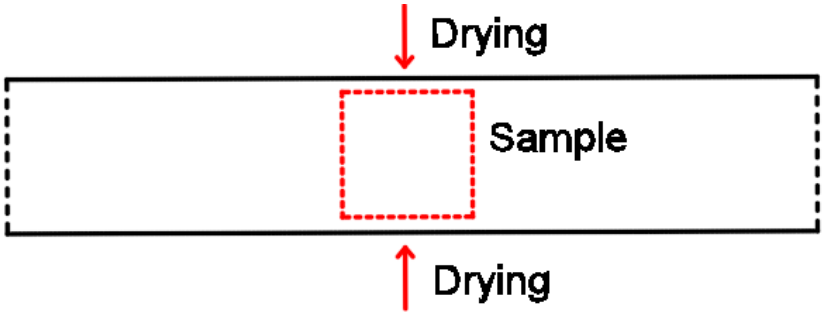

Figure 6.2: Unequal drying of printed beams.

capacity of the concrete pump, i.e. the maximum pressure the pump can handle, instead of the maximum open time of the concrete mixture.

6.1.2. Tensile splitting strength

The results of the tensile splitting tests showed no great differences between the tested parameters. The splitting strength was approximately 4 MPa for the perpendicular loading direction, which was 8% higher than the parallel loading direction. There was almost no difference between the tested parameters, except for the samples cured with a wet burlap. This strength was about 8-22% higher for the perpendicular and parallel loading direction, respectively. The same tests were performed by other researchers. The results of Wolfs et al. (2019) showed exactly the same results, without a significant difference between the testing directions. Also the strength values were approximately the same, although the materials were different. The results from Ma et al. (2019) showed a great strength difference between the testing directions. Differences could be related to the loading rate of the splitting test, which was 50% lower in the research of Ma et al. (2019), compared to this research and the research of Wolfs et al. (2019). Information on the exact test setup used by Ma et al. (2019) was not known, and could not be compared to this research, although the calculation of the tensile strength was the same. The test procedure of Wolfs et al. (2019) was exactly the same as in this research.

Since the tensile splitting strength is a measure for the tensile strength of the material, the results were expected to have approximately the same ratio for the different parameters as the direct tensile bond strength. This was however not the case, and therefore the question remains which test was performed more accurate. First of all the remark must be made that the accuracy of the tensile splitting test could not be qualified. The positioning of sample in the compression machine was a manual task, and sensitive for mistakes, because no loading jig was available. Misalignment of the packing strip was possible, although no failure planes other than the interface were observed. Rotation of the samples during loading was observed, and possibly had an influence on the samples. Some results were deleted, because the samples touched the loading plates, due to the rotation. On the other hand, the relative standard deviation of the samples was between 5-8% with one outlier of 11%. This is an indication that all tests were performed the same.

6.1.3. Tensile bond strength

Due to detailed experiments and careful sample preparation, lots of information has been gathered from the tensile bond strength tests. The full stress-displacement curves provided useful information on both the results of the test, but also on the validity of the results. First the test methods and samples are analyzed.

Discussion of the test method and samples

Based on standard concrete fracture mechanics, the stress-displacement curves should look like the graph presented in Figure 6.3. This curve shows a linear elastic branch up to the point where the micro cracks start to develop. After the peak value the micro cracks are fully developed and, as the loading continues, the load on the sample decreases until full strength loss.

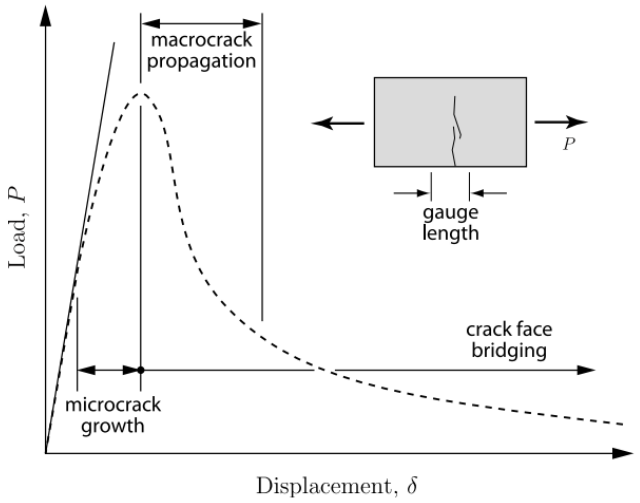

Figure 6.3: Good looking results of a direct tensile test of unreinforced concrete, shown as reference for the discussion (Landis and Bolander, 2009).

The results obtained for the samples printed with different time intervals, showed similar graphs compared to Figure 6.3. Samples with a nozzle standoff distance of 5mm, showed more noise in the results, showed a more brittle failure pattern and the micro cracking started earlier. The results of the samples printed with a 3 hour time interval and different curing conditions, showed this pattern even more clear, although the remark must be made that the samples with 3H time intervals were larger [1], which led to a much higher force on the sample, leading to more sudden failure.

Bending of the samples
During the tensile bond strength test, bending was observed. Both the obtained stress-displacement graphs and the DIC results showed this phenomena. Several explanations can be thought of, and below possible explanations for bending have been presented:

- The first possible explanation can be best described by looking at Figure 6.4. The notches were sawn manually, during the sample preparation. The cutting blade was only three millimeters thick, which made it difficult to position the centre of the notch exactly at the position of the interface. For this reason, some notches had to be made wider afterwards, to ensure that the full perimeter of the notch was positioned at the interface. The notches shown in the figure do not have the same width. According to Pluvinage (1998), the radius of the notch has an influence on the stress intensity at the crack tip. The sharper the angle of the notch is, the less stress is needed in order to initiate a crack, due to a higher stress intensity at the tip of the notch. This information can be directly related to the samples from this research. The notch on the left, shown in the figure, has a curvature, while the notch at the right has a larger width. This means that the crack starts at the left, due to the higher stress intensity at the tip of the notch. Early cracking of the sample from one side, leads to bending in the sample, from which it is impossible to obtain the same ultimate strength of the sample, compared to a sample loaded in uniaxial tension.

- A second possible explanation is that the surfaces that were glued to the loading plates, were not in all cases perfectly perpendicular. This was due to sample preparation, as was also mentioned for the cubic samples for the compression test. This led in some cases to samples that were not perfectly vertical aligned with the loading device. When loading the sample, the exerted load tried too pull the sample vertical, leading to bending of the sample, and crack initiation from one side.

- Finally, also the composition of the interface might cause crack initiation from one side. The tested cross section was only 100 mm^2, so it is possible that voids or large aggregates were non-

[1] The dimensions for the samples with 3H time intervals and different curing conditions were 30x30x40mm, including a notch.

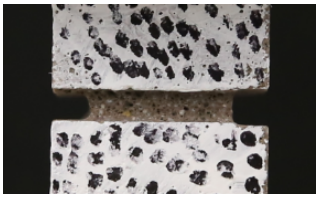

(a) Side view of a tested sample, showing the notch.

Plate with a crack	Notched plate with infinite acuity (zero notch radius)	notched plate with a notch radius ρ
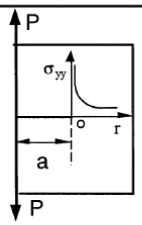	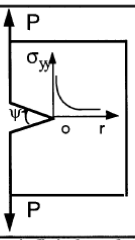	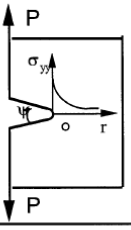
K_I for a crack	K^*_I for an infinitely sharp notch	K_ρ for a notch with a notch radius ρ
$K_I = \lim_{r \to 0} \sqrt{2\pi r}\ \sigma_{yy}$	$K_I^* = \lim_{r \to 0} 2\pi^{\alpha}\ \sigma_{yy} r^{\alpha}$	$\sigma_{yy} = \frac{K_\rho}{\sqrt{2\pi r^{\alpha}}}$

(b) Influence of the notch geometry.

Figure 6.4: Influence of the notch geometry on the crack initiation of the sample (Pluvinage, 1998).

uniformly distributed over the interface, having a significant influence on the overall strength of the sample. This could cause a non-uniform strength of the interface, again leading to bending.

It is most likely that a combination of these factors led to the behaviour that was observed during the tests. Moreover, LVDTs were placed on two sides of the sample, which means that bending can only be observed in one direction. Also from the results of the DIC analysis, bending in the other direction could not be observed. It is still possible that samples with good looking curves bent in the other direction, which resulted in a lower over all strength.

Qualitative analysis of the results

The results were analyzed based on both the strength and the standard deviation of the samples, and are compared to literature.

Different time intervals

The results obtained from samples printed with different time intervals, showed a clear trend of decreasing tensile bond strength with increasing time intervals between printed filaments. These same trend was obtained by other researchers. The main difference compared to the results of Panda et al. (2018), is that for each filament a new batch of concrete was prepared. During this research, the same batch was used for all filaments, which means that stiffness of the material that still had to be printed, was higher, leading to a worse adhesion between two adjacent filaments. The same procedure, with a different material, was performed by Tay et al. (2019). Their results showed a much stronger rate of decreasing bond strength, because of different mix design properties. According to literature, decreasing bond strength with increasing time intervals, is partially due to the temporary adsorption of water by the VMA (Chen et al., 2019a), evaporation of water (Sanjayan et al., 2018), and differences in longitudinal shrinkage of different filaments. The latter was visually observed during the experiments. The chemical bonding between the two filaments becomes less.

Different nozzle standoff distance

The results of the samples printed with a different nozzle standoff distance showed no clear pattern in the results. The time interval was 1 minute, and the printing speed was kept constant. All results that

were shown in the literature review, were obtained from nozzles with vertical extrusion. The influence of the nozzle standoff distance was then significant, because a certain pressure was exerted on printed filaments. In this research however, horizontal extrusion did not result in any pressure on the printed filaments, except for the gravitational weight of the filament. The positioning of the filaments became more inaccurate with an increasing nozzle standoff distance, resulting in inaccurate positioning of the filaments. Consequently, misalignment could lead to unequally distributed stresses, causing early failure of the printed element due to buckling of the printed elements or plastic failure (squeezing) of the first filament. The differences between relative standard deviations became larger when the nozzle standoff distance increased. This result is in agreement with the explanation in this paragraph.

No clear trend in average values was observed. The strength of the 5mm samples was expected to lie in between the 1mm and 10mm samples, but this was not the case. The only difference that could explain these results, is the temperature during the printing session of the 5mm samples. The first printing session for the 5mm samples failed, so the beams were printed a second time in mid-summer. Everything looked normal during the printing session, but the room temperature was approximately 30-35°C, while the other printing sessions took place at a room temperature of 20°C. The influence of the room temperature was not investigated, but the hypothetical conclusion could be drawn that the room temperature had a significant influence on the drying and hardening process of the printed samples.

Different curing conditions
Samples printed with a 3 hour time interval, were cured with specific curing regimes. The room temperature during the printing session was also 30-35 °C. However, all 3 hour time interval samples were printed under the same conditions, so a comparison can still be made. Significant differences were observed between the different curing regimes:

- The first observation was that curing of the samples results in higher bond strength, compared to the samples that were not cured. This was expected on beforehand. The relative standard deviation of samples that were not cured was however much lower compared to the samples that were cured.

- Curing the samples in wet curing regimes, like the wet burlap and the mist spray, resulted in high strength, but also in a very high standard deviation. The reason for this can again be related to the presence of water/mist/moisture on the printing surface. The same reason was mentioned for the low compressive strength of the samples, due to the large quantity of voids present in the interface. A simple relation can then be made between the chemical bonding and the bond strength of the sample: a high moisture content results in a large quantity of voids (leading to a lower compressive strength), but the chemical bonding between the filaments is better compared to samples that were not cured with moisture/water.

- The samples that were covered with a plastic film, also show a very good relative standard deviation of only 8.8%. Also the CT scanning results showed visibly good compaction, the voids in the interface were less compared to the samples cured with wet measures. This leads to a second hypothetical conclusion that the bond strength of the samples covered with plastic is less than the samples cured with wet measures, but that the contact area between the two filaments is larger, which results in a smaller standard deviation.

6.1.4. Digital Image Correlation

DIC was performed to check the results of the tensile bond strength test. The distinction between samples cracking from one side, and samples cracking symmetrical (from both edges at the same time), could be made. However, the first results, showing the linear deformation of the sample, showed a lot of noise in the results. This might be caused by the rough dot pattern, which are large black dots on the surface. A finer, more random pattern, will most likely lead to more accurate results. This conclusion is supported by Pan et al. (2009).

6.1.5. CT scanning

The CT scanning results all showed the same brightness and resolution. The voids could be seen visually, as well as the location of the interfaces. The cast samples contained larger pores than the printed samples, from which could be concluded that the compaction between printed samples and cast samples was not the same. Any comparison between printed samples and cast samples is therefore useless. Also can be said that the developed material by Y. Chen, is not suitable as traditional self compacting concrete. The VMA added in the concrete mix outweighs the effects of superplasticizer to expel the air.

The filaments looked good when they were inspected visually. No visible pores could be seen in the filaments, except for the 5mm nozzle standoff distance. The temperature at the day of printing and the open time of the mixture may have had a significant influence on the fresh mix properties, and the hardening process of the concrete, as explained before. The trend of decreasing bond strength with increasing time intervals, can also be observed on the CT scans. The bond strength of the 3 hour cured samples, showed again much larger and much more voids compared to all the other samples with different parameters.

Open time of the concrete mix

The final very important observation is about a parameter that was not part of this research, namely the open time of the mixture. As mentioned before, the samples were all printed from different batches of concrete, mixed with time intervals of 10 minutes. This means that the open time of the concrete could not be exactly measured. Printing samples with time intervals of 10 minutes, took in total 30 minutes to print (four filaments), which theoretically means that the concrete could have been from the same batch. Although the printability window of the mixture was over one hour, the printability of the material decreased, hardened C-S-H chains were broken, and more air was entrapped in the material. Differences in the porosity between two subsequent filaments can be visually observed in the CT scans, as shown in Figure 6.5. The influence of the early age of the material on the bond strength and the porosity of the filaments could not be qualified.

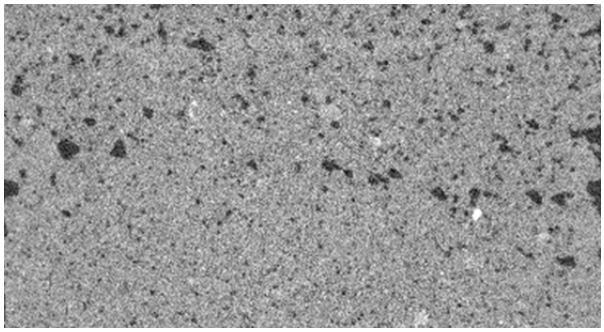

Figure 6.5: Influence of the open time of the concrete mix on the porosity of the filaments, in this case samples printed with a nozzle standoff distance of <1mm.

6.1.6. General use of the parameters in practice

Now the last questions that remain are which parameters are suitable for the use in practice, and how the quality obtained in the laboratory can also be obtained in outdoor printing conditions, with construction workers that might not have the same attention for detail as scientific researchers.

- The samples printed with a time interval of 20 seconds and 1 minute, are not representative for use in practice, both from the viewpoint of the buildability of the mixture, and related to the desired continuous printing path. Printing with a path of 1 minute means that the nozzle has to be back at its starting position within one minute, and 3,6 meters of printed filament.
- The ten minute time interval is realistic for larger structures, since maximum 36 meters of a wall can be printed (with the standard printing speed of 60 mm/sec). The remaining tensile bond strength after 10 minutes is only 20% lower compared to filaments printed after 20 seconds.

- If the structure is too large and the work should be stopped overnight, it is good to know that the material properties decrease significantly. With good curing it is still possible to minimize the decrease in bond strength. However, only three hour time intervals were tested.
- The curing conditions all led to better bond strength of the printed elements. However, some of them are not advised to be used in practice, due to possible stability problems of the printed elements. If walls are covered with wet burlaps, or plastic films, the top filaments are touched. Touching the top filaments may lead to modified surface properties of the printed filament, which can have a negative influence on the bond with the subsequent filament. What also should be taken into account is that during the experimental research the complete samples were covered, so in fact the hole sample was cured. In practice, curing the sides of the walls with a plastic cover/wet burlap is either not possible, or at least less effective. Touching of the walls may also lead to small misalignment's of the wall, since the concrete has not hardened when the curing is applied. Printing the next filaments can then lead to eccentric loading. Also buckling of the (not hardened) printed walls is plausible to occur when the walls are touched. Also bad weather conditions like strong wind may lead to buckling of the printed walls, but were not considered in this research. Printing in a tent might then be a good solution.

  A curing measure that can be applied from a distance is therefore be the best. Spraying a mist layer on the wall, both on the top surface and the edges, is a curing measure that can be applied easily in practice for curing of the wall. Attention should be paid the the amount of moisture on the top surface of the wall when the printing session is restarted. This surface should be visibly dry in order to avoid large voids in the interface, as has been mentioned before.

6.2. Numerical material model

The material model was critically analyzed for its application in practice. The development of the the material model, together with the development of the case study, gave an idea of the possibilities for the use in practice.

A remark has to be made by for the use of the material model. The shear strength of the interfaces was not known. The shear forces acting on the structure could not be checked and were assumed to fulfill the requirements. The shear strength of the filaments complied with the codes. If structures are designed where the shear forces are critical, the consideration should be made whether to build the structure or not, because it is likely that the shear strength of the interfaces is less compared to the filaments.

A second point of attention is the third loading direction, which is the lateral loading direction. The compressive strength in these directions was less compared to the printing direction, but this could not be modelled. The reason for this is the following: the filaments have been modelled as normal strength concrete. This is a standard material available in DIANA, and is heterogeneous. Multiple reasons have been provided in section 6.1. Summarized: the printing process, drying of the samples from the edges, and directional compaction all possibly have a share in the lower lateral compressive strength. If compressive loading of a wall in lateral direction is the case, then the developed model cannot be used safely.

It has to be kept in mind that the material is still brittle, although the simulation of the tensile bond stress curve suggests that the material has a long post cracking curve. If the peak value is reached at a certain point, that part of the material does not contribute anymore to the bond strength of the material. In the case of the simple wall element this means that the wall fails immediately.

6.3. Case study

The case study is discussed based on the feasibility of the project, including the structural verification. A 3D printed shelter can be seen as an innovation that can partially replace the common shelter solutions.

Structural verification
The final result of the full wind load calculation was that wind combination 2 did not fulfill the ULS requirements, with a unity check of 1.1. The conclusion should be that the structure is unsafe in extreme wind condition. The ultimate loads on the building is however discussed:

- The wind loads are based on a return period of 50 years. It is unlikely that the shelter will be build for a period of 50 years, so the the wind load can be reduced. If a time period of 10 years is taken as reference, the wind speed should be multiplied with a factor 0.9, resulting in an extreme wind pressure of 2.41 kN/m^2, which is 3.12 kN/m^2 in the ULS. So, depending on the design period, the building fulfills the requirements or not.
- A second remark must be made that the wind speeds in Mali are extreme and that most of the countries in Africa have much lower wind speeds, resulting in extreme wind pressures from which the shelter does not collapse.
- Finally, also the thickness of the walls can be increased to increase the capacity of the walls. This should always be checked with the pump capacity and the nozzle dimensions.

Summarizing: the shelter has sufficient capacity for most of the African countries, and based on the return period of extreme wind load conditions, the safety of the shelter should not be a problem in any country.

Variation of the chosen wall system
In literature, one wall system was mentioned often for printing walls. This wall system is based on contour crafting. Two outer shells are connected internally by means of curved filaments, as shown in Figure 6.6. This construction system provides the following advantages:

Figure 6.6: Alternative wall system (3Dnatives.com).

1) The hollow wall system provides good insulation properties, due to the air inside the wall. The walls can also be filled with insulation materials.
2) A smaller quantity of concrete is needed to obtain the same structural performance.
3) A standard, circular, nozzle type with down-flow can be used. Changes in print path direction are easy to make.
4) Thick walls are easy to make, and therefore are expected to provide better structural stability, due to a larger internal lever arm.
5) Internal walls are easier to connect to perpendicular walls, since the print path can still be partially continuous.

However, the reasons why in this case study solid walls were chosen, are the following:

1) A rectangular nozzle with back flow was used during the experimental research. A rectangular nozzle is difficult to use for the alternative wall system, because this requires the use of a rotating nozzle. Also according to literature, adding a curvature to a horizontally extruded filament, can lead to stretching or compressing the filaments, causing deviating material properties.
2) The shear strength of the samples has not been investigated. In order to make a reliable material model, where the filaments also touch each other vertically, requires additional research to obtain the shear strength of the laterally connected filaments. The material model would be unreliable if the shear strength is not considered.

Roof solution
The roof was designed in timber, which may nullify the advantages of the printable walls. The amount of labour and time that is needed to construct the roof is in contradiction with the design philosophy of the project. Nevertheless, for this study the decision was made to construct the roof in timber because the printed roof solution was not considered feasible yet, and the styrofoam roof solution was too hypothetical. Furthermore, the loads on the timber roof could be applied according to the code.

7

Conclusions

At the beginning of this thesis, a research framework was presented. Research questions have served as the red line for the elaboration of this research, and now, with the results and the discussion finished, conclusions were drawn. The conclusions are formulated such, that all research questions are provided with an answer.

How do the process parameters influence the mechanical properties?

- Increasing time intervals between printed filaments had a negative influence on the tensile bond strength of printed elements. The compressive strength of cubic samples was almost not influenced by the increasing time intervals between printing two adjacent filaments.
- The nozzle standoff distance had no significant influence on both the tensile splitting strength and the compressive strength, because new filaments exerted no pressure on previous filaments, except for their gravitational weight. However, inaccurate positioning of filaments could lead to early failure due to buckling and eccentric loading.
- From the tensile splitting strength tests, no clear distinction could be made between the strength of the samples, printed with different parameters. This was in contradiction with the tensile bond strength test results. The test method was discussed and questioned, but the relative standard deviations gave no reason to doubt the results. Loading a structure in lateral or longitudinal printing direction should therefore not be critical.
- Several curing regimes could be applied to improve the bond strength of printed elements, up to 101% compared to air-cured samples. Curing with a mist spray led to larger voids, decreasing the mechanical interaction between filaments and therefore led to a lower compressive strength. On the other hand, the tensile bond strength increased by curing with a mist layer, due to increasing chemical bonding in the interfaces between two filaments. Air-curing of the samples led to the best compressive strength of printed elements, however the tensile bond strength was the lowest of all tested parameters. The major point of attention is application in practice. Curing regimes with a wet burlap also showed good compressive and tensile behaviour of the sample. However, applying this curing method in practice, means that the printed walls are touched, which could lead to early collapse of the walls, due to other failure mechanisms like buckling and eccentric loading. Furthermore, the whole structure is cured if a mist layer is applied.
- The CT scanning results indicated that the porosity of two adjacent filaments was different. That observation was related to the open time of the concrete mixtures, which influenced the compaction of the filaments. Older concrete behaves stiffer, and the self compacting property of the concrete becomes less significant.

Can the material behaviour in different directions be captured numerically, using a finite element program?

- It was possible to create a reliable finite element model, exactly matching the tensile bond strength and the compressive strength in two directions. It was not possible to model the lateral loading direction based on the fact that the filaments were modeled as heterogeneous materials. Possible explanations for the anisotropic properties are directional compaction, drying from the longitudinal edges of the printed beams, and printing parameters, like the printing speed.
- When the material model is used for calculations of structures, it is essential to keep in mind that the compressive strength in lateral loading direction has not been modelled, and in reality has a lower strength. Also the shear strength of the interfaces has not been modelled, and a numerical calculation can therefore not diverge due to a shear failure.
- The splitting strength of the material was not modelled, because this material property was not necessary for the elaboration of the case study. If, in a later stage, structures are loaded parallel to the interfaces, the splitting strength becomes important and the consideration has to be made whether to use this model or not.

How can the obtained knowledge about both the printing process and the material model be used to design a 3D printed emergency shelter?

- It is very important to design the structure based on the construction procedure. In the end it must be possible to build the structure, so the construction procedure must be leading during the design stage. The buildability of the structure, general design aspects like continuous filaments for the walls, a significant corner radius, and wall openings all the way to the top of the wall, are important aspects. Simplicity is important for emergency shelters, especially because of the desired construction speed, and to prevent any mistakes during the construction process.
- The material model can serve as a tool to check the final shelter design. The simplicity of the design makes it possible to use the simplified material model, and the final conclusion is that the structure is safe to be built anywhere in Africa, and possibly other continents as well.
- The new way of thinking for future shelter solutions offers numerous advantages, like a better indoor environment, contribution to the well-being of the people living in a shelter, and safety. Also the possibility to upgrade the shelters in the future, to serve as long term housing, makes this solution convenient and sustainable.

8

Recommendations

Looking back at this research, there are always results that lead to new questions. Additional research should be performed find the answers to these questions. A list of recommendations for future research is presented below, to optimize the printing process, or simply to find additional evidence for the results.

- Samples with different nozzle standoff distances were tested in order to obtain the mechanical properties when printed structures show slump. This problem can be overcome if a printing technique is developed where the nozzle standoff distance is constantly corrected by sensors that measure the exact standoff distance. The advise is to further develop this tool for accurate printing.
- What turned out to be a critical parameter is the open time of the mixture. Based on the CT scanning results, the conclusion could be made that the open time of the material had a significant influence on the compaction of the material. To quantify the influence of the open time of the mixture, the advise is to perform additional research on the decreasing mechanical properties with increasing open time of the mixture. CT scanning can provide evidence in this test.
- The suspicion is that the room temperature had a significant influence on the rate of drying and the rate of hydration of the concrete. The samples with 5mm nozzle standoff distance showed a small strength decrease, compared to samples printed at a room temperature which was 15°C lower. It is advised to test the influence of the room temperature, in combination with the relative humidity.
- The buildability of the printed filaments is only based on the green strength of the material with a maximum strain criterion of 5%. The buildability of a wall is however also dependant on the small misalignment of filaments and buckling of the wall. It is advised to do further research on these additional failure mechanisms.
- The tensile bond strength tests were performed on samples with a notch. Bending of the samples led to high standard deviations and lower strength values. It is advised to perform the tests without a notch, to see if bending still occurs and if the results get more accurate.
- The difficulty that printable mixtures must be both extrudable and buildable, could be solved by the use of a nozzle type that can change the rheology of the fresh mixture at the nozzle. By injecting VMA or an accelerator at the nozzle, a flowable mixture could be changed to a buildable mix. It is advised to further investigate this technique.
- During the elaboration of the case study design, the assumption was made that the dimensions of the cross section of the nozzle opening can be scaled with a factor 3, to dimensions of 120x30mm. The buildability and extrudabuility of filaments printed with a larger nozzle should be tested, in order to verify that the buildability of the filaments remains the same.

- The final recommendation is about the development of an emergency shelter. The first steps of a feasible emergency shelter design have been presented, but the next step is to further develop the interior design, for long term use of the shelters. Maybe it is even possible to print the furniture, like a sofa, dining table or a bed, so when the shelter is finished, people can move in directly. Also upgrade measures should be further investigated, to make the shelter suitable for long term use. Upgrade measures could include a permanent roof design, but could also be based on safety and indoor climate.

Bibliography

AF Ab Ghani, MB Ali, S DharMalingam, and J Mahmud. Digital image correlation (dic) technique in measuring strain using opensource platform ncorr. *Journal of Advanced Research in Applied Mechanics*, 26(1):10–21, 2016.

Domenico Asprone, Ferdinando Auricchio, Costantino Menna, and Valentina Mercuri. 3d printing of reinforced concrete elements: Technology and design approach. *Construction and Building Materials*, 165:218 – 231, 2018a. ISSN 0950-0618. doi: https://doi.org/10.1016/j.conbuildmat.2018.01.018. URL http://www.sciencedirect.com/science/article/pii/S0950061818300187.

Domenico Asprone, Costantino Menna, Freek P. Bos, Theo A.M. Salet, Jaime Mata-Falcón, and Walter Kaufmann. Rethinking reinforcement for digital fabrication with concrete. *Cement and Concrete Research*, 112:111 – 121, 2018b. ISSN 0008-8846. doi: https://doi.org/10.1016/j.cemconres.2018.05.020. URL http://www.sciencedirect.com/science/article/pii/S0008884618300309. SI : Digital concrete 2018.

ASTM. Standard test method for tensile strength of concrete surfaces and the bond strength or tensile strength of concrete repair and overlay materials by direct tension (pull-off method), 2004.

Abdulrahman Bashawri, Stephen Garrity, and Krisen Moodley. An overview of the design of disaster relief shelters. *Procedia Economics and Finance*, 18:924–931, 2014.

Frederick Bester. *Benchmark Structures for 3D printing of Concrete*. PhD thesis, 10 2018.

Freek Bos, Rob Wolfs, Zeeshan Ahmed, and Theo Salet. Additive manufacturing of concrete in construction: potentials and challenges of 3d concrete printing. *Virtual and Physical Prototyping*, 11(3): 209–225, 2016. ISSN 1745-2759.

Othmane Boukendakdji, El-Hadj Kadri, and Said Kenai. Effects of granulated blast furnace slag and superplasticizer type on the fresh properties and compressive strength of self-compacting concrete. *Cement and concrete composites*, 34(4):583–590, 2012.

R.A. Buswell, W.R. Leal de Silva, S.Z. Jones, and J. Dirrenberger. 3d printing using concrete extrusion: A roadmap for research. *Cement and Concrete Research*, 112:37 – 49, 2018. ISSN 0008-8846. doi: https://doi.org/10.1016/j.cemconres.2018.05.006. URL http://www.sciencedirect.com/science/article/pii/S0008884617311924. SI : Digital concrete 2018.

Y Chen, S Figueiredo, Z Li, Z Chang, K Jansen, and O Copuroglu. Improving 3d printability of limestone and low-grade calcined clay-based sustainable cementitious materials by using viscosity modifying admixture. 2020 (submitted).

Yu Chen, Fred Veer, and Oguzhan Copuroglu. A critical review of 3d concrete printing as a low co2 concrete approach. *Heron*, 62(3), 2017.

Yu Chen, Stefan Chaves Figueiredo, Çağlar Yalçinkaya, Oğuzhan Çopuroğlu, Fred Veer, and Erik Schlangen. The effect of viscosity-modifying admixture on the extrudability of limestone and calcined clay-based cementitious material for extrusion-based 3d concrete printing. *Materials*, 12(9), 2019a. ISSN 1996-1944. URL http://www.mdpi.com/1996-1944/12/9/1374.

Yu Chen, Zhenming Li, Stefan Chaves Figueiredo, Oğuzhan Çopuroğlu, Fred Veer, and Erik Schlangen. Limestone and calcined clay-based sustainable cementitious materials for 3d concrete printing: A fundamental study of extrudability and early-age strength development. *Applied Sciences*, 9(9), 2019b. ISSN 2076-3417. URL http://www.mdpi.com/2076-3417/9/9/1809.

Sang-Yeop Chung, Tong-Seok Han, and Yong-Woo Kim. Spatial distribution of voids in insulating concrete analyzed by micro-ct images and probability functions. *Advances in Materials Science and Engineering*, 2015, 2015.

C. Borg Costanzi, Z.Y. Ahmed, H.R. Schipper, F.P. Bos, U. Knaack, and R.J.M. Wolfs. 3d printing concrete on temporary surfaces: The design and fabrication of a concrete shell structure. *Automation in Construction*, 94:395 – 404, 2018. ISSN 0926-5805. doi: https://doi.org/10.1016/j.autcon.2018.06.013. URL http://www.sciencedirect.com/science/article/pii/S0926580517306556.

Geert De Schutter, Karel Lesage, Viktor Mechtcherine, Venkatesh Naidu Nerella, Guillaume Habert, and Isolda Agusti-Juan. Vision of 3d printing with concrete—technical, economic and environmental potentials. *Cement and Concrete Research*, 112:25–36, 2018.

J Del Viso, J Carmona, and G Ruiz. Size and shape effects on the compressive strength of high strength concrete. In *6th International conference on fracture mechanics of concrete and concrete structures*, pages 1297–1304, 2007.

Stefan Chaves Figueiredo, Claudia Romero Rodríguez, Zeeshan Y. Ahmed, D.H. Bos, Yading Xu, Theo M. Salet, Oğuzhan Çopuroğlu, Erik Schlangen, and Freek P. Bos. An approach to develop printable strain hardening cementitious composites. *Materials Design*, 169:107651, 2019. ISSN 0264-1275. doi: https://doi.org/10.1016/j.matdes.2019.107651. URL http://www.sciencedirect.com/science/article/pii/S0264127519300887.

Izabela Hager, Anna Golonka, and Roman Putanowicz. 3d printing of buildings and building components as the future of sustainable construction? *Procedia Engineering*, 151:292 – 299, 2016. ISSN 1877-7058. doi: https://doi.org/10.1016/j.proeng.2016.07.357. URL http://www.sciencedirect.com/science/article/pii/S1877705816317453. Ecology and new building materials and products 2016.

François Hild and Stéphane Roux. Digital image correlation: from displacement measurement to identification of elastic properties–a review. *Strain*, 42(2):69–80, 2006.

Akihiko Ito and Rota Wagai. Global distribution of clay-size minerals on land surface for biogeochemical and climatological studies. *Scientific data*, 4:170103, 2017.

Kumar Neeraj Jha. *Formwork for concrete structures*. Tata McGraw Hill Education Private Limited, 2012.

Vl Kadleček and S Modrỳ. Size effect of test specimens on tensile splitting strength of concrete: general relation. *Materials and Structures*, 35(1):28, 2002.

Jamal M. Khatib, Oussama Baalbaki, and Adel A. ElKordi. 15 - metakaolin. In Rafat Siddique and Paulo Cachim, editors, *Waste and Supplementary Cementitious Materials in Concrete*, Woodhead Publishing Series in Civil and Structural Engineering, pages 493 – 511. Woodhead Publishing, 2018. ISBN 978-0-08-102156-9. doi: https://doi.org/10.1016/B978-0-08-102156-9.00015-8. URL http://www.sciencedirect.com/science/article/pii/B9780081021569000158.

Behrokh Khoshnevis. Automated construction by contour crafting—related robotics and information technologies. *Automation in construction*, 13(1):5–19, 2004.

Nathalie Labonnote, Anders Rønnquist, Bendik Manum, and Petra Rüther. Additive construction: state of the art, challenges and opportunities. *Automation in Construction*, 72, 09 2016. doi: 10.1016/j.autcon.2016.08.026.

EN Landis and JE Bolander. Explicit representation of physical processes in concrete fracture. *Journal of Physics D: Applied Physics*, 42(21):214002, 2009.

S Laustsen, D Bentz, Marianne Hasholt, and O.M. Jensen. Ct measurement of sap voids in concrete. 01 2010.

T. T. Le, S. A. Austin, S. Lim, R. A. Buswell, A. G. F. Gibb, and T. Thorpe. Mix design and fresh properties for high-performance printing concrete. *Materials and Structures*, 45(8):1221–1232, Aug 2012a. ISSN 1871-6873. doi: 10.1617/s11527-012-9828-z. URL https://doi.org/10.1617/s11527-012-9828-z.

T.T. Le, S.A. Austin, S. Lim, R.A. Buswell, R. Law, A.G.F. Gibb, and T. Thorpe. Hardened properties of high-performance printing concrete. *Cement and Concrete Research*, 42(3):558 – 566, 2012b. ISSN 0008-8846. doi: https://doi.org/10.1016/j.cemconres.2011.12.003. URL http://www.sciencedirect.com/science/article/pii/S0008884611003255.

L Lei and J Plank. Synthesis, working mechanism and effectiveness of a novel cycloaliphatic superplasticizer for concrete. *Cement and Concrete Research*, 42(1):118–123, 2012.

Sungwoo Lim, Thanh Le, John Webster, Richard Buswell, A Austin, Alistair Gibb, and Tony Thorpe. Fabricating construction components using layered manufacturing technology. pages 512–520, 2009.

Guowei Ma, Zhijian Li, Li Wang, Fang Wang, and Jay Sanjayan. Mechanical anisotropy of aligned fiber reinforced composite for extrusion-based 3d printing. *Construction and Building Materials*, 202: 770–783, 2019.

Viktor Mechtcherine, Venkatesh Naidu Nerella, Frank Will, Mathias Näther, Jens Otto, and Martin Krause. Large-scale digital concrete construction–conprint3d concept for on-site, monolithic 3d-printing. *Automation in Construction*, 107:102933, 2019.

Christian Melaun, Antje Werblow, Sarah Cunze, Sina Zotzmann, Lisa K Koch, Heinz Mehlhorn, Dorian D Dörge, Katrin Huber, Oliver Tackenberg, and Sven Klimpel. Modeling of the putative distribution of the arbovirus vector ochlerotatus japonicus japonicus (diptera: Culicidae) in germany. *Parasitology research*, 114(3):1051–1061, 2015.

Shazim Ali Memon, Muhammad Ali Shaikh, and Hassan Akbar. Utilization of rice husk ash as viscosity modifying agent in self compacting concrete. *Construction and building materials*, 25(2):1044–1048, 2011.

William A Mitchell. Reconstruction after disaster: The gediz earthquake of 1970. *Geographical Review*, pages 296–313, 1976.

NcorrV1.2. Ncorr v1.2. URL http://ncorr.com/index.php.

Venkatesh Naidu Nerella, Simone Hempel, and Viktor Mechtcherine. Effects of layer-interface properties on mechanical performance of concrete elements produced by extrusion-based 3d-printing. *Construction and Building Materials*, 205:586–601, 2019.

Hiroki Ogura, Venkatesh Nerella, and Viktor Mechtcherine. Developing and testing of strain-hardening cement-based composites (shcc) in the context of 3d-printing. *Materials*, 11(8):1375, 2018.

Bing Pan, Kemao Qian, Huimin Xie, and Anand Asundi. Two-dimensional digital image correlation for in-plane displacement and strain measurement: a review. *Measurement science and technology*, 20 (6):062001, 2009.

Biranchi Panda, Suvash Chandra Paul, and Ming Jen Tan. Anisotropic mechanical performance of 3d printed fiber reinforced sustainable construction material. *Materials Letters*, 209:146 – 149, 2017. ISSN 0167-577X. doi: https://doi.org/10.1016/j.matlet.2017.07.123. URL http://www.sciencedirect.com/science/article/pii/S0167577X17311679.

Biranchi Panda, Suvash Chandra Paul, Nisar Ahamed Noor Mohamed, Yi Wei Daniel Tay, and Ming Jen Tan. Measurement of tensile bond strength of 3d printed geopolymer mortar. *Measurement*, 113:108 – 116, 2018. ISSN 0263-2241. doi: https://doi.org/10.1016/j.measurement.2017.08.051. URL http://www.sciencedirect.com/science/article/pii/S0263224117305560.

Suvash Chandra Paul, Gideon PAG van Zijl, Ming Jen Tan, and Ian Gibson. A review of 3d concrete printing systems and materials properties: Current status and future research prospects. *Rapid Prototyping Journal*, 24(4):784–798, 2018.

Arnaud Perrot, Damien Rangeard, and Alexandre Pierre. Structural built-up of cement-based materials used for 3d-printing extrusion techniques. *Materials and Structures*, pages 1–8, 02 2015. doi: 10.1617/s11527-015-0571-0.

Guy Pluvinage. Fatigue and fracture emanating from notch; the use of the notch stress intensity factor. *Nuclear Engineering and Design*, 185(2-3):173–184, 1998.

Hans W Reinhardt, Hans AW Cornelissen, and Dirk A Hordijk. Tensile tests and failure analysis of concrete. *Journal of structural engineering*, 112(11):2462–2477, 1986.

Marine Rubio, M Sonebi, and S Amziane. 3d printing of fibre cement-based materials: Fresh and rheological performances. 2017.

Theo A. M. Salet, Zeeshan Y. Ahmed, Freek P. Bos, and Hans L. M. Laagland. Design of a 3d printed concrete bridge by testing. *Virtual and Physical Prototyping*, 13(3):222–236, 2018. doi: 10.1080/17452759.2018.1476064. URL https://doi.org/10.1080/17452759.2018.1476064.

Jay G. Sanjayan, Behzad Nematollahi, Ming Xia, and Taylor Marchment. Effect of surface moisture on inter-layer strength of 3d printed concrete. *Construction and Building Materials*, 172:468 – 475, 2018. ISSN 0950-0618. doi: https://doi.org/10.1016/j.conbuildmat.2018.03.232. URL http://www.sciencedirect.com/science/article/pii/S0950061818307384.

Claire Scott. Chinese construction company 3d prints an entire two-story house on-site in 45 days. *3Dprint.com*, page 16, 06 2016.

Seung-Jun Shin, Suk-Hwan Suh, and Ian Stroud. Reincarnation of g-code based part programs into step-nc for turning applications. *Computer-Aided Design*, 39(1):1 – 16, 2007. ISSN 0010-4485. doi: https://doi.org/10.1016/j.cad.2006.08.005. URL http://www.sciencedirect.com/science/article/pii/S0010448506001667.

M Sonebi, Mohamed Lachemi, and KMA Hossain. Optimisation of rheological parameters and mechanical properties of superplasticised cement grouts containing metakaolin and viscosity modifying admixture. *Construction and Building Materials*, 38:126–138, 2013.

Rory Stott. Chinese company constructs the world's tallest 3d printed building. 2015. URL https://www.archdaily.com/591331/chinese-company-creates-the-world-s-tallest-3d-printed-building.

Yi Wei Daniel Tay, Guan Heng Andrew Ting, Ye Qian, Biranchi Panda, Lewei He, and Ming Jen Tan. Time gap effect on bond strength of 3d-printed concrete. *Virtual and Physical Prototyping*, 14(1):104–113, 2019. doi: 10.1080/17452759.2018.1500420. URL https://doi.org/10.1080/17452759.2018.1500420.

Marcel R.A. van Vliet and Jan G.M. van Mier. Experimental investigation of size effect in concrete and sandstone under uniaxial tension. *Engineering Fracture Mechanics*, 65(2):165 – 188, 2000. ISSN 0013-7944. doi: https://doi.org/10.1016/S0013-7944(99)00114-9. URL http://www.sciencedirect.com/science/article/pii/S0013794499001149.

Vicente, Mínguez, and González. The use of computed tomography to explore the microstructure of materials in civil engineering: From rocks to concrete, computed tomography. *Journal of Advanced Research in Applied Mechanics*, 2017. doi: DOI:10.5772/intechopen.69245. URL https://www.intechopen.com/books/computed-tomography-advanced-applications/the-use-of-computed-tomography-to-explore-the-microstructure-of-materials-in-civil

Xiaofeng Wang, Zhenjun Yang, and Andrey P Jivkov. Monte carlo simulations of mesoscale fracture of concrete with random aggregates and pores: a size effect study. *Construction and Building Materials*, 80:262–272, 2015.

Wolfs. Early age mechanical behaviour of 3d printed concrete: Numerical modelling and experimental testing. *Cement and Concrete Research*, 106:103–116, 02 2018. doi: 10.1016/j.cemconres.2018.02.001.

R.J.M. Wolfs, F.P. Bos, and T.A.M. Salet. Hardened properties of 3d printed concrete: The influence of process parameters on interlayer adhesion. *Cement and Concrete Research*, 119:132 – 140, 2019. ISSN 0008-8846. doi: https://doi.org/10.1016/j.cemconres.2019.02.017. URL http://www.sciencedirect.com/science/article/pii/S0008884618310482.

Peng Wu, Jun Wang, and Xiangyu Wang. A critical review of the use of 3-d printing in the construction industry. *Automation in Construction*, 68:21–31, 2016.

Ming Xia, Behzad Nematollahi, and Jay G Sanjayan. Development of powder-based 3d concrete printing using geopolymers. pages 223–240, 2019.

Seong-Tae Yi, Eun-Ik Yang, and Joong-Cheol Choi. Effect of specimen sizes, specimen shapes, and placement directions on compressive strength of concrete. *Nuclear Engineering and Design*, 236(2): 115–127, 2006.

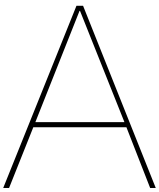

Appendix A - Input data 3DCP machine

An example of the G-code that was used to print beams of 800mm is added.

```
;reset g2 g3 motion to XY plane
        g17
        ;reset back to mm mode
        g21
        ;cancel radius compensation
        g40
        ;cancel height compensation
        g49
        ;smooth motion mode 0.1mm radius allowed (only when needed)
        G64P0.1
        ;revert back to absolute programming
        g90
        ;revert back to units per minute mode
        g94


        ;from here the actual G-code starts



        ;feed rate
#101 = 2700
#102 = 2700
#103 = 3600

F[#103] G1 Z200


F[#102] G1 X0 Y40.0000
G4 P15
F[#103] G1 Z0
F[#101] G1 X-980.0000 Y40.0000
F[#103] G1 Z200

F[#102] G1 X0 Y40.0000
G4 P30
F[#103] G1 Z12
F[#101] G1 X-980.0000 Y40.0000
F[#103] G1 Z200

F[#102] G1 X0 Y40.0000
G4 P30
F[#103] G1 Z24
F[#101] G1 X-980.0000 Y40.0000
F[#103] G1 Z200

F[#102] G1 X0 Y40.0000
G4 P30
F[#103] G1 Z36
F[#101] G1 X-980.0000 Y40.0000
F[#103] G1 Z200

F[#102] G1 X0 Y40.0000
G4 P30
F[#103] G1 Z48
F[#101] G1 X-980.0000 Y40.0000
F[#103] G1 Z200
```

Figure A.1: Example of a G-code used to print beams of 800mm in length, consisting of 4 layers.

B

Appendix B - Experimental data

This appendix shows the raw data obtained during the experimental research. On this page the data from the tensile splitting strength test are presented, on page 102 the data from the tensile bond strength tests are presented, and on page 103 the data from the compressive strength tests are presented.

All tables include the average data, and the (relative) standard deviations.

Experimental data obtained during tensile splitting strength tests

Description	***Direction 1***			***Direction 2***		
	Average	St. dev.	RSD	Average	St. dev.	RSD
Reference material	4.33	0.23	5.3%	-	-	-
1 minute	4.16	0.16	3.8%	3.77	0.21	5.6%
3H open	4.02	0.23	5.7%	3.72	0.19	5.1%
3H mist (30 minutes)	4.27	0.26	6.1%	3.88	0.19	4.9%
3H mist (1 hour)	4.01	0.25	6.2%	3.79	0.31	8.2%
3H plastic cover	3.91	0.22	5.6%	3.64	0.40	11.0%
3H wet cover	4.89	0.30	6.1%	4.00	0.22	5.5%

Table B.1: Explanation of the loading directions.

For a clear understanding of the loading directions, figure B.1 has been added, presenting the loading directions in compression and tensile splitting.

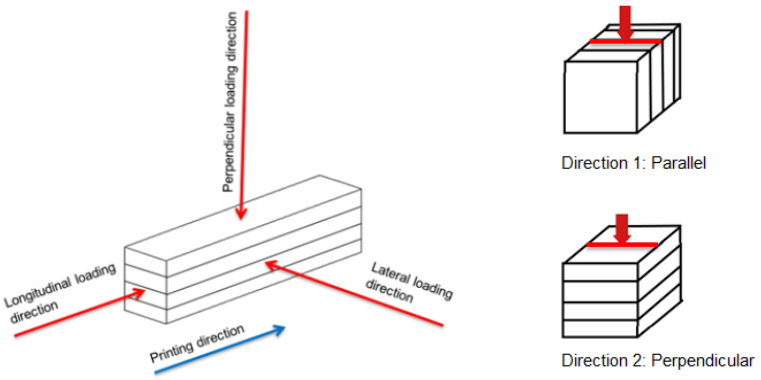

(a) Loading directions in compression.

(b) Loading directions in tensile splitting.

Figure B.1: Explanation of the loading directions.

Experimental data obtained during tensile bond strength test

Description	*Strength of the samples [MPa]*					*Average*	*Standard deviation*	*RSD*
	Sample 1	Sample 2	Sample 3	Sample 4	Sample 5			
Reference material	3.14	3.11	2.80	2.87	2.88	2.96	0.15	5.2%
Time intervals								
20 seconds	3.12	2.83	2.87			2.94	0.16	5.3%
1 minute	3.01	2.87	2.80			2.89	0.11	3.7%
10 minutes	2.50	2.58	2.00			2.36	0.31	13.3%
Nozzle standoff distance								
<1mm	3.12	2.83	2.87			2.94	0.16	5.3%
5mm	2.52	2.46	2.40	2.66		2.51	0.11	4.4%
10mm	2.58	2.68	3.07			2.78	0.26	9.3%
Curing conditions								
Open	0.60	0.69	0.77			0.69	0.09	12.4%
Plastic cover	1.16	0.98	1.03			1.06	0.09	8.8%
Wet cover	1.53	1.48	1.15			1.39	0.21	14.9%
Mist spray (30 minutes)	1.43	0.90	1.38	0.89		1.15	0.30	25.7%
Mist spray (1 hour)	0.82	1.17	1.06			1.02	0.18	17.6%

Table B.2: Experimental data of the tensile bond strength tests.

Experimental data obtained during compressive strength tests

Description	***Perpendicular loading direction***			***Longitudinal loading direction***			***Lateral loading direction***		
	Average	St. dev.	RSD	Average	St. dev.	RSD	Average	St. dev.	RSD
Reference material	33.51	1.46	4.3%	-	-	-	-	-	-
1 minute	45.98	1.69	3.7%	55.16	0.94	1.7%	45.70	1.66	3.6%
3H open	46.06	2.71	5.9%	56.35	1.96	3.5%	51.17	1.66	3.2%
3H mist (30 minutes)	41.15	1.79	4.3%	52.27	2.43	4.6%	47.92	2.48	5.2%
3H mist (1 hour)	42.03	2.14	5.1%	53.97	2.43	4.5%	44.75	1.57	3.5%
3H plastic cover	44.29	2.18	4.9%	55.74	1.99	3.6%	47.41	1.93	4.1%
3H wet cover	42.49	2.61	6.1%	55.93	1.98	3.5%	49.59	2.49	5.0%

Table B.3: Experimental data of the compressive strength tests.

C

Appendix C - Wind load calculation

The wind loads in Africa were calculated according to the South African National Standard, which is based on the Eurocode. Below the calculation is performed step by step:

The peak wind speed is dependant on both the roughness factor and the orography factor. The terrain roughness factor depends on both the height of the structure above ground level and the ground roughness. The ground roughness was chosen as a horizontal terrain, with negligible vegetation, Category A. The orography factor was taken as 1.0, and therefore the assumption was made that the shelter is not located close to hills, where the wind speed increases with more than 5%. The peak wind speed was calculated according to formula (C.1):

$$v_p(z) = C_r(z) \cdot C_0(z) \cdot v_{b,peak} \tag{C.1}$$

where:
$C_r(z)$ = 1.02 (terrain roughness factor)
$C_0(z)$ = 1.0 (orography factor)
$v_{b,peak}$ = 69 m/s (peak wind speed)
So: $v_p(3m)$ = 70.4 m/s

The next step was the calculation of the peak wind speed pressure. This calculation is dependant on the density of the air, and the peak wind speed. The density of the air was taken at sea level. The peak wind speed pressure could be calculated according to (C.2):

$$q_p(z_e) = \frac{1}{2} \cdot \rho \cdot {v_p}^2(z) \tag{C.2}$$

where:
ρ = 1,2 kg/m^3 (air density)
and $v_p(z)$ = 70.4 m/s
So: $q_p(z_e)$ = 2.97 kN/m^2

The final step in the wind load calculation was the determination of the wind pressure coefficients. Figure C.1, on the next page, shows the areas where pressure coefficients should be applied, including an explanation of the positive and negative signs.

Taking the dimensions of the shelter into account, b = 5, d = 3, h = 3, e = 5, the external pressure coefficients are the following:

A = - 1.2
B = - 0.8
D = + 0.8
E = - 0.5

The internal pressures were taken as +0.2 and -0.3, for the positive and negative pressure coefficients respectively.

A simplification was made for the perpendicular walls. The pressure coefficient was taken as -1.0 for the complete width of the wall. This assumption is conservative, but on the safe side. If the structure is safe with this assumption, no further calculations needed to be made. The governing pressure coefficients for the directly loaded walls were +1.0 (= +0.8 + 0.2). This means that the walls must be able to withstand a characteristic windload of 2.97 kN/m^2. This load was taken as the characteristic load for the wall element calculation.

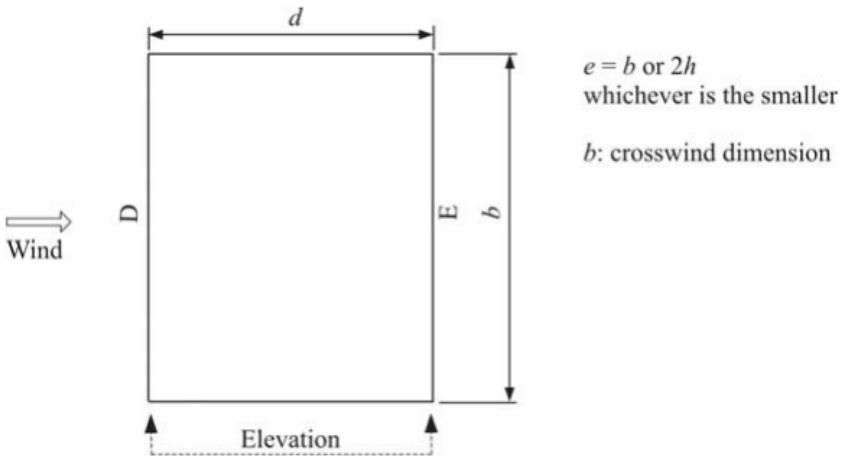

(a) Floor plan

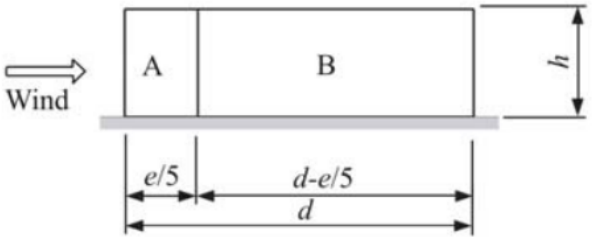

(b) Perpendicular walls

(c) Explanation of the signs

Figure C.1: Wind pressure coefficients for a rectangular building.

C.1. Wind loads on the complete shelter

The wind loads on the complete shelter were based on numerous internal end external pressure coefficients. Below, the three load combinations are shown in figure C.2.

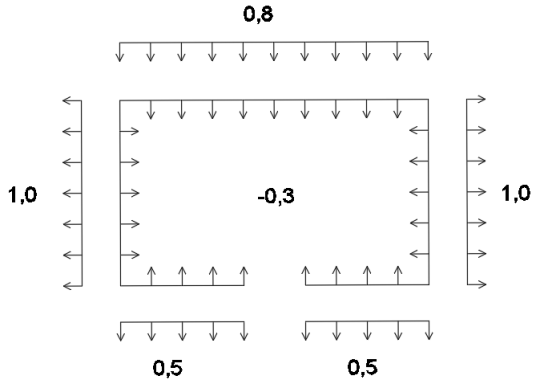

(a) Negative internal pressure coefficient.

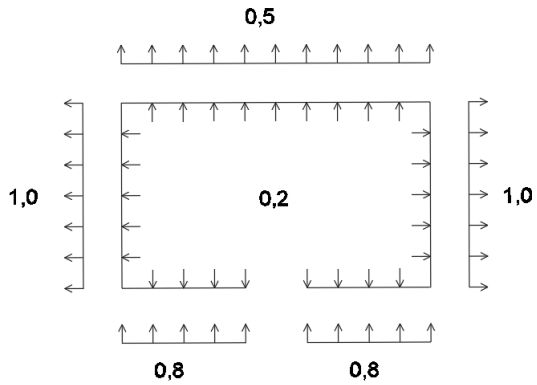

(b) Positive internal pressure coefficient.

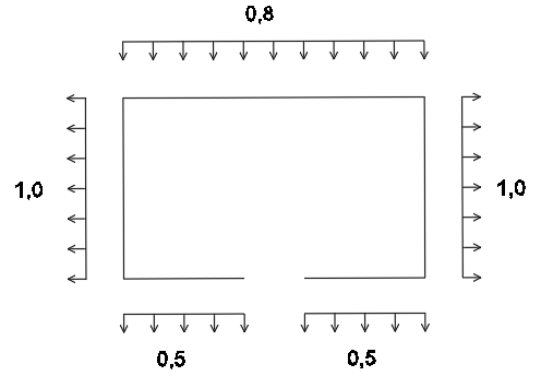

(c) No internal pressure coefficient.

Figure C.2: Load combinations based on the wind direction and internal pressure coefficients.

These pressure coefficients should be multiplied with the peak wind speed pressure. In the case of the shelter, a much higher peak wind pressure was chosen, to be able to calculate the failure wind pressure of the shelter.